Electronic Supporting Information for

Supramolecular chemistry of two new bis(1,2,3-triazolyl)pyridine macrocycles: metal complexation, self–assembly and anion binding

Arthur H. G.David,[a,b†] Rosemary J. Goodwin,[a] Nicholas G. White[*a]

[a] Research School of Chemistry, Australian National University, Canberra, ACT, Australia
[b] Institut des Sciences Chimiques de Rennes, Université de Rennes 1, 35042 Rennes, France
[†] Current address: MOLTECH-Anjou, CNRS, Université d'Angers, 49000 Angers, France

[*]E-mail: nicholas.white@anu.edu.au Website: www.nwhitegroup.com

Table of Contents

1. Experimental section **S3**

1.1. General methods S3

1.2. ^{1}H and ^{13}C NMR spectra of new compounds S4

1.3. Synthesis and characterisation of **2** and **4** S12

1.4. Alternative methods for the preparation of tetra-triazole macrocycle **3** S17

2. ^{1}H NMR studies of metal and anion complexation **S18**

2.1. Complexation of **btp** diazide **1** with Zn^{2+} S18

2.2. Complexation of macrocycle **8** with Zn^{2+} S20

2.3. Complexation of macrocycle **8** with Pd^{2+} S21

2.4. Anion binding by macrocycle **8** S23

2.5. Anion complexation by $[Pd\cdot\mathbf{8}\cdot CH_3CN](BF_4)_2$ S29

3. Single crystal X-ray diffraction analysis **S31**

3.1. General remarks S31

3.2. Structure of **3** S32

3.3. Structure of **8** S33

3.4. Structure of TBA·**8**·Br S34

3.5. Structure of $[Pd\cdot\mathbf{8}\cdot Cl]BF_4$ S35

3.6. Structure of $[Pd\cdot\mathbf{8}\cdot Br]BF_4$ from acetonitrile S36

3.7. Structure of $[Pd\cdot\mathbf{8}\cdot Br]BF_4$ from chloroform/methanol S37

3.8. Structure of $[Pd\cdot\mathbf{8}\cdot I]BF_4$ S38

3.9. Structure of $[Zn\cdot\mathbf{8}\cdot(OH_2)_2\cdot MeOH]^{2+}$ S39

3.10. Structure of $[Zn\cdot\mathbf{1}_2]^{2+}$ S40

3.11. Table of crystallographic data S42

3.12. Survey of Pd···Pd interactions in the Cambridge Structural Database S43

4. Computational modelling **S44**

4.1. Simulation protocol S44

4.2. Computational modelling of $[Zn\cdot\mathbf{3}_2]^{2+}$ S45

4.3. Computational modelling of $[Zn\cdot\mathbf{8}_2]^{2+}$ S46

5. References **S47**

1. Experimental section

1.1. General methods

TBTA,[1] 2,6-diethynylpyridine,[2] and dimethylcarbinol-protected 2-bromo-6-ethynylpyridine **S1**[3] were prepared as previously described, as were TBA_2·oxalate,[4] TBA_2·isophthalate[5] and TBA_2·terephthalate.[6] The bottle of isophthaloyl chloride used was quite old and contained a solid which was insoluble in dichloromethane (presumably the carboxylic acid). This was removed by taking up in dichloromethane, filtering and taking the resulting solution to dryness under reduced pressure. The resulting white crystals were stored in a freezer until needed. Other reagents and solvents were purchased from commercial suppliers and used as received.

NMR spectra were recorded on a Bruker Avance (400 MHz) spectrometer at a constant temperature of 298 K. Chemical shifts are given in ppm and referenced to the signal of the residual protiated solvent or the ^{13}C signal of the solvents.[7] Electrospray ionisation mass spectrometry data were acquired on a Micromass Waters ZMD spectrometer.

Azides and perchlorates are potentially explosive; no issues were encountered during this work but the use of care and small reaction scales is recommended.

1.2. ^{1}H and ^{13}C NMR spectra of new compounds

Diazide 1:

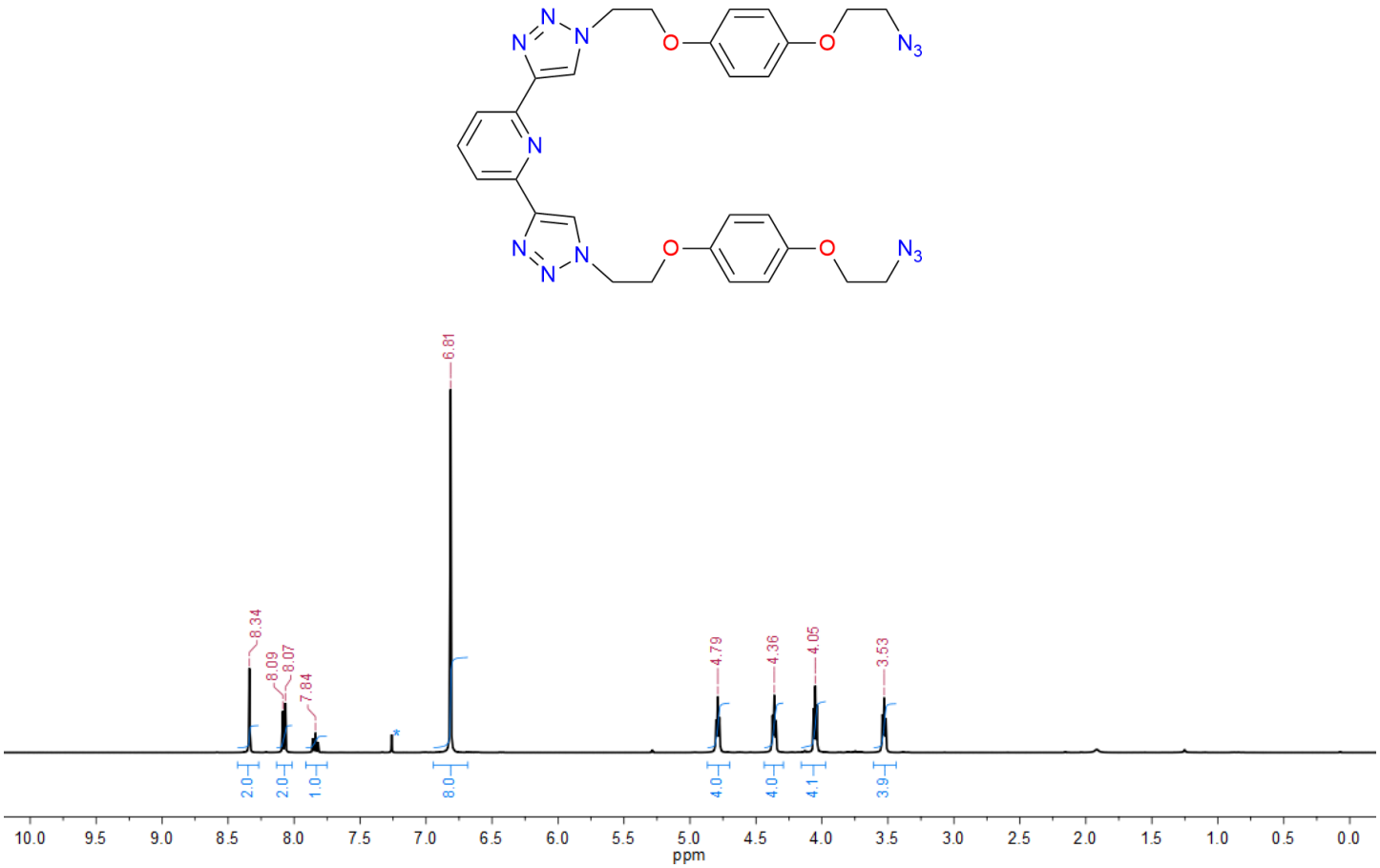

Figure S1. ^{1}H NMR spectrum of **1**, * indicates residual NMR solvent ($CDCl_3$, 400 MHz, 298 K).

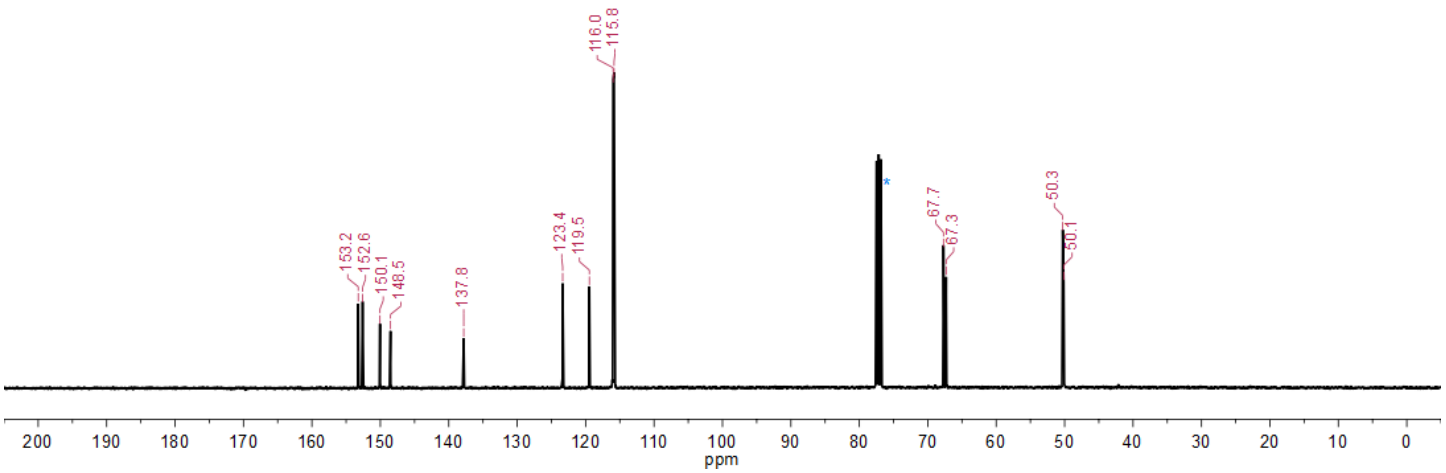

Figure S2. ^{13}C NMR spectrum of **1,** * indicates residual NMR solvent ($CDCl_3$, 101 MHz, 298 K).

TIPS-protected azide alkyne 5:

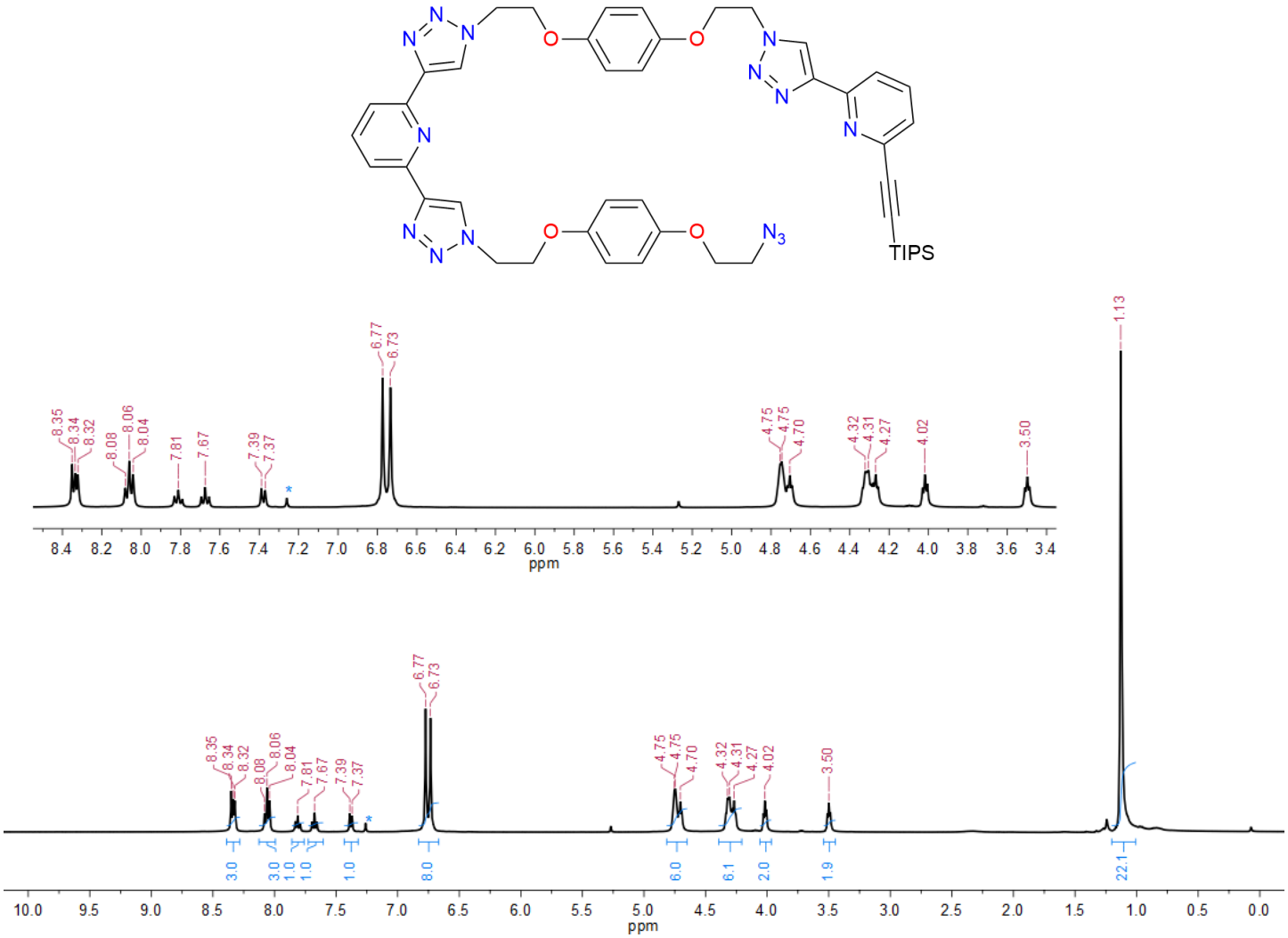

Figure S3. ^{1}H NMR spectrum of **5**, * indicates residual NMR solvent ($CDCl_3$, 400 MHz, 298 K).

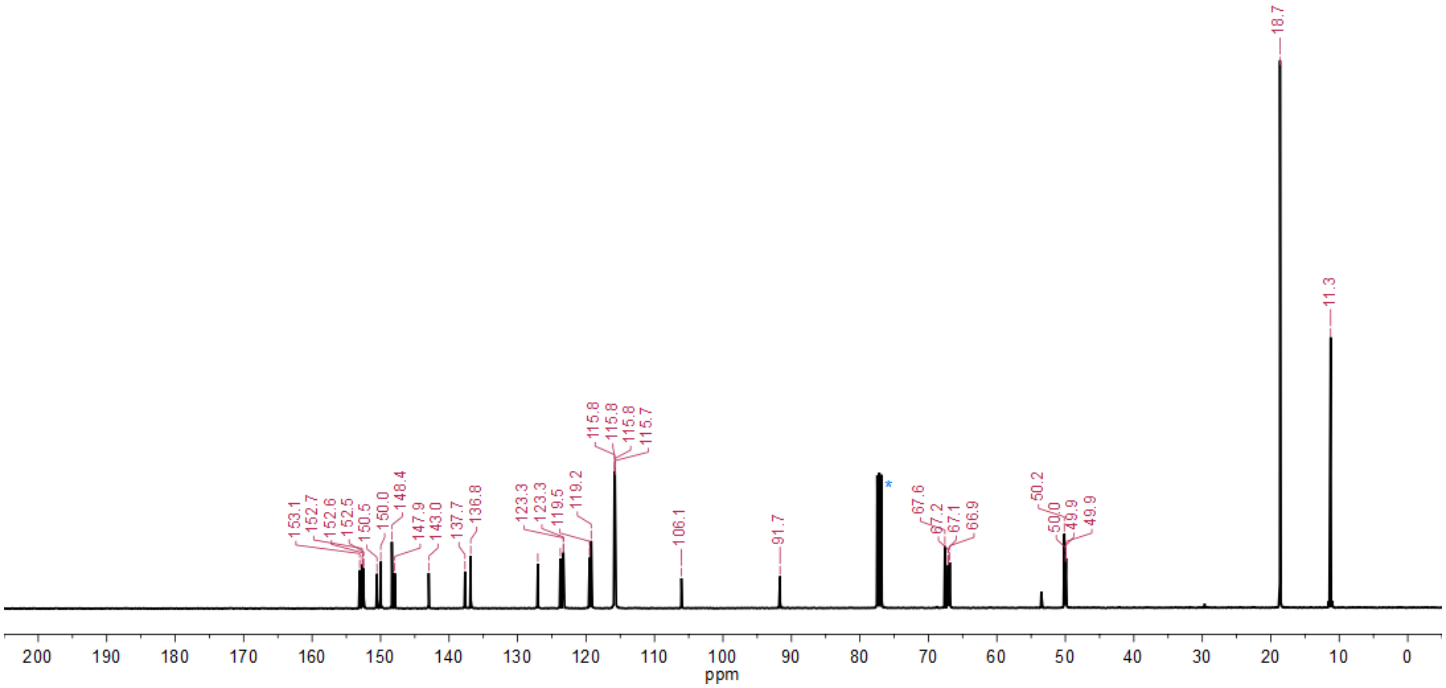

Figure S4. ^{13}C NMR spectrum of **5,** * indicates residual NMR solvent ($CDCl_3$, 101 MHz, 298 K).

Azide alkyne 6:

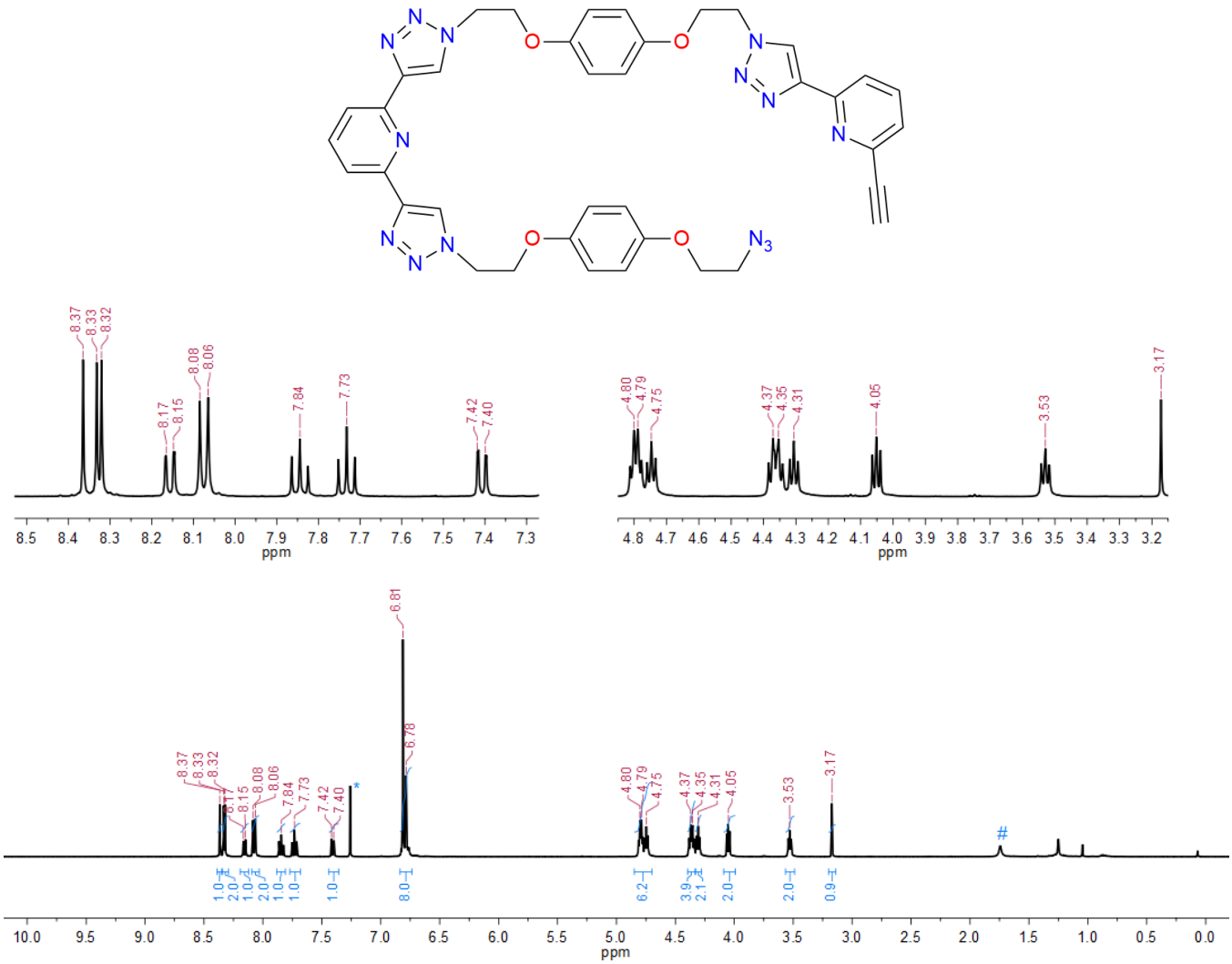

Figure S5. ^{1}H NMR spectrum of **6**, * indicates residual NMR solvent, # indicates water ($CDCl_3$, 400 MHz, 298 K).

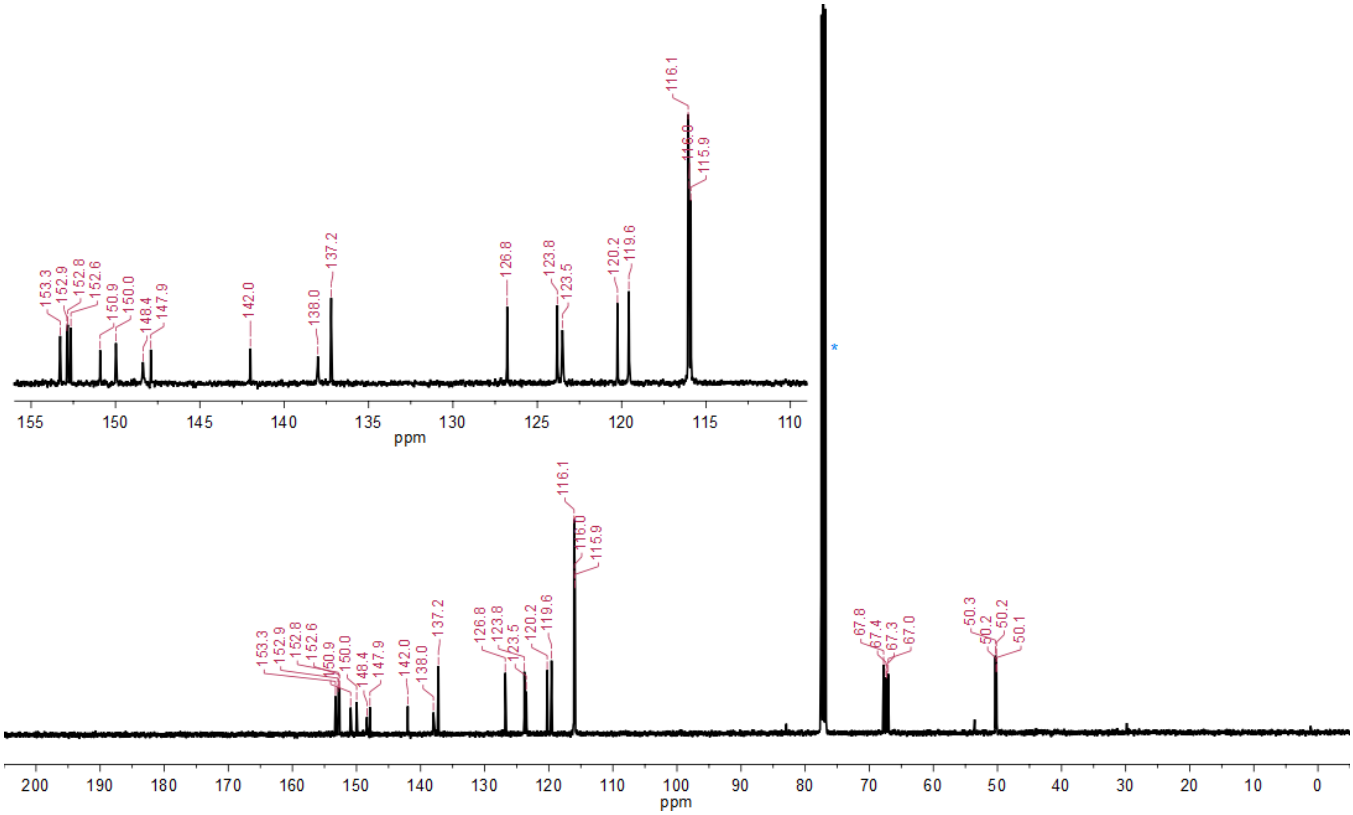

Figure S6. ^{13}C NMR spectrum of **6,** * indicates residual NMR solvent ($CDCl_3$, 101 MHz, 298 K).

Tetra-triazole macrocycle 3:

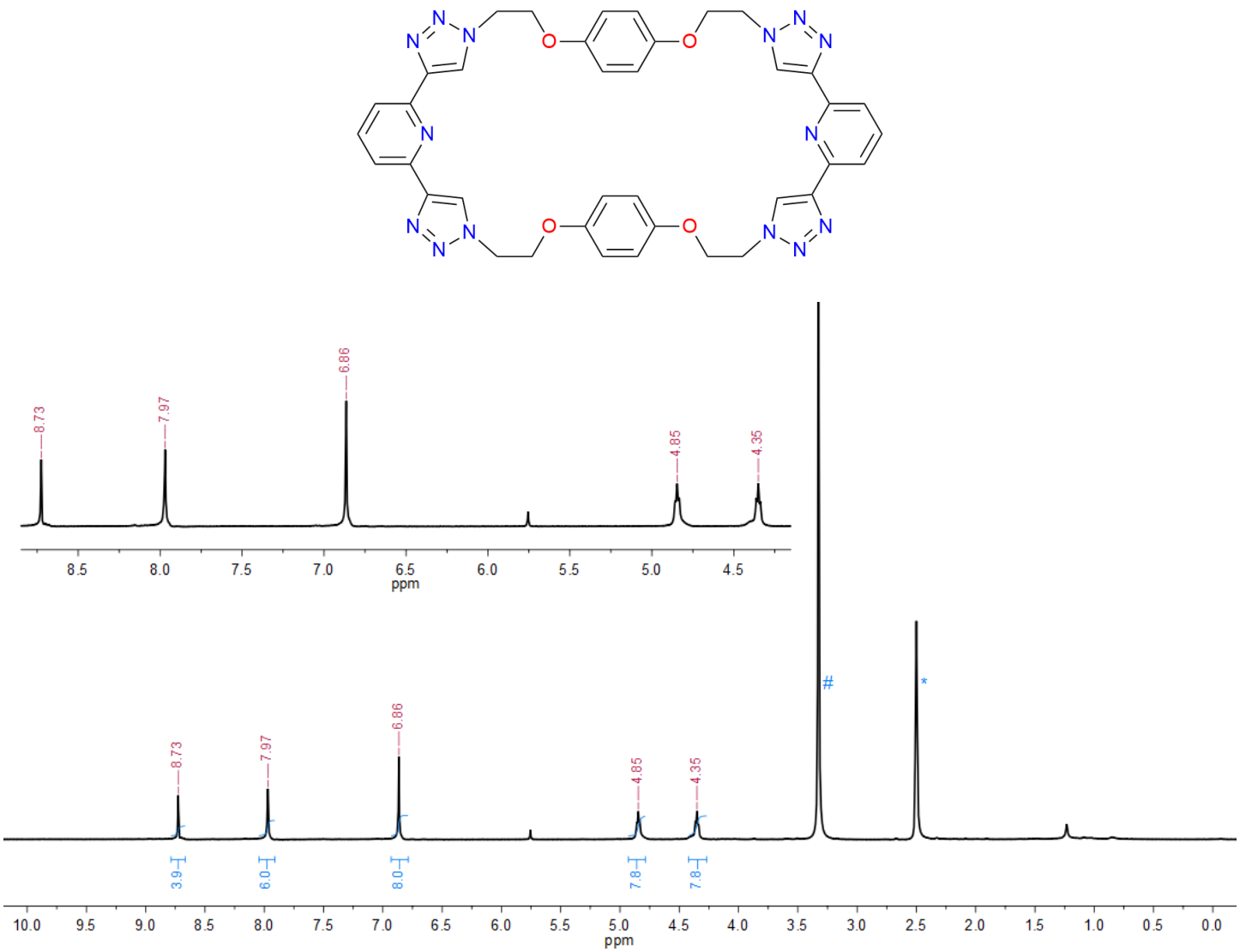

Figure S7. ^{1}H NMR spectrum of **3**, * indicates residual NMR solvent, # indicates water (d_6-DMSO, 400 MHz, 298 K).

Unfortunately, the compound was too insoluble to acquire ^{13}C NMR data (we have found that DMSO is the best solvent for this compound, but even then the solubility is < 2 mg mL^{-1}).

Diamine 7:

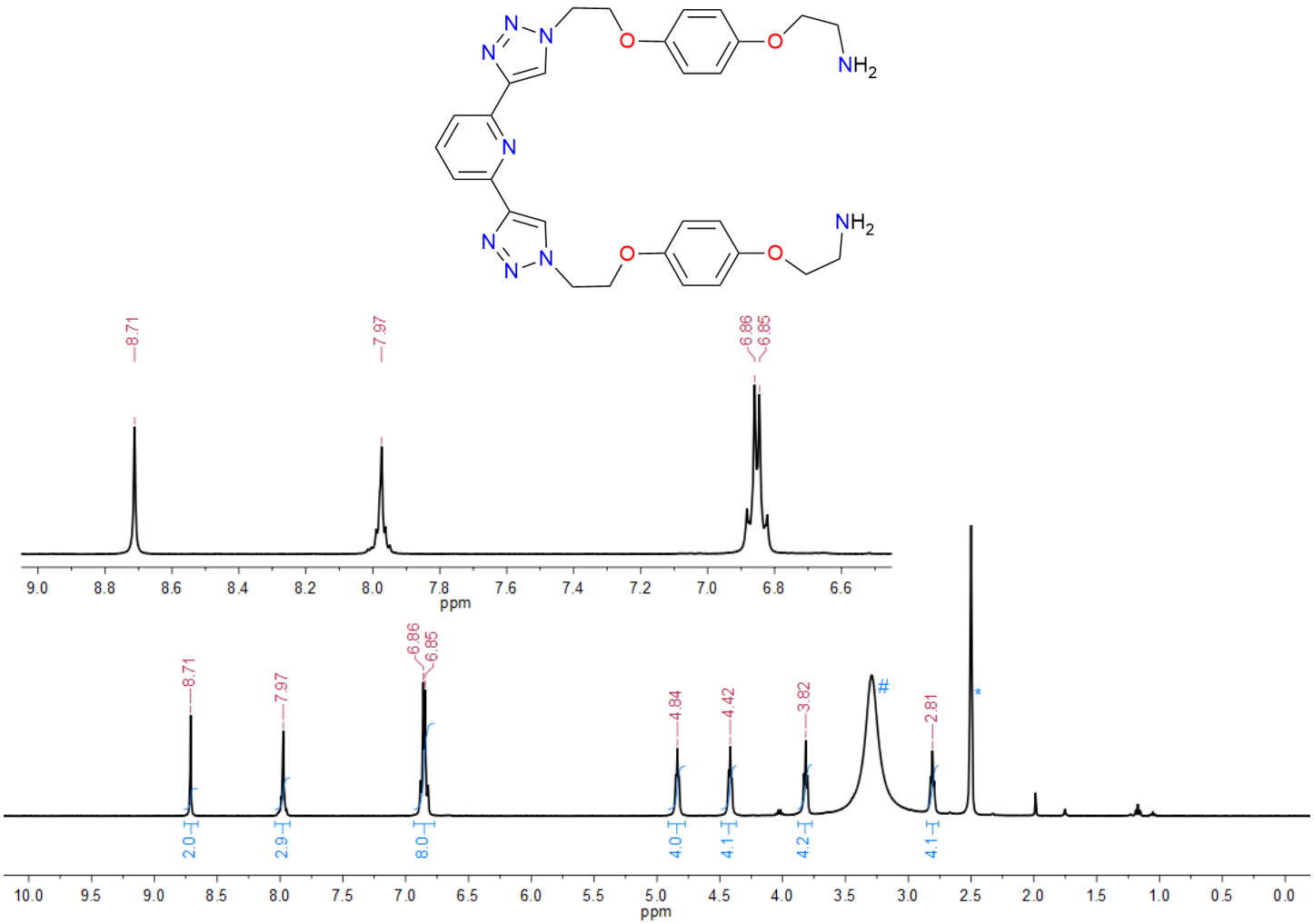

Figure S8. ^{1}H NMR spectrum of **7**, * indicates residual NMR solvent, # indicates water (d_6-DMSO, 400 MHz, 298 K).

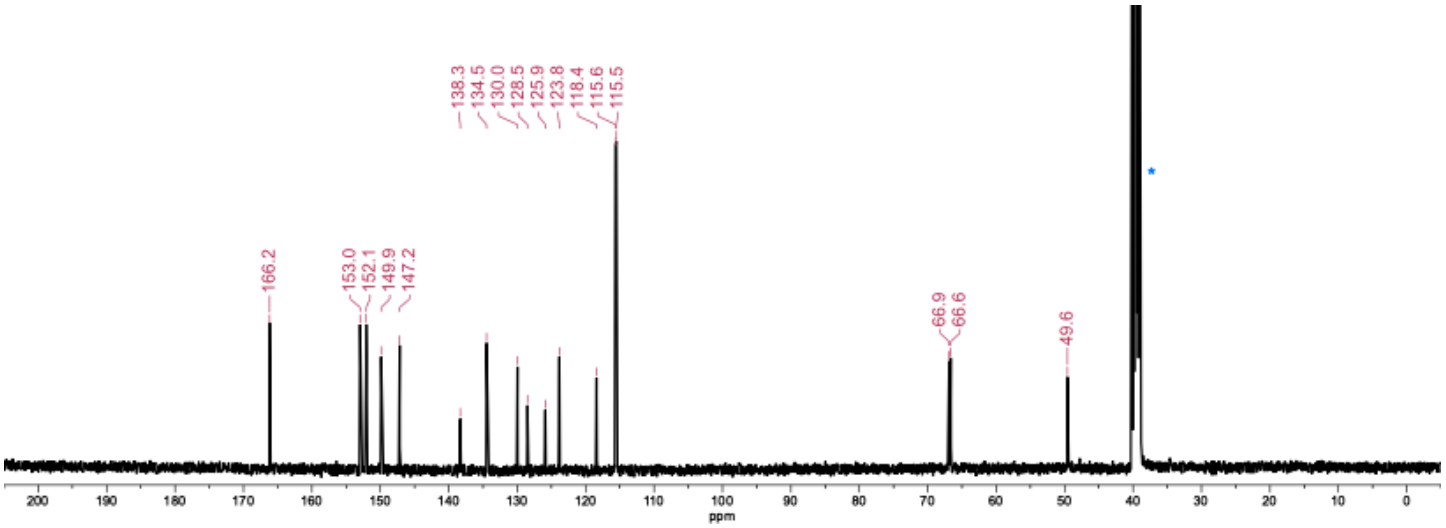

Figure S9. ^{13}C NMR spectrum of **7**, * indicates residual NMR solvent (d_6-DMSO, 101 MHz, 298 K).

Ditriazole diamide macrocycle 8:

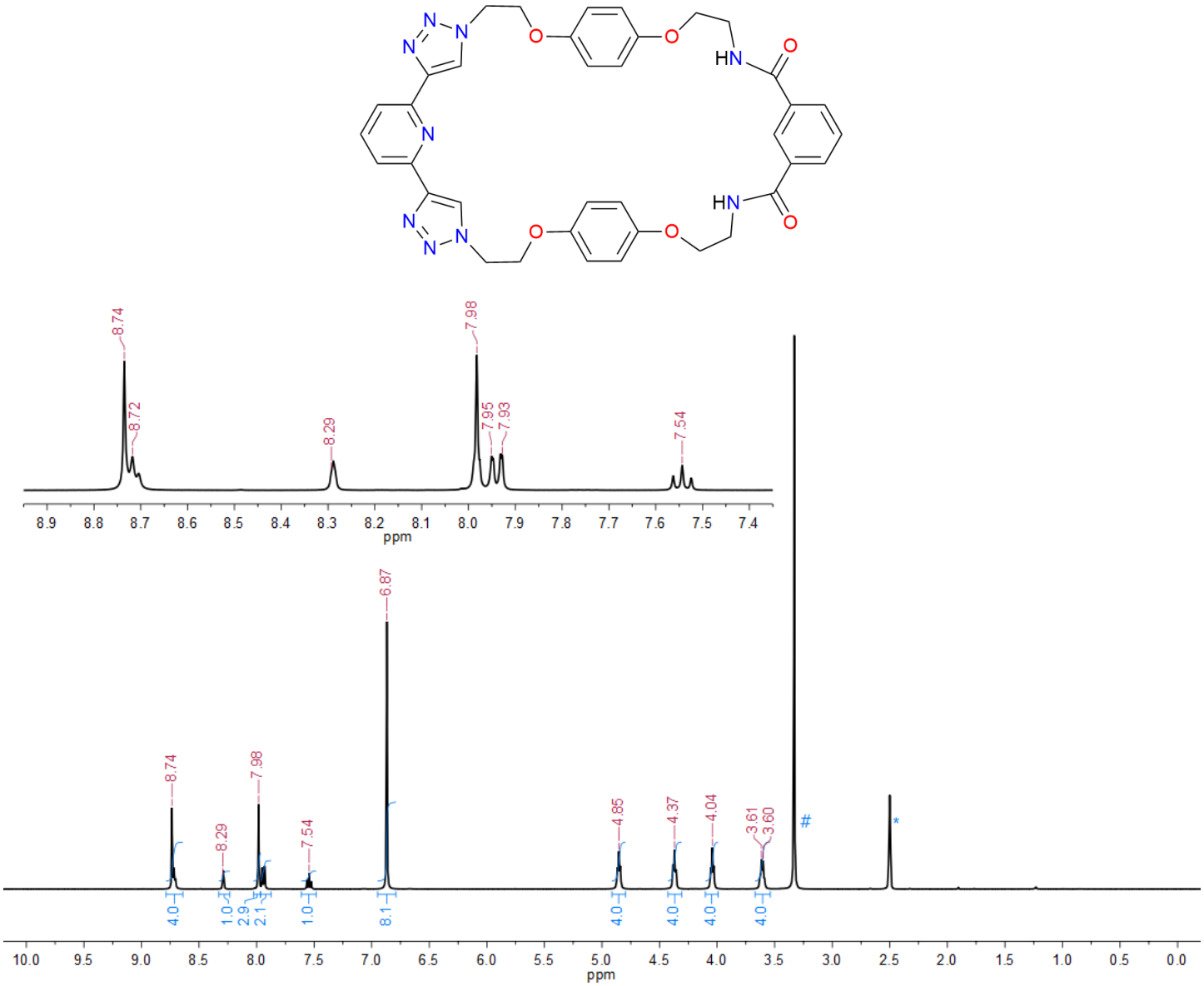

Figure S10. ^{1}H NMR spectrum of **8**, * indicates residual NMR solvent, # indicates water (d_6-DMSO, 400 MHz, 298 K).

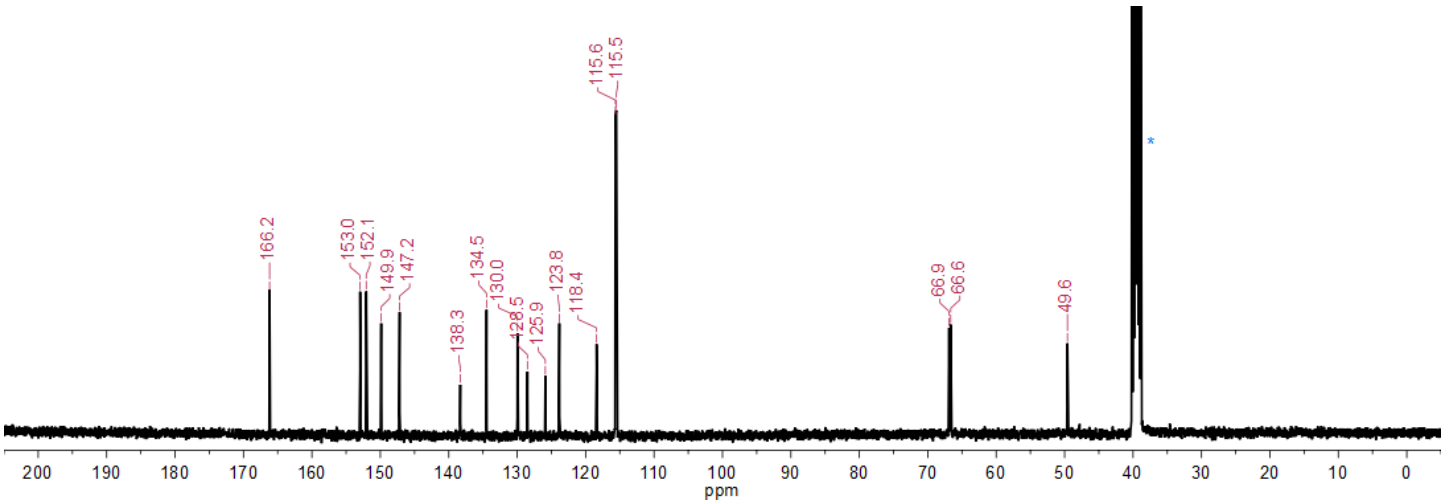

Figure S11. ^{13}C NMR spectrum of **8**, * indicates residual NMR solvent (d_6-DMSO, 101 MHz, 298 K).

Palladium(II) complex of 8, [Pd·8·MeCN](BF$_4$)$_2$:

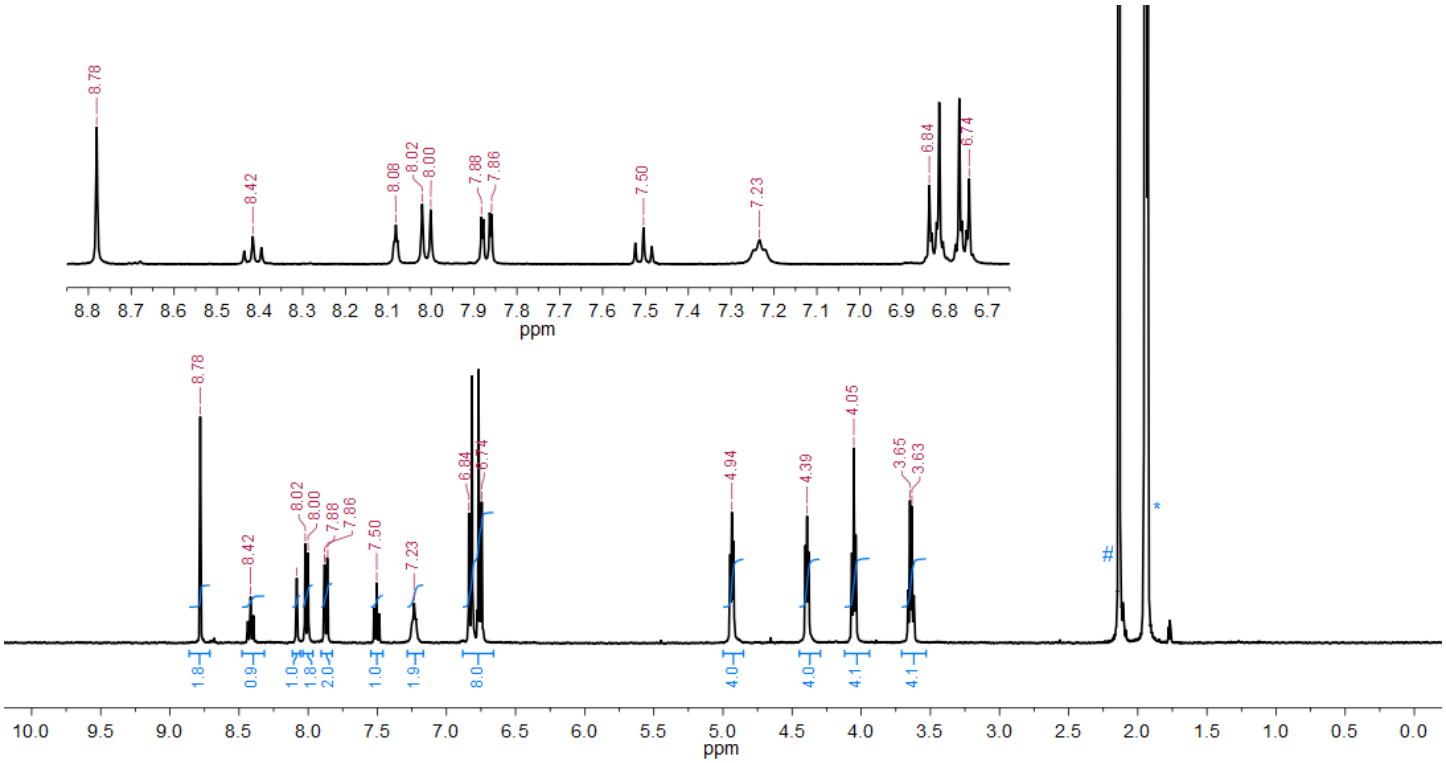

Figure S12. ^{1}H NMR spectrum of [Pd·**8**·MeCN](BF$_4$)$_2$, * indicates residual NMR solvent, # indicates water (CD$_3$CN, 400 MHz, 298 K).

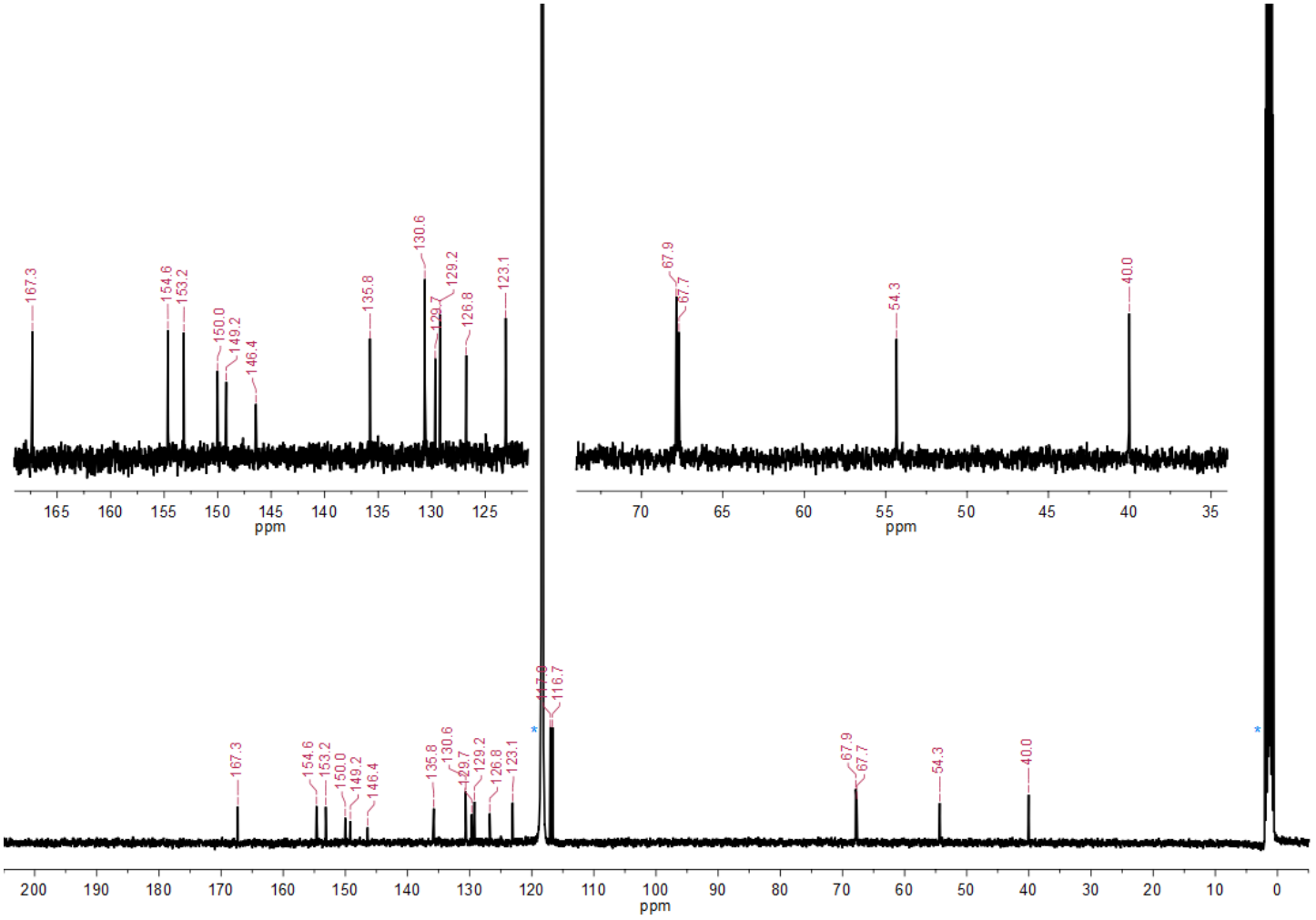

Figure S13. ^{13}C NMR spectrum of [Pd·**8**·MeCN](BF$_4$)$_2$, * indicates residual NMR solvent (CD$_3$CN, 101 MHz, 298 K).

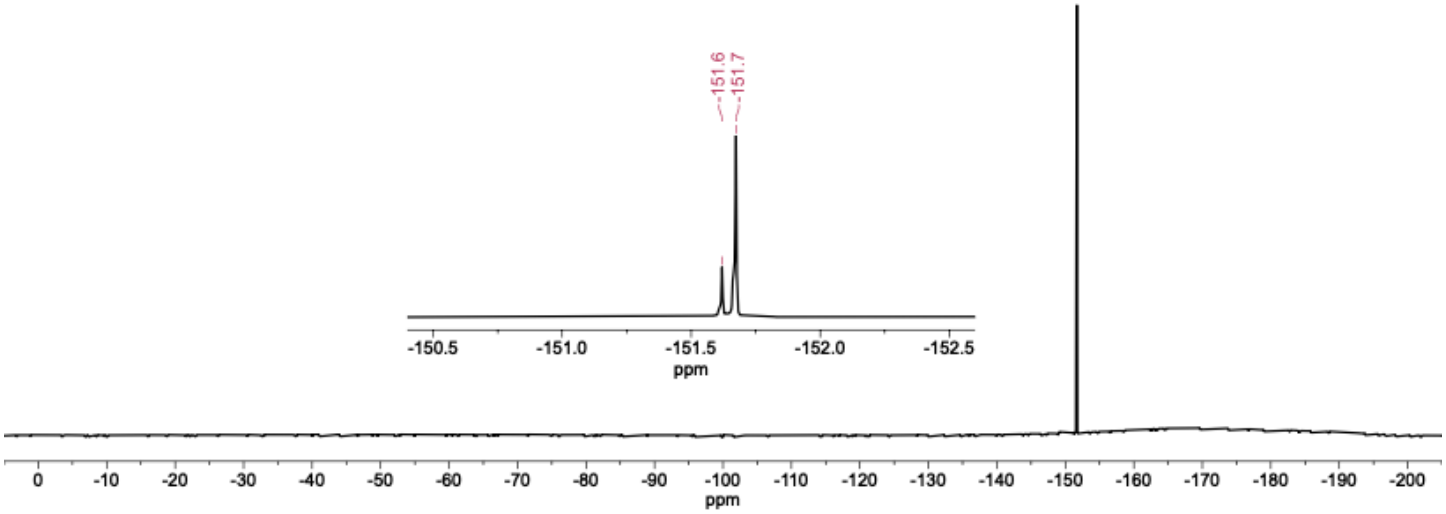

Figure S14. ^{19}F NMR spectrum of [Pd·**8**·MeCN]$(BF_4)_2$ (CD_3CN, 376 MHz, 298 K).

1.3. Synthesis and characterisation of 2 and 4

Diazide 2:

The synthesis of diazide **2** has been reported previously by Beer.[8] We have modified Beer's procedure to conduct the mesylate to azide transformation at room temperature in DMSO,[9] rather than at elevated temperatures in DMF (Scheme S1).

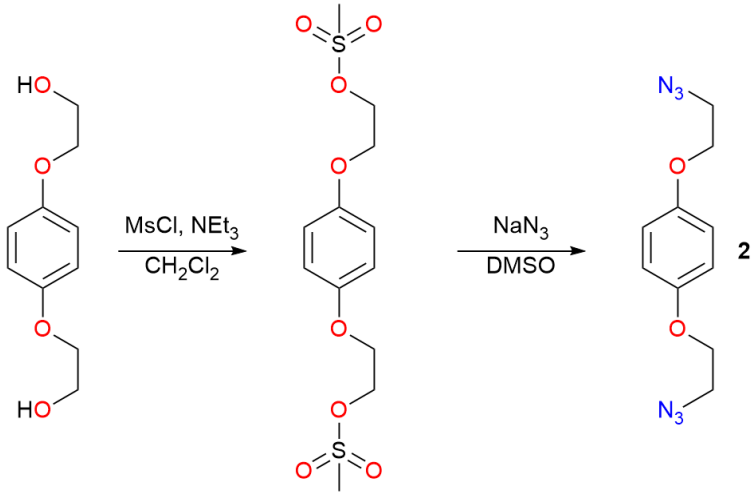

Scheme S1. Synthesis of diazide **2**.

To a degassed solution of hydroquinone bis(2-hydroxyethyl) ether (1.98 g, 10.0 mmol) in CH_2Cl_2 (4 mL) at 0 °C, were added Et_3N (4.2 mL, 3.1 g, 30 mmol) and then methanesulfonyl chloride (2.3 mL, 3.4 g, 30 mmol) dropwise. The solution was allowed to warm to room temperature and was stirred for 3 hours under a nitrogen atmosphere. It was washed with $HCl_{(aq)}$ (1.0 M, 2 × 30 mL), then brine (30 mL) and dried over anhydrous $MgSO_4$. The solvent was evaporated under reduced pressure to give the dimesylate as a colourless oil. A 1:1 mixture of ethyl acetate and toluene (40 mL) was added and this removed under reduced pressure to ensure that all traces of dichloromethane were removed, as dichloromethane can form explosive mixtures upon reaction with sodium azide[10] (used in the next step). Complete removal of dichloromethane was further checked by ^{1}H NMR spectroscopy.

^{1}H NMR ($CDCl_3$): 6.85 (s, 4H), 4.53 – 4.56 (m, 4H), 4.18 – 4.21 (m, 4H), 3.09 (s, 6H) ppm.

All of the dimesylate prepared in the previous step was dissolved in DMSO (20 mL). To this solution was added sodium azide (1.63 g, 25.0 mmol) and the suspension was stirred for 3 days at room temperature. During this time, all material dissolved and then a pale precipitate formed. Water (40 mL) was added to the resulting mixture and the aqueous layer was extracted with Et_2O (3 × 20 mL). The combined organic extracts were washed with H_2O (2 × 20 mL) and brine (20 mL) and dried over anhydrous $MgSO_4$. The solvent was removed under reduced pressure to afford **2** as a yellow oil, which solidified upon standing to give a white solid. Yield: 1.83 g (7.36 mmol, 74%). ^{1}H NMR spectroscopy indicated that this product was approximately 95% pure (Figure S15), and this was generally used in subsequent experiments without further purification.

Alternatively, the yellow oil could be taken up in methanol (~ 10 mL solvent per gram) and left to stand. This gave white crystals, which were isolated by filtration, washed with methanol and air-dried to give pure **2** (Figure S16), but in lower yields (~ 50% overall yield) due to the relatively high solubility of the product in methanol.

^{1}H NMR ($CDCl_3$): 6.87 (s, 4H), 4.11 (t, J = 5.0 Hz, 4H), 3.57 (t, J = 5.0 Hz, 4H) ppm. ^{13}C NMR ($CDCl_3$): 152.9, 115.7, 67.7, 50.2 ppm.

NMR data are consistent with literature values.[8]

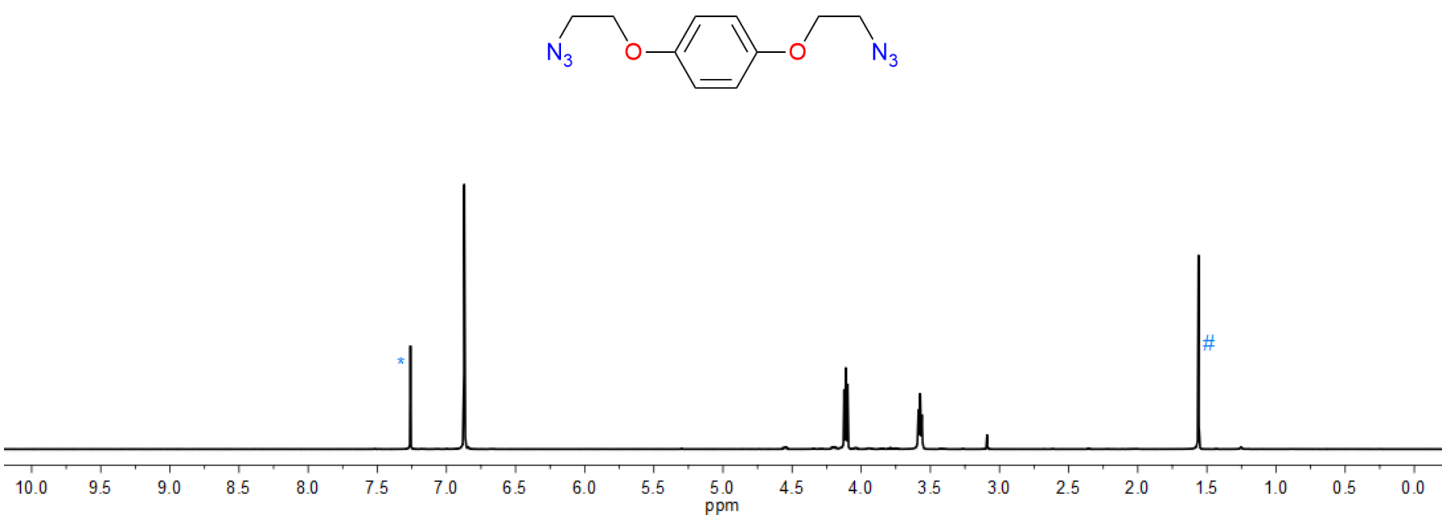

Figure S15. ^{1}H NMR spectrum of **2** without purification, * indicates residual NMR solvent, # indicates water ($CDCl_3$, 400 MHz, 298 K).

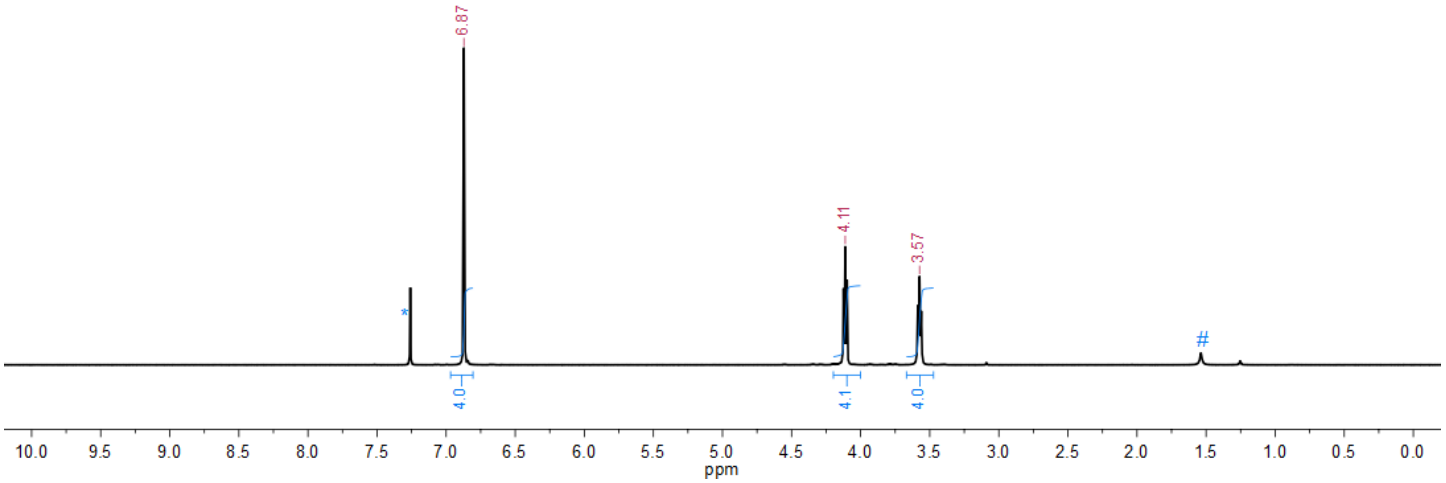

Figure S16 ^{1}H NMR spectrum of **2** after purification by crystallisation from methanol, * indicates residual NMR solvent, # indicates water ($CDCl_3$, 400 MHz, 298 K).

TIPS-protected diethynylpyridine 4:

This compound has been previously prepared by selective Sonogashira coupling of 2-bromo-6-iodopyridine with TIPS-acetylene,[11] or by reacting 2,6-dibromobenzene with one equivalent of TIPS-acetylene, then one equivalent of TMS-acetylene, followed by selective deprotection of the TMS group.[12,13] However, 2-bromo-6-iodopyridine is expensive and not easy to make, and we found purification of mixtures of TIPS-ethynyl, TMS-ethynyl and bromopyridine difficult as these columns have similar R_f values. We instead reacted 2,6-dibromopyridine statistically with dimethyl ethynyl carbinol to give dimethylcarbinol-protected 2-bromo-6-ethynylpyridine **S1**,[3] which can be purified relatively easily by column chromatography. We then reacted this with TIPS-acetylene to give **S2**, and then removed the dimethylcarbinol group to give **4** (Scheme S2).

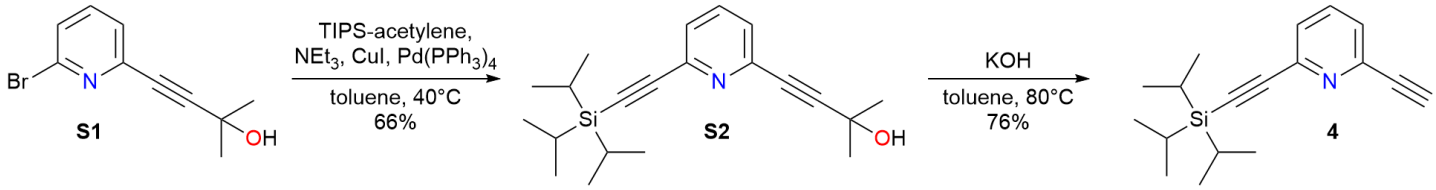

Scheme S2. Synthesis of TIPS-protected alkyne **4**.

Compound S2:

To a solution of **S1**[3] (1.5 g, 6.3 mmol) in toluene (80 mL) was added Et_3N (5.7 mL, 4.2 g, 41 mmol). The solution was deoxygenated for 10 min with bubbling N_2 and then triisopropylsilylacetylene (2.8 mL, 13 mmol), CuI (0.12 g, 0.64 mmol) and $Pd(PPh_3)_4$ (0.36 g, 0.31 mmol) were added. The resulting solution was stirred for 16 hours at 40 °C under a nitrogen atmosphere. The solvent was removed under reduced pressure and the solid was dissolved in CH_2Cl_2 (150 mL). An aqueous solution of EDTA and NH_3 (0.05 M EDTA, 1 M NH_3, 60 mL) was added and the mixture was stirred for 10 min. The layers were separated and the organic phase was dried over anhydrous $MgSO_4$. The solvent was removed and the crude material was purified by column chromatography (eluent: 9:1 pet. spirits:EtOAc) to yield **S2** as an orange solid. Yield: 1.4 g (4.2 mmol, 66%).

^{1}H NMR (400 MHz, $CDCl_3$): 7.60 (t, *J* = 7.8 Hz, 1H), 7.40 (dd, *J* = 7.8, 1.1 Hz, 1H), 7.35 (dd, *J* = 7.8, 1.1 Hz, 1H), 1.63 (s, 6H), 1.13 – 1.15 (m, 21H) ppm. ^{13}C NMR (101 MHz, $CDCl_3$): 143.8, 143.3, 136.3, 127.3, 126.5, 105.4, 94.3, 92.7, 81.4, 65.6, 31.3, 18.8, 11.4 ppm. ESI-MS (pos.): 342.3, calc. for $[C_{21}H_{31}NOSi{\cdot}H]^+$ = 342.2 Da.

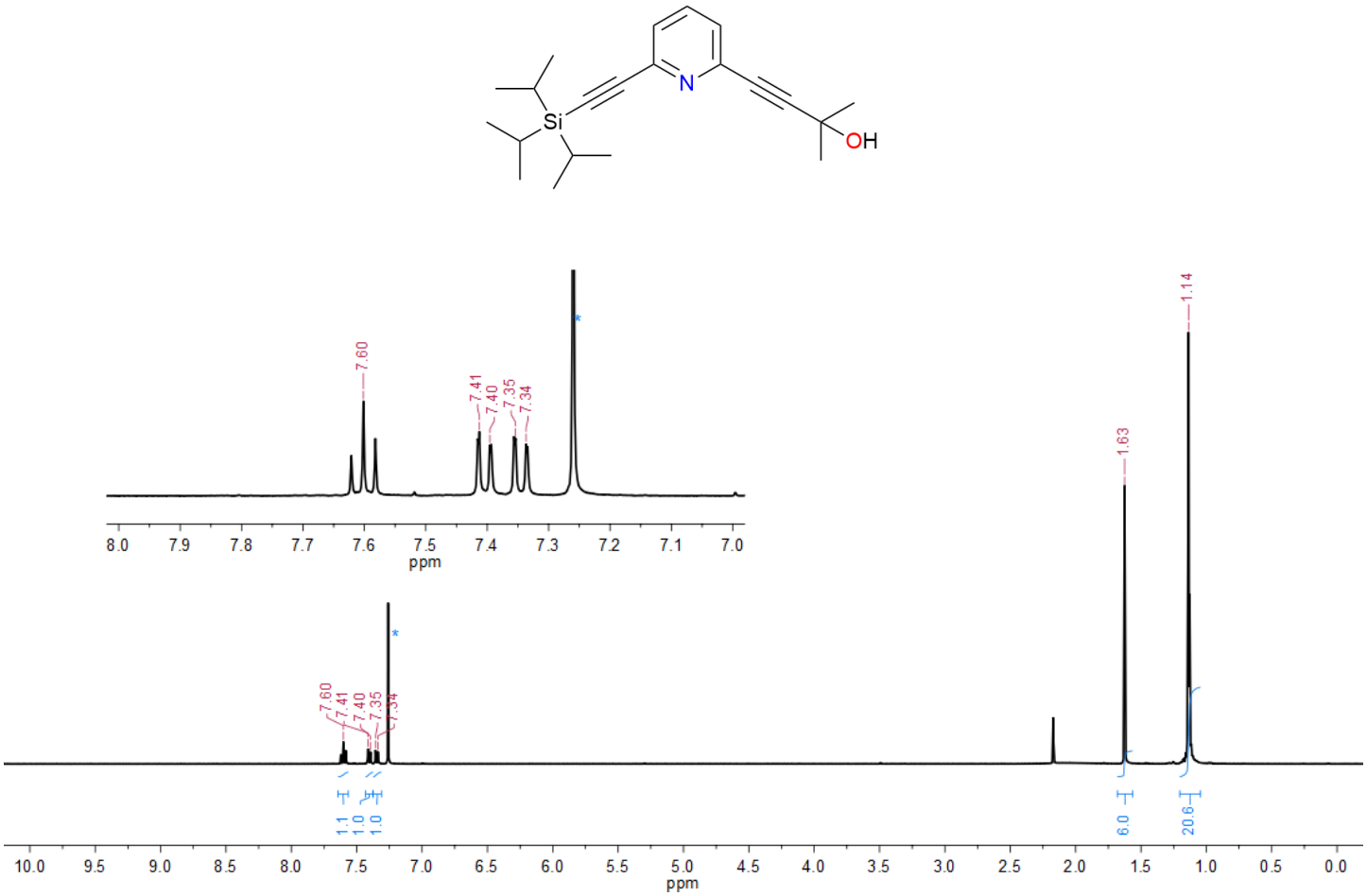

Figure S17. ^{1}H NMR spectrum of **S2**, * indicates residual NMR solvent ($CDCl_3$, 400 MHz, 298 K).

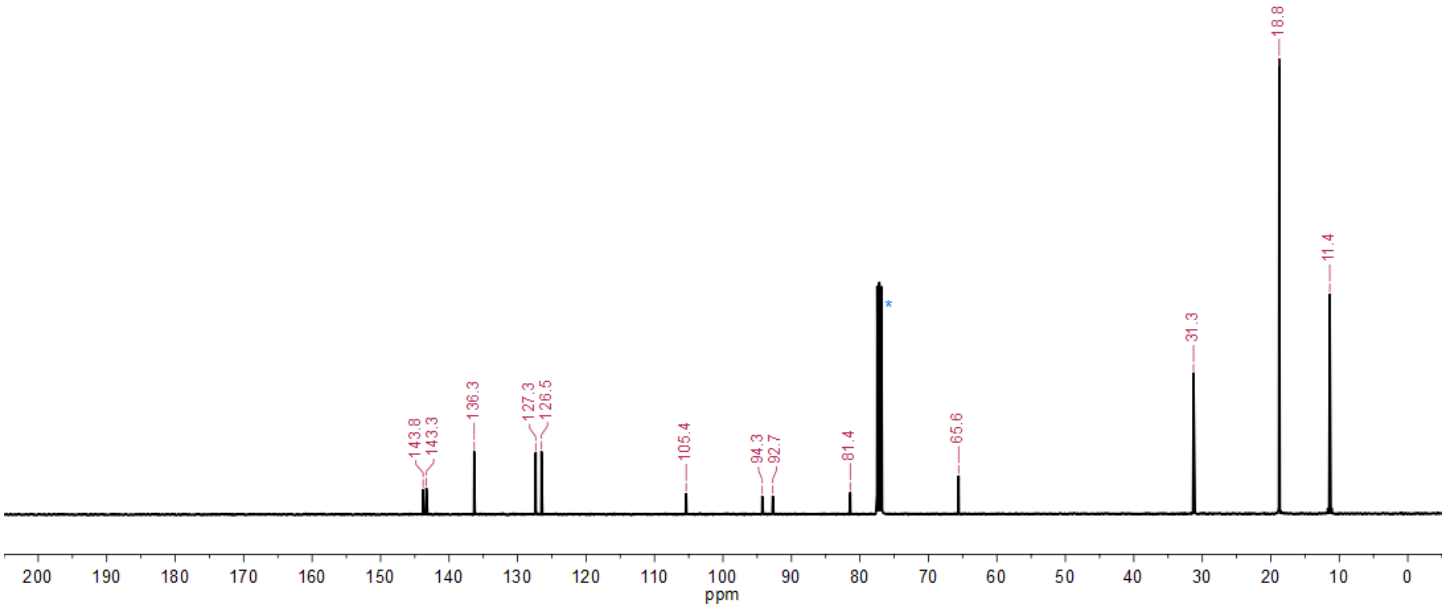

Figure S18. ^{13}C NMR spectrum of **S2,** * indicates residual NMR solvent ($CDCl_3$, 101 MHz, 298 K).

TIPS-protected diethynylpyridine 4:

To a deoxygenated solution of **S2** (97 mg, 0.29 mmol) in dry toluene (20 mL) was added KOH (87 mg, 1.6 mmol). The solution was stirred at 80 °C for 19 hours under a nitrogen atmosphere. The reaction was then taken to dryness under reduced pressure. The resulting solid was dissolved in CH_2Cl_2 (30 mL) and washed with water (2 × 30 mL). The organic layer was dried over anhydrous $MgSO_4$ and the solvent was evaporated under vacuum. The crude material was purified by column chromatography (eluent: 98:2 pet. spirits:EtOAc) to give **4** as a yellow oil. Yield: 63 mg (0.22 mmol, 76%).

^{1}H NMR (400 MHz, $CDCl_3$): 7.61 (t, *J* = 7.8 Hz, 1H), 7.43 (dd, *J* = 7.8, 1.1 Hz, 1H), 7.40 (dd, *J* = 7.8, 1.1 Hz, 1H), 3.15 (s, 1H), 1.12 – 1.14 (m, 21H) ppm. ^{13}C NMR (101 MHz, $CDCl_3$): 143.9, 142.6, 136.4, 127.8, 126.7, 105.3, 92.7, 82.5, 77.7, 18.8, 11.4 ppm. ESI-MS (pos.): 284.2, calc. for $[C_{18}H_{25}NSi{\cdot}H]^+$ = 284.2 Da.

NMR data are consistent with those previously reported.[11]

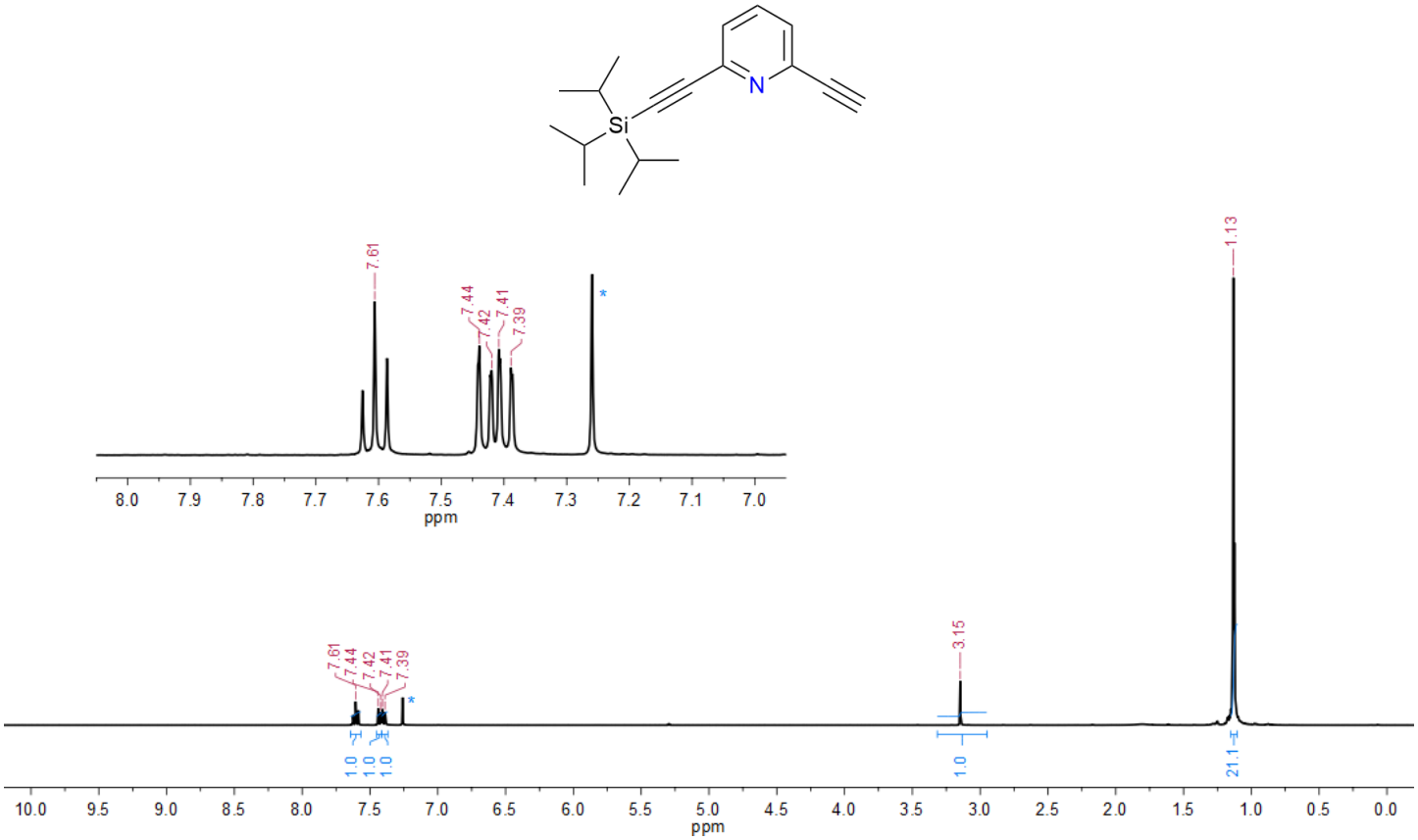

Figure S19. ^{1}H NMR spectrum of **4**, * indicates residual NMR solvent ($CDCl_3$, 400 MHz, 298 K).

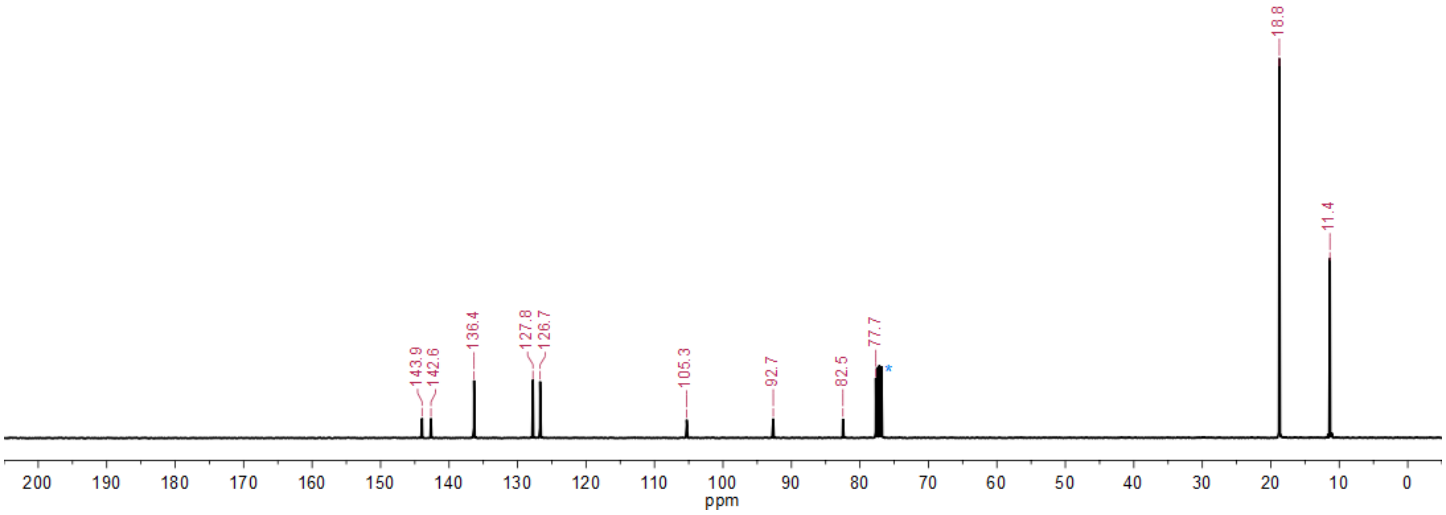

Figure S20. ^{13}C NMR spectrum of **4, *** indicates residual NMR solvent ($CDCl_3$, 101 MHz, 298 K).

1.4. Alternative methods for the preparation of tetra-triazole macrocycle 3

From diazide 1: Diazide **1** (62 mg, 0.10 mmol), 2,6-diethynylpyridine (13 mg, 0.10 mmol), TBTA (5.3 mg, 0.010 mmol) and $[Cu(CH_3CN)_4]BF_4$ (3.1 mg, 0.010 mmol) were placed in a flask. Dichloromethane (200 mL) was added, followed by diisopropylethylamine (17 µL, 13 mg, 0.10 mmol) and the resulting bright yellow solution was stirred at room temperature under a nitrogen atmosphere for 7 days. After this time, a solution containing EDTA (29 mg, 0.10 mmol) and $NH_{3(aq)}$ (26%, 5 mL) in water (100 mL) was added and the biphasic mixture stirred vigorously for one hour. The organic layer was taken, dried ($MgSO_4$), and taken to dryness under reduced pressure. The resulting pale yellow solid was dissolved in hot DMF (2 mL) and cooled to room temperature resulting in the formation of white crystals. These were isolated by filtration, washed with DMF (2 × 1 mL), diethyl ether (3 × 2 mL) and thoroughly air-dried. This gave 20 mg (24%) of macrocycle **3**·DMF, which was approximately 90% pure according to ^{1}H NMR spectroscopy.

A clean sample was obtained by a second recrystallization from hot DMF: a sample of ~90% pure macrocycle (9.7 mg) was dissolved in hot DMF (1 mL), then cooled to room temperature resulting in the formation of white crystals. These were isolated by filtration, washed with DMF (0.5 mL) and thoroughly air dried. Yield: 6.9 mg (70% for this recrystallization, 17% from diazide **1**).

*Spectroscopic data matched those of **3** prepared from **6**, except that a small amount of residual DMF was present in the ^{1}H NMR spectrum (Figure S21). This DMF could not be removed even with extensive drying in vacuo.*

From diazide 2: Diazide **2** (99 mg, 0.40 mmol), 2,6-diethynylpyridine (51 mg, 0.40 mmol), TBTA (21 mg, 0.040 mmol) and $[Cu(CH_3CN)_4]BF_4$ (13 mg, 0.040 mmol) were placed in a flask. Dichloromethane (400 mL) was added, followed by diisopropylethylamine (70 µL, 52 mg, 0.40 mmol) and the resulting bright yellow solution was stirred at room temperature under a nitrogen atmosphere for 7 days. After this time, a solution containing EDTA (58 mg, 0.20 mmol) and $NH_{3(aq)}$ (26%, 10 mL) in water (100 mL) was added and the biphasic mixture stirred vigorously for one hour. The organic layer was taken, dried ($MgSO_4$) and taken to dryness under reduced pressure. The resulting pale yellow solid was dissolved in hot DMF (2 mL) and cooled to room temperature resulting in the formation of white crystals. These were isolated by filtration, washed with DMF (2 × 0.5 mL) and thoroughly air-dried to give **3**. Yield: 5.3 mg (3.2%).

*Spectroscopic data matched those of **3** prepared from **6**, except that a small amount of residual DMF was present in the ^{1}H NMR spectrum. This DMF could not be removed even with extensive drying in vacuo.*

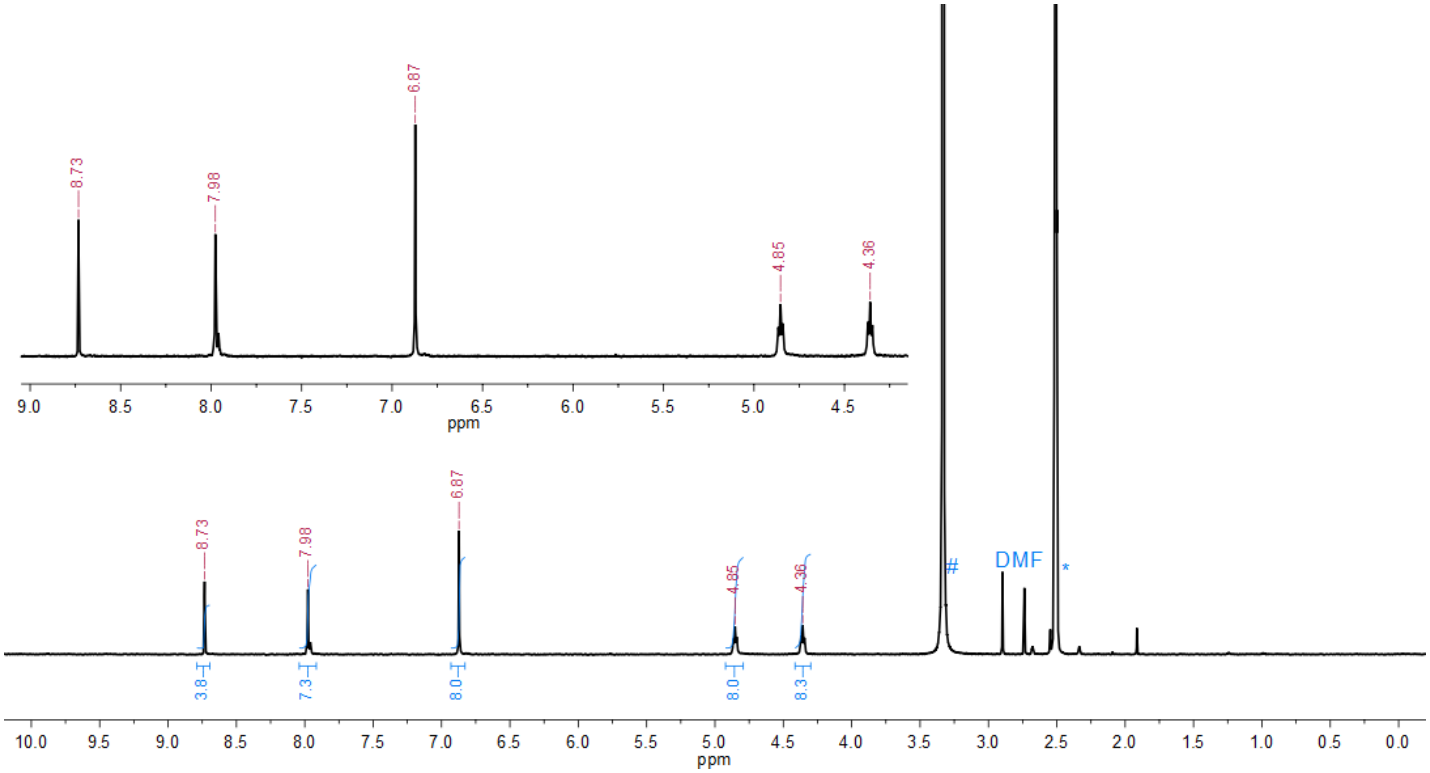

Figure S21. ^{1}H NMR spectrum of **3** prepared from **1**, * indicates residual NMR solvent, # indicates water; the peak at 7.98 ppm integrates to a higher than expected value due to overlap with DMF that could not be removed even after extensive drying (d_6-DMSO, 400 MHz, 298 K).

2. ^{1}H NMR studies of metal and anion complexation

2.1 Complexation of btp diazide 1 with Zn^{2+}

We studied the complexation of **btp** diazide **1** with $[Zn(OH_2)_6](ClO_4)_2$ using ^{1}H NMR spectroscopy. Studies were conducted in CD_3CN, d_6-DMSO, and 1:1 $CDCl_3$:CD_3OD. A 2.0 mM solution of **1** was prepared and aliquots of a 100 mM solution of $[Zn(OH_2)_6](ClO_4)_2$ were added and the complexations monitored by ^{1}H NMR spectroscopy. As discussed in the main text of the manuscript, in CD_3CN (Figure S22) and 1:1 $CDCl_3$:CD_3OD (Figure S23) it appears that an initial ML_2 species forms, which is eventually replaced by a ML complex when more metal ion is added. In d_6-DMSO, negligible complexation is observed (Figure S24).

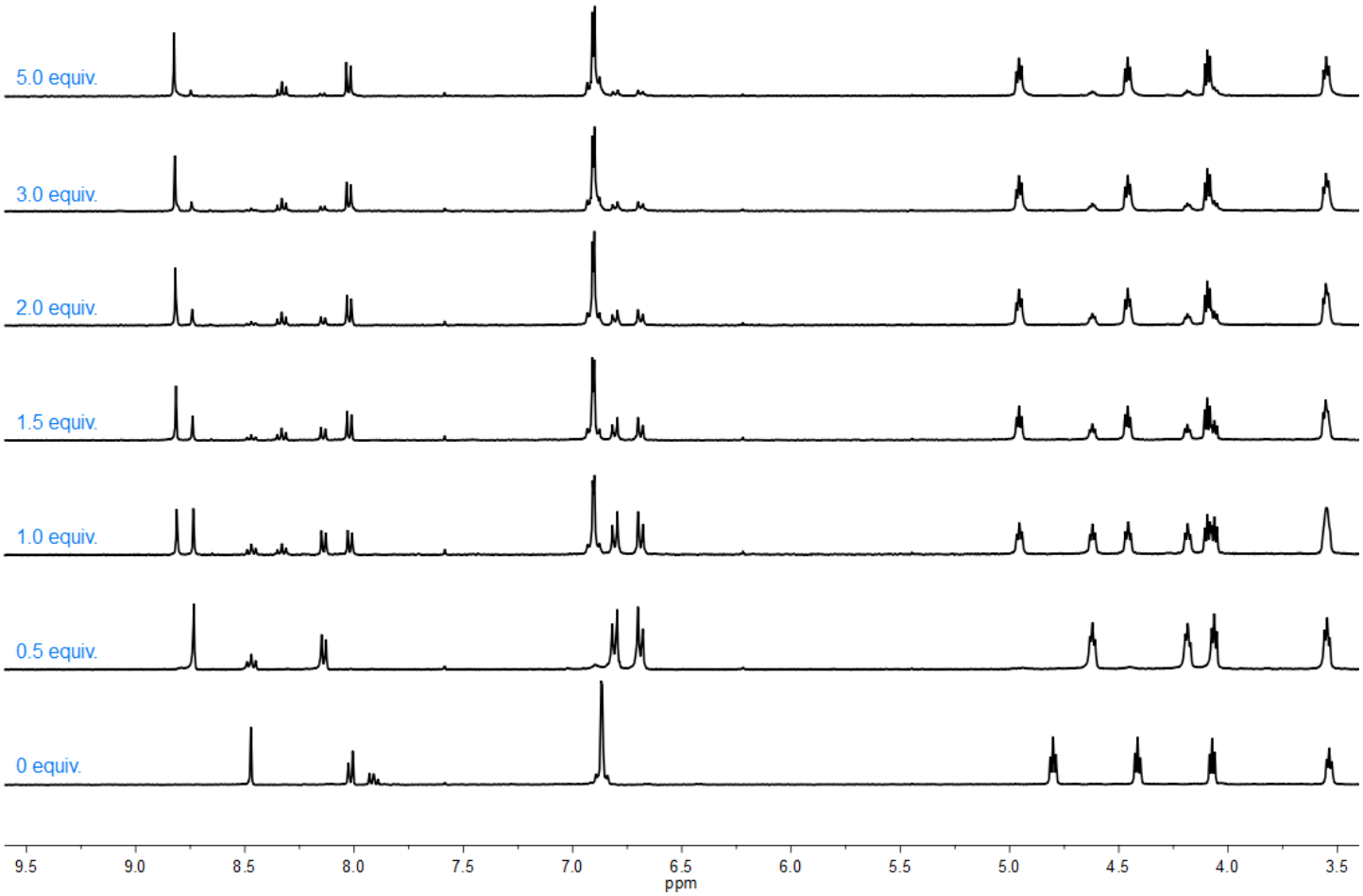

Figure S22. Partial ^{1}H NMR spectra of **1** on addition of $[Zn(OH_2)_6](ClO_4)_2$ in CD_3CN (400 MHz, 298 K). Note: a partial version of this figure is shown in the main text of the manuscript.

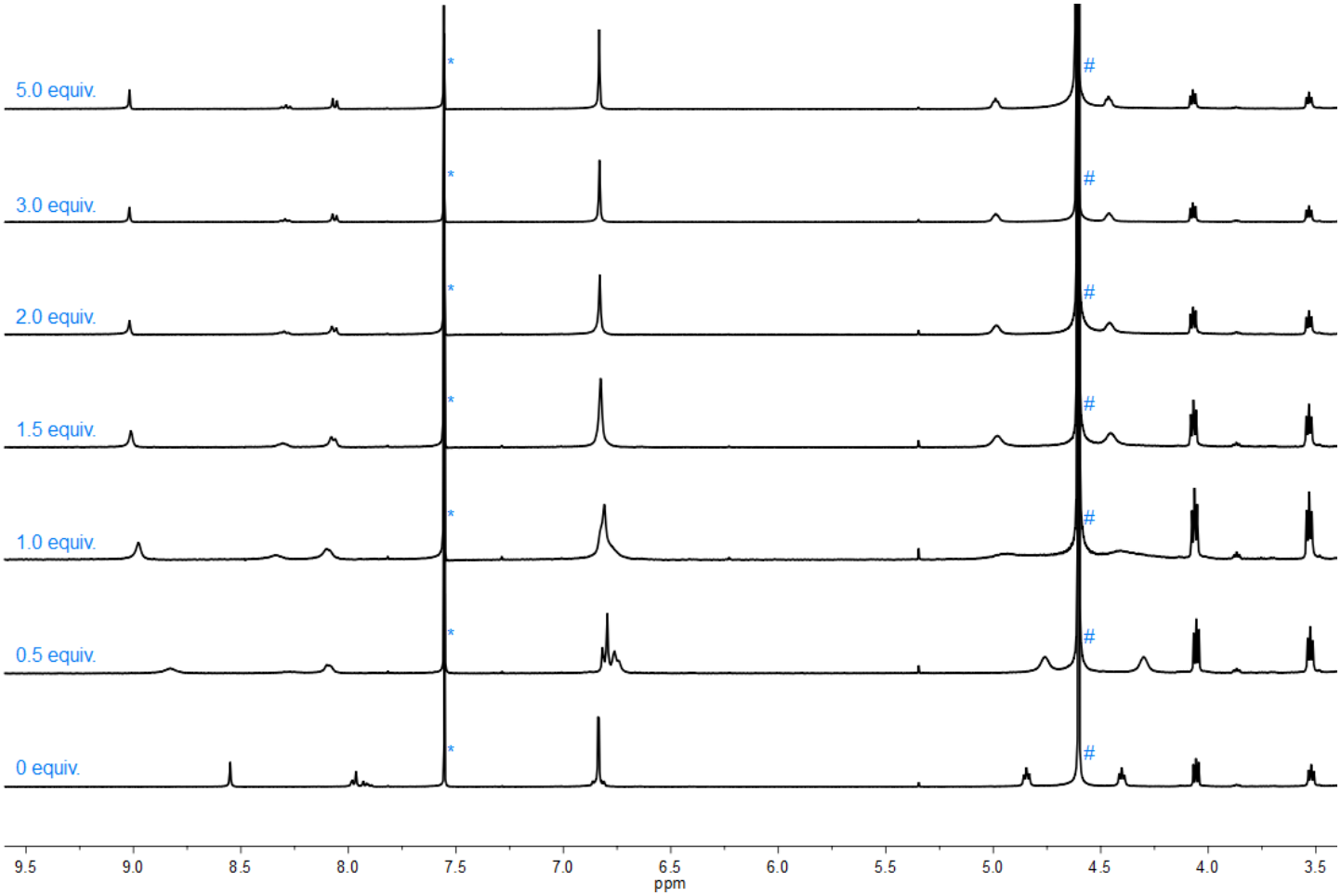

Figure S23. Partial ^{1}H NMR spectra of **1** on addition of $[Zn(OH_2)_6](ClO_4)_2$ in 1:1 $CDCl_3$:CD_3OD, * indicates residual NMR solvent peak, # indicates water (400 MHz, 298 K).

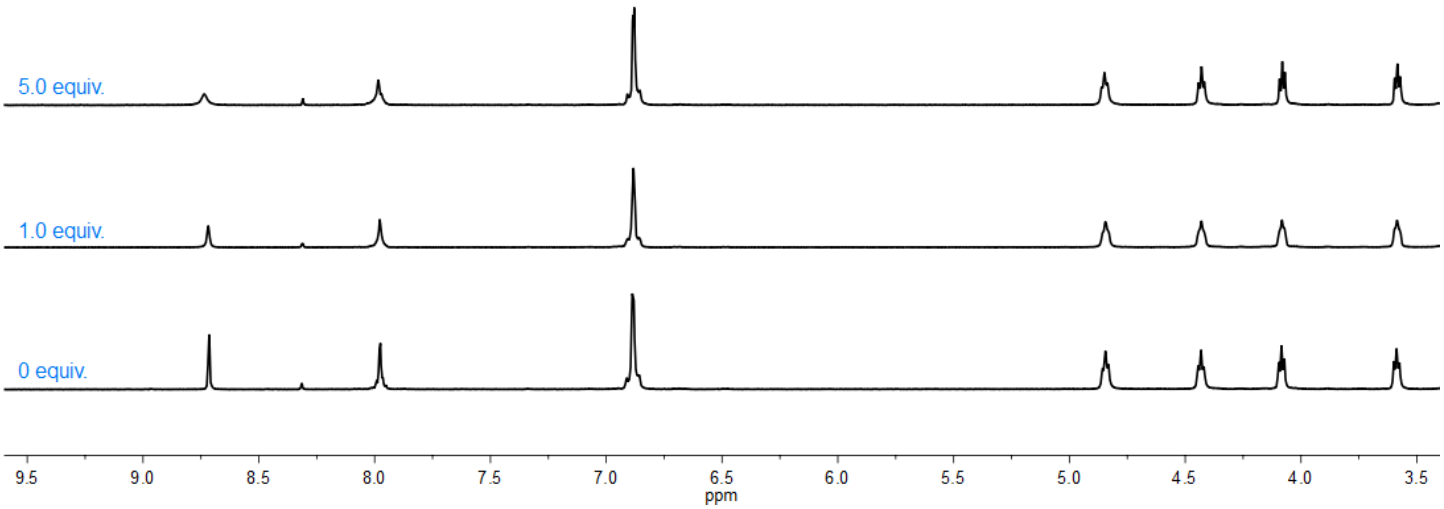

Figure S24. Partial ^{1}H NMR spectra of **1** on addition of $[Zn(OH_2)_6](ClO_4)_2$ in d_6-DMSO (400 MHz, 298 K).

2.2 Complexation of macrocycle 8 with Zn^{2+}

We studied the complexation of **btp** macrocycle **8** with $[Zn(OH_2)_6](ClO_4)_2$ using ^{1}H NMR spectroscopy. Studies were conducted in d_6-DMSO, and 1:1 $CDCl_3$:CD_3OD (the macrocycle does not have sufficient solubility in CD_3CN to conduct studies at the same concentration used for other metal complexation studies, *i.e.* 2.0 mM). A 2.0 mM solution of **8** was prepared and aliquots of a 100 mM solution of $[Zn(OH_2)_6](ClO_4)_2$ were added and the complexations monitored by ^{1}H NMR spectroscopy. As discussed in the main text of the manuscript, in 1:1 $CDCl_3$:CD_3OD (Figure S25) it appears that a species in fast exchange with the free macrocycle forms, as well as a trace of a minor by-product in slow exchange on the ^{1}H NMR timescale. In d_6-DMSO, negligible complexation is observed (Figure S26).

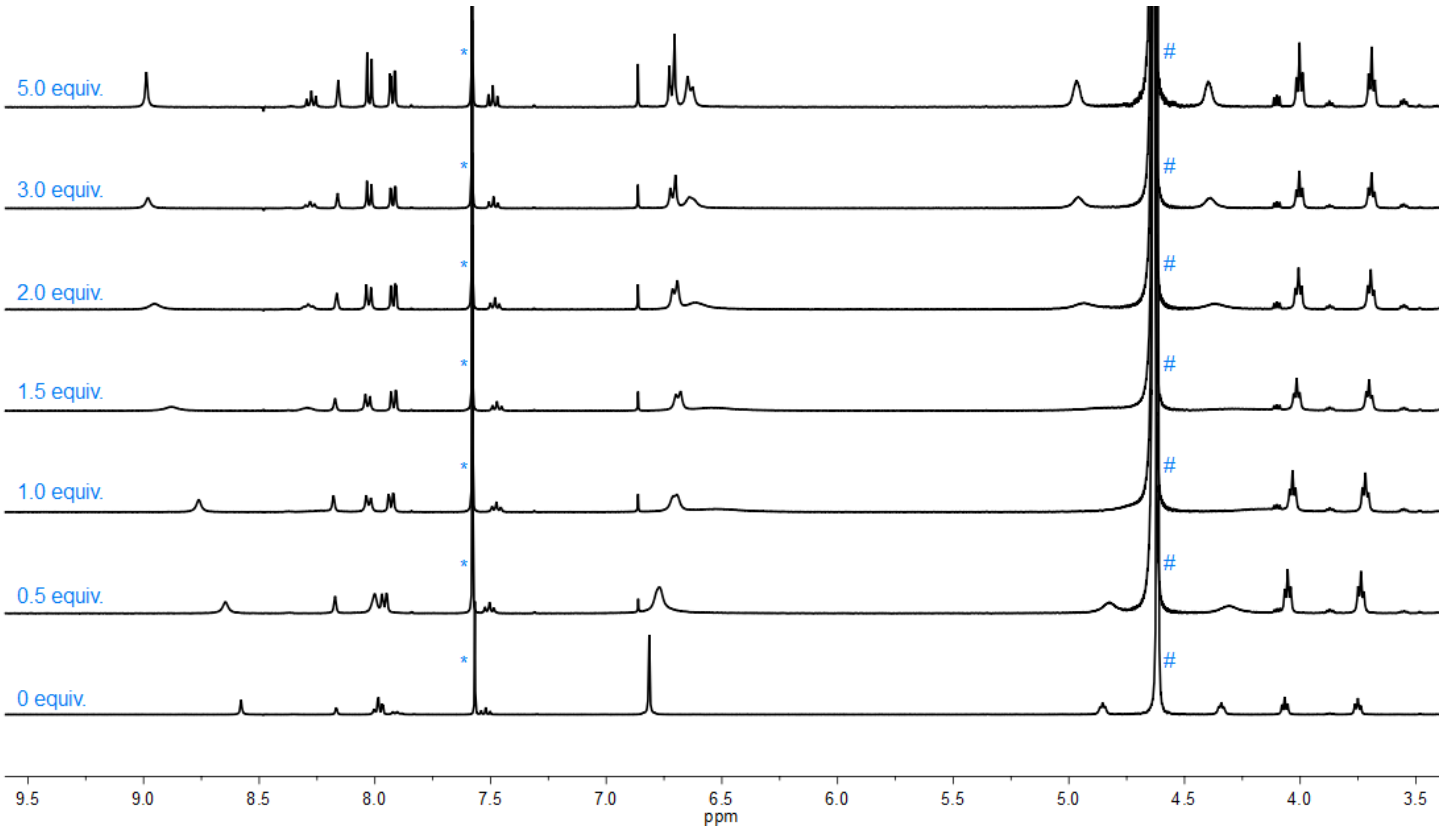

Figure S25. Partial ^{1}H NMR spectra of **8** on addition of $[Zn(OH_2)_6](ClO_4)_2$ in 1:1 $CDCl_3$:CD_3OD, * indicates residual NMR solvent peak, # indicates water (400 MHz, 298 K).

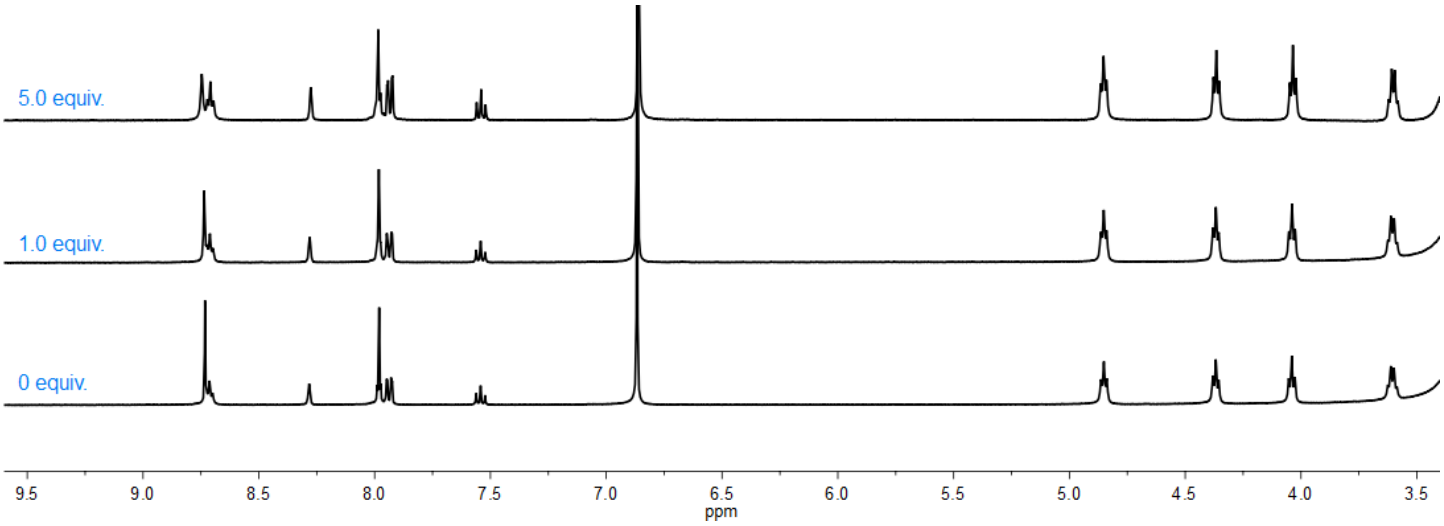

Figure S26. Partial ^{1}H NMR spectra of **8** on addition of $[Zn(OH_2)_6](ClO_4)_2$ in d_6-DMSO (400 MHz, 298 K).

2.3 Complexation of ditriazole diamide macrocycle 8 with Pd^{2+}

We studied the complexation of **btp** macrocycle **8** with $[Pd(CH_3CN)_4](BF_4)_2$ using ^1H NMR spectroscopy. Studies were conducted in d_6-DMSO, and 1:1 $CDCl_3$:CD_3OD (the macrocycle does not have sufficient solubility in CD_3CN to conduct studies at the same concentration used for other metal complexation studies, *i.e.* 2.0 mM). A 2.0 mM solution of **8** was prepared and aliquots of a 100 mM solution of $[Pd(CH_3CN)_4](BF_4)_2$ were added and the complexations monitored by ^1H NMR spectroscopy. In 1:1 $CDCl_3$:CD_3OD, two complexation events are observed, both in slow exchange with each other and with free macrocycle (Figure S27). It is unclear what the nature of these two products is. In d_6-DMSO, clean conversion is seen to a product believed to be $[Pd{\cdot}\mathbf{8}{\cdot}DMSO]^{2+}$ and this is in slow exchange on the ^1H NMR timescale with free **8** (Figure S28).

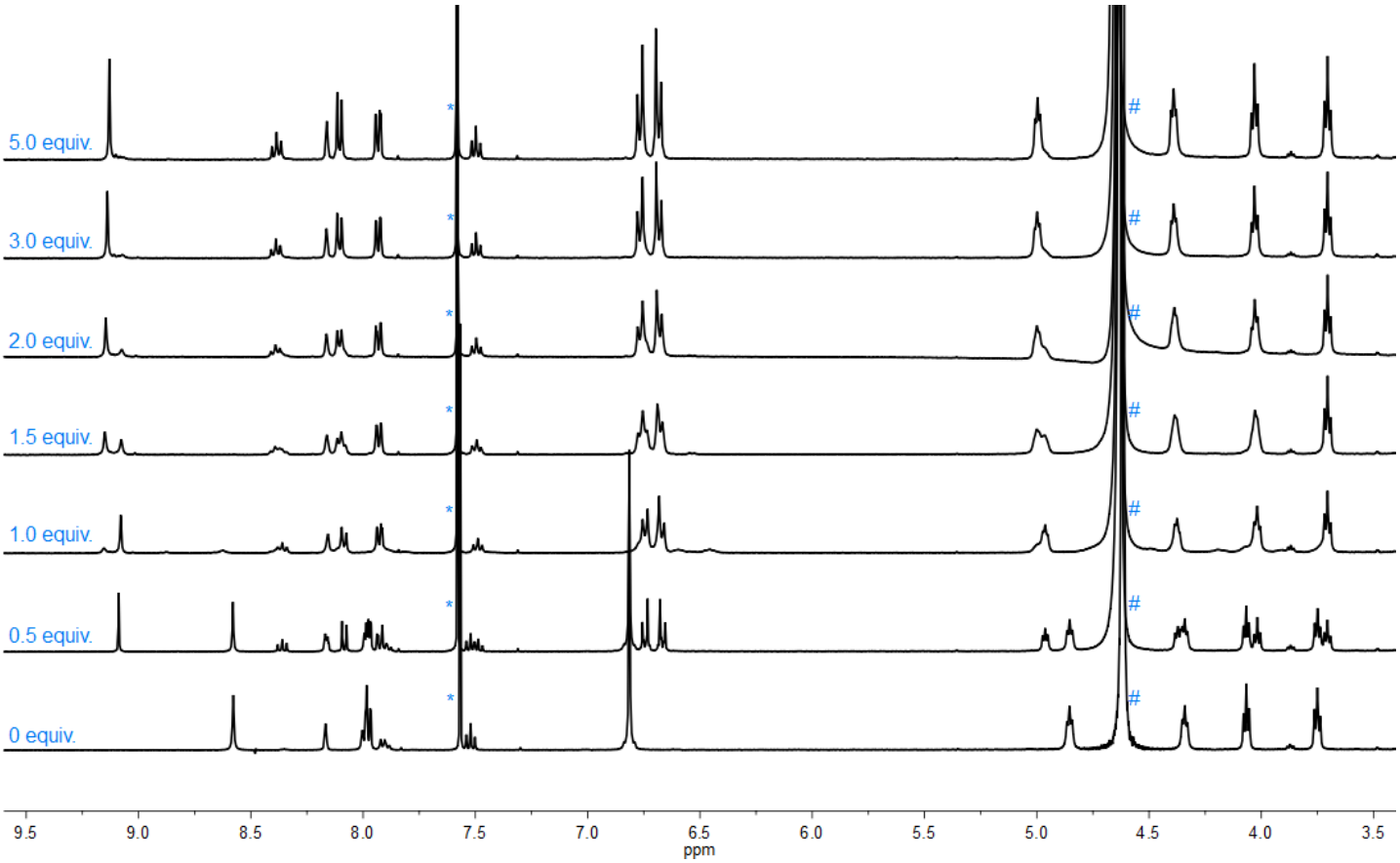

Figure S27. Partial ^1H NMR spectra of **8** on addition of $[Pd(CH_3CN)_4](BF_4)_2$ in 1:1 $CDCl_3$:CD_3OD, * indicates residual NMR solvent peak, # indicates water (400 MHz, 298 K).

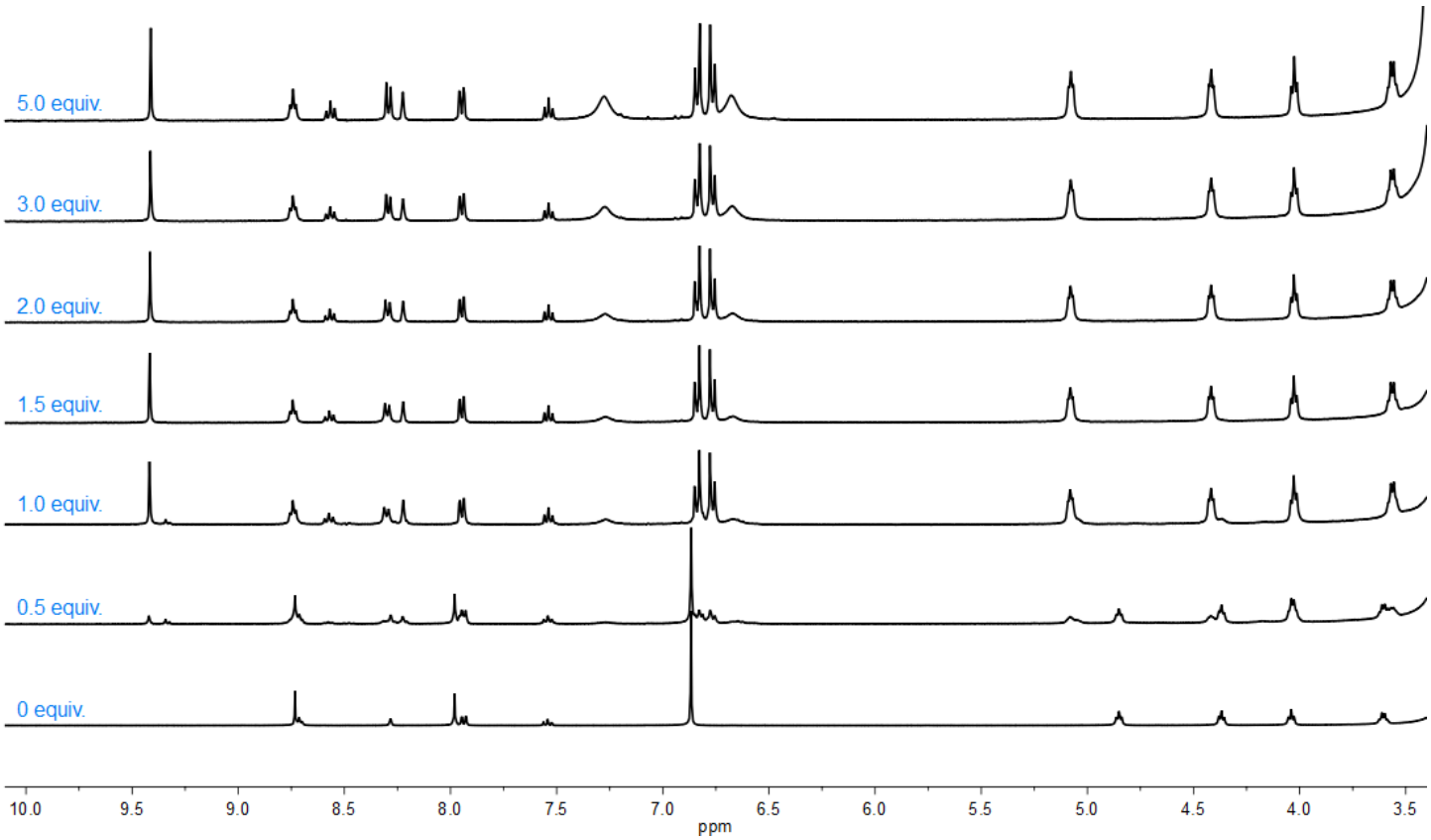

Figure S28. Partial ^{1}H NMR spectra of **8** on addition of $[Pd(CH_3CN)_4](BF_4)_2$ in d_6-DMSO (400 MHz, 298 K).

2.4 Anion binding by macrocycle 8

We studied the binding of anions by **8** using ^{1}H NMR spectroscopy. Studies were conducted in CD_3CN, with 50 mM solutions of the anions as their *n*-tetrabutylammonium (TBA^+) salts added to a 1.0 mM solution of **8**. Due to the difficulties in accurately measuring the small volumes of anion solution, approximate numbers of equivalents of anions were added, and then the actual number of equivalents determined by integration of the macrocycle and TBA^+ peaks. No evidence of halide or oxalate anions interacting with the **btp** group was observed, with these binding solely at the isophthalamide part of the macrocycle. In contrast, terephthalate and isophthalate bind at both the isophthalamide and **btp** parts of the molecule.

Binding of chloride

The movement of the amide and phenylene protons were globally fitted to a 1:1 binding isotherm with K_a = 396 ± 4 M^{-1}. Fitting the amide peak movement alone gave a value of 395 ± 5 M^{-1}, fitting the phenylene peak movement alone gave a value of 398 ± 5 M^{-1}.

Bindfit link: http://app.supramolecular.org/bindfit/view/0b748020-18f7-4e20-8693-b0d340fdf9b0

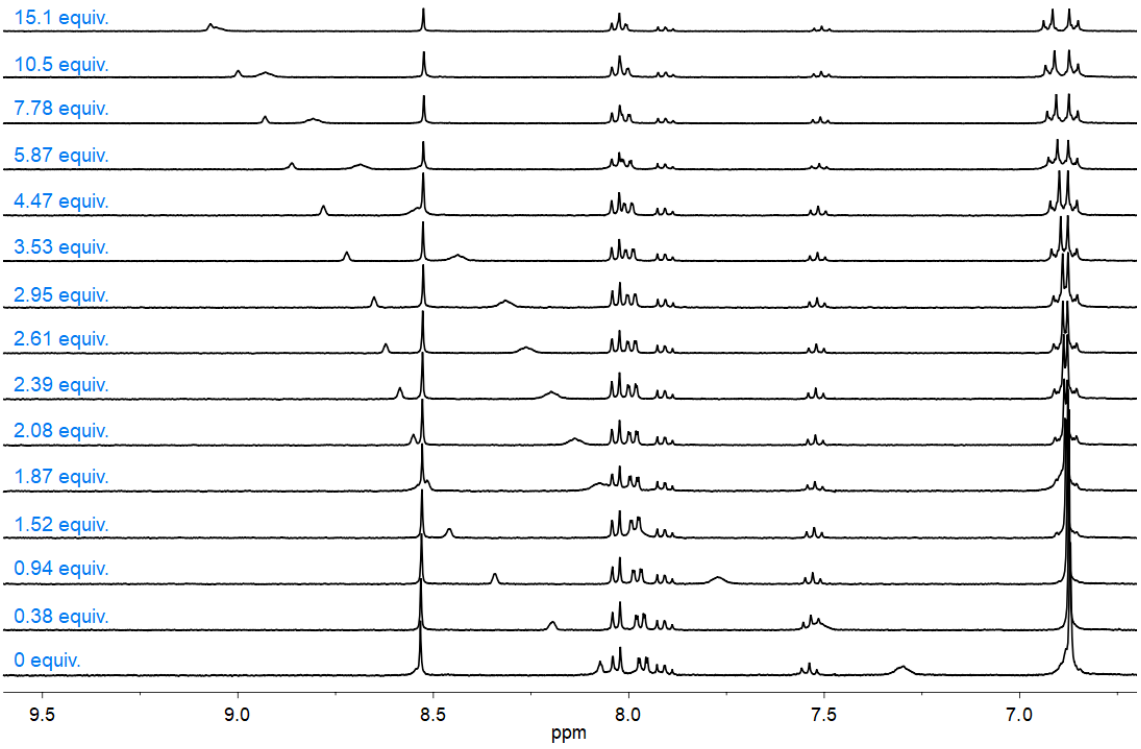

Figure S29. Partial ^{1}H NMR spectra of **8** upon addition of TBA·Cl in CD_3CN, the number of equivalents of anion (determined by integration of the ^{1}H NMR spectra) is indicated (1.0 mM **8** in CD_3CN 400 MHz, 298 K).

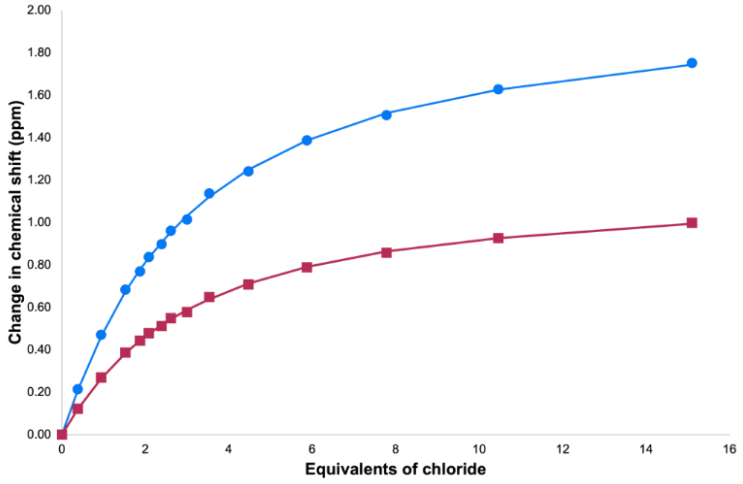

Figure S30. Change in chemical shifts of peaks corresponding to amide N–H (blue circles) and interior C–H phenylene group (maroon squares) of isophthalamide motif upon addition of chloride (points represent data, curves represent 1:1 binding isotherms fitted using *Bindfit*[14]).

Binding of bromide

The movement of the amide and phenylene protons were globally fitted to a 1:1 binding isotherm with K_a = 91 ± 2 M^{-1}. Fitting the amide peak movement alone gave a value of 91 ± 3 M^{-1}, fitting the phenylene peak movement alone gave a value of 93 ± 2 M^{-1}.

For two titration points (7.81 and 9.19 equiv.), the amide N–H peak could not be resolved due to overlap with other peaks. For this reason, the amide and global fits miss these points (so 16 data points are used), while the phenylene fit includes all 18 data points.

Bindfit link: http://app.supramolecular.org/bindfit/view/4864b110-2155-40f3-92a1-3187e80f8430

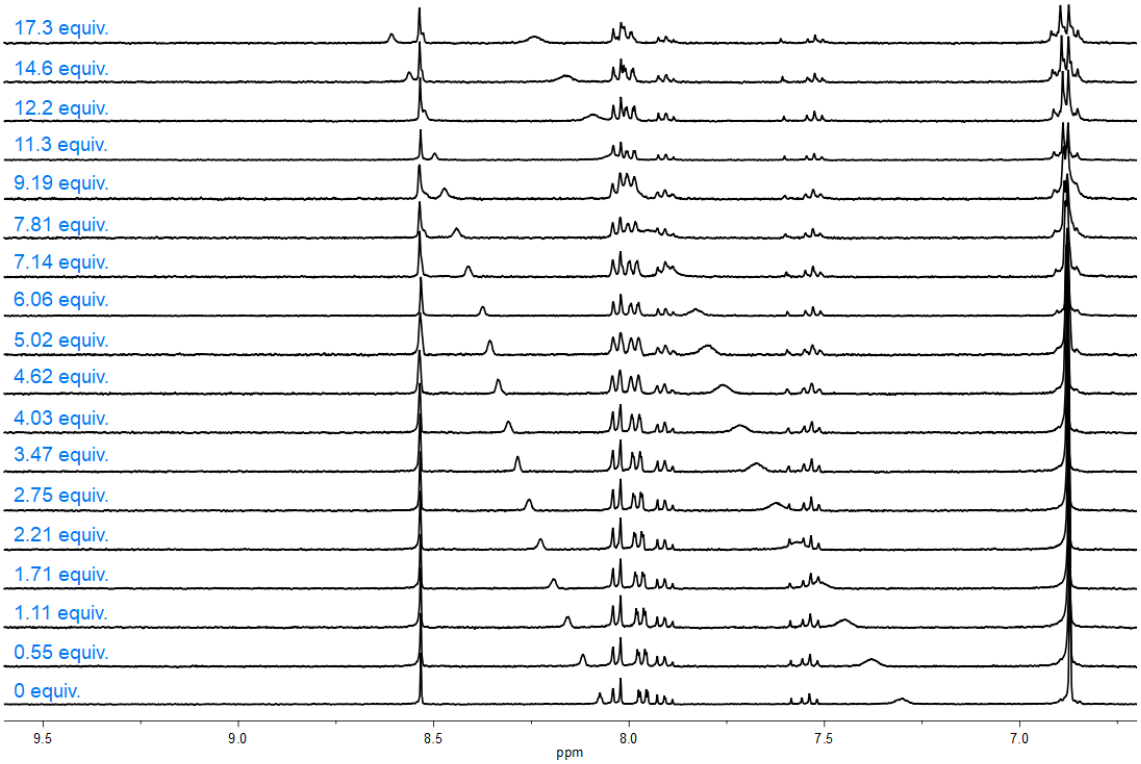

Figure S31. Partial ^{1}H NMR spectra of **8** upon addition of TBA·Br in CD_3CN, the number of equivalents of anion (determined by integration of the ^{1}H NMR spectra) is indicated (1.0 mM **8** in CD_3CN 400 MHz, 298 K).

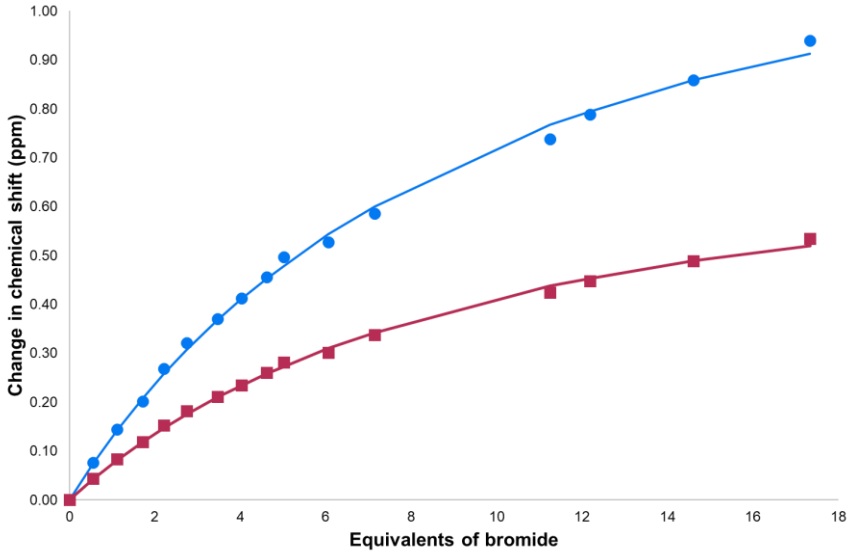

Figure S32. Change in chemical shifts of peaks corresponding to amide N–H (blue circles) and interior C–H phenylene group (maroon squares) of isophthalamide motif upon addition of bromide (points represent data, curves represent 1:1 binding isotherms fitted using *Bindfit*[14]).

Binding of iodide

The movement of the amide and phenylene protons were globally fitted to a 1:1 binding isotherm with K_a = 28 ± 1 M^{-1}. Fitting the amide peak movement alone gave a value of 30 ± 1 M^{-1}, fitting the phenylene peak movement alone gave a value of 22 ± 1 M^{-1}.

Bindfit link: http://app.supramolecular.org/bindfit/view/dd3827b3-d0d7-421d-977f-86bd937deb82

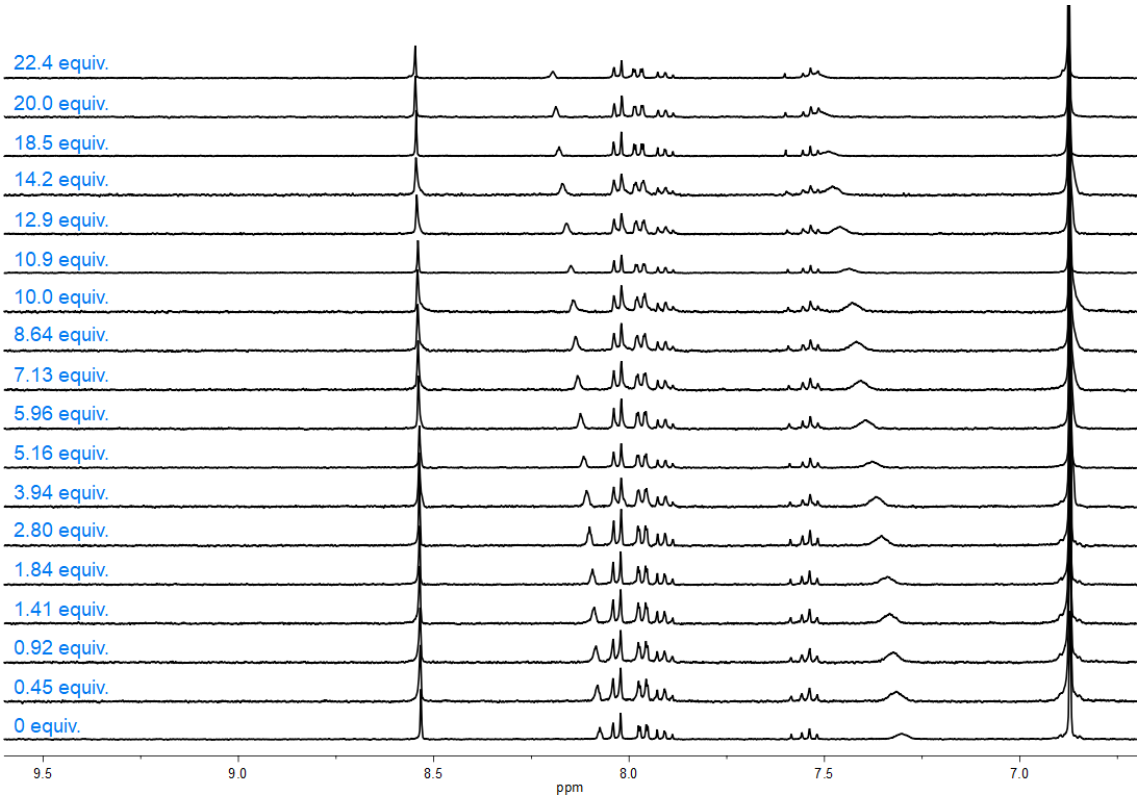

Figure S33. Partial ^{1}H NMR spectra of **8** upon addition of TBA·I in CD_3CN, the number of equivalents of anion (determined by integration of the ^{1}H NMR spectra) is indicated (1.0 mM **8** in CD_3CN 400 MHz, 298 K).

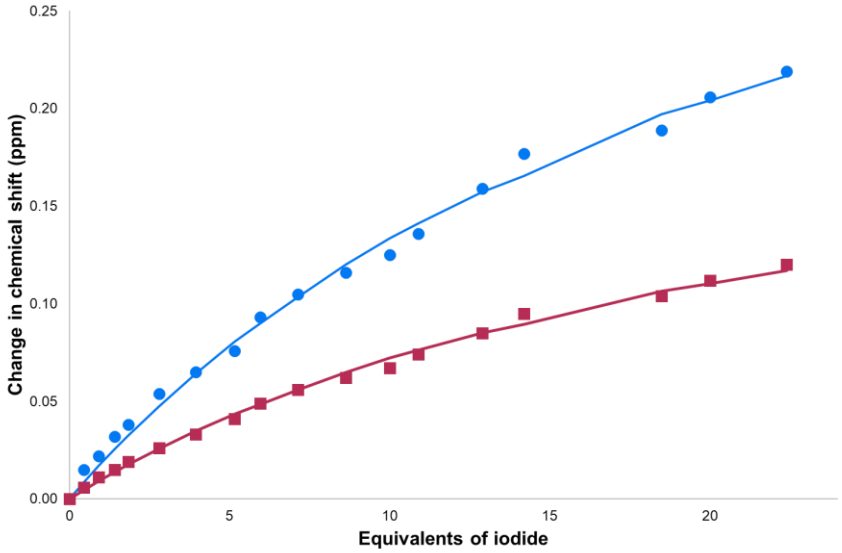

Figure S34. Change in chemical shifts of peaks corresponding to amide N–H (blue circles) and interior C–H phenylene group (maroon squares) of isophthalamide motif upon addition of iodide (points represent data, curves represent 1:1 binding isotherms fitted using *Bindfit*[14]).

Binding of terephthalate

Binding was too strong to be quantified by ^{1}H NMR titration experiments, but appears to be approximately 5×10^4 M^{-1}. Significant peak broadening was observed at low equivalents of anion meaning that these peaks could not be resolved. **Bindfit link:** http://app.supramolecular.org/bindfit/view/ce1ff95d-6a8d-4808-b48b-73cd67a7cf74

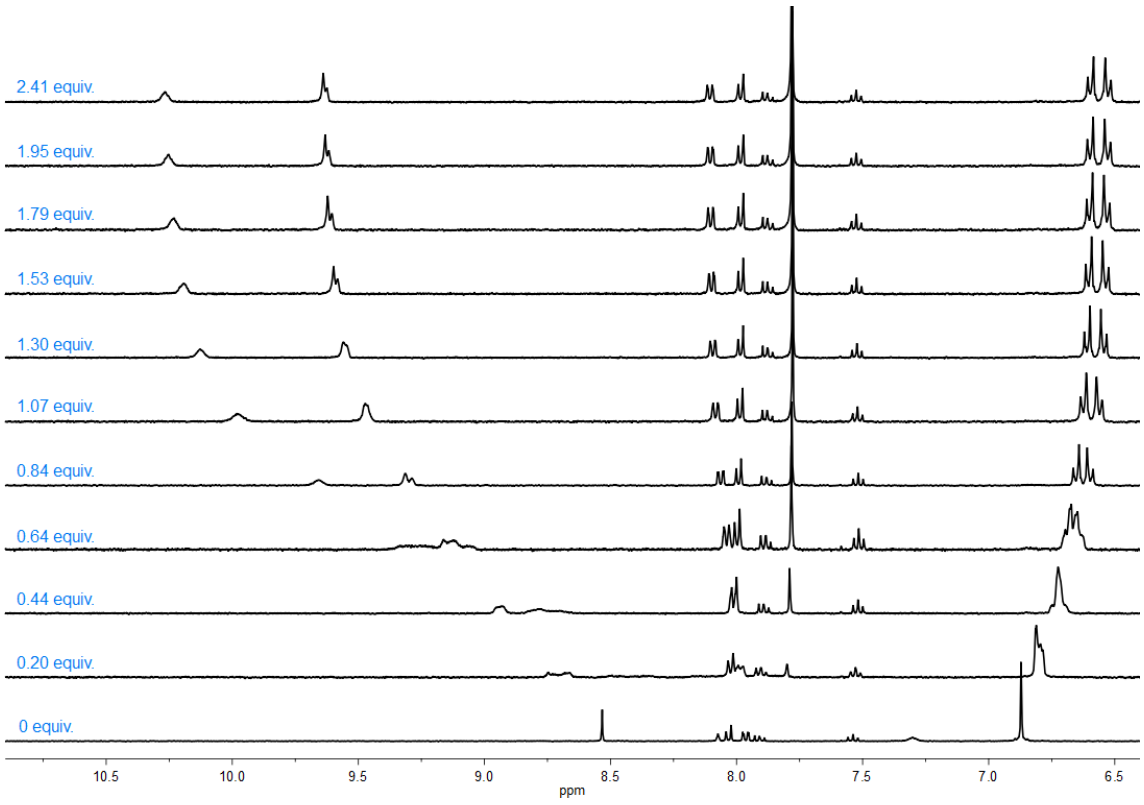

Figure S35. Partial ^{1}H NMR spectra of **8** upon addition of TBA_2·terephthalate in CD_3CN, the number of equivalents of anion (determined by integration of the ^{1}H NMR spectra) is indicated (1.0 mM **8** in CD_3CN 400 MHz, 298 K).

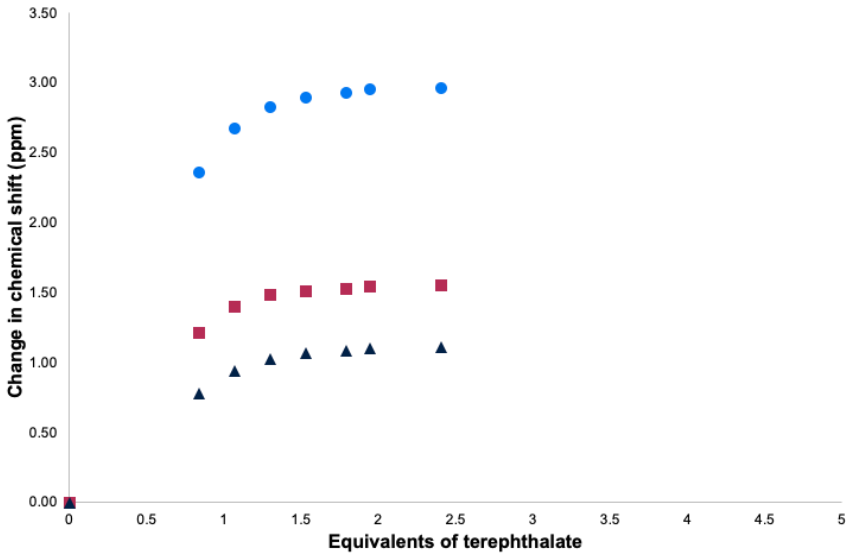

Figure S36. Change in chemical shifts of peaks corresponding to amide N–H (blue circles), interior C–H phenylene group (maroon squares) of isophthalamide motif and triazole group (navy triangles) upon addition of terephthalate (points represent data, due to the high binding strength an isotherm could not be fitted).

Binding of isophthalate

Binding was too strong to be quantified by ^{1}H NMR titration experiments, but appears to be approximately 5×10^4 M^{-1}. Significant peak broadening was observed at low equivalents of anion meaning that these peaks could not be resolved. **Bindfit link:** http://app.supramolecular.org/bindfit/view/321ef60c-e415-4690-adc3-e1c1edd90cfa

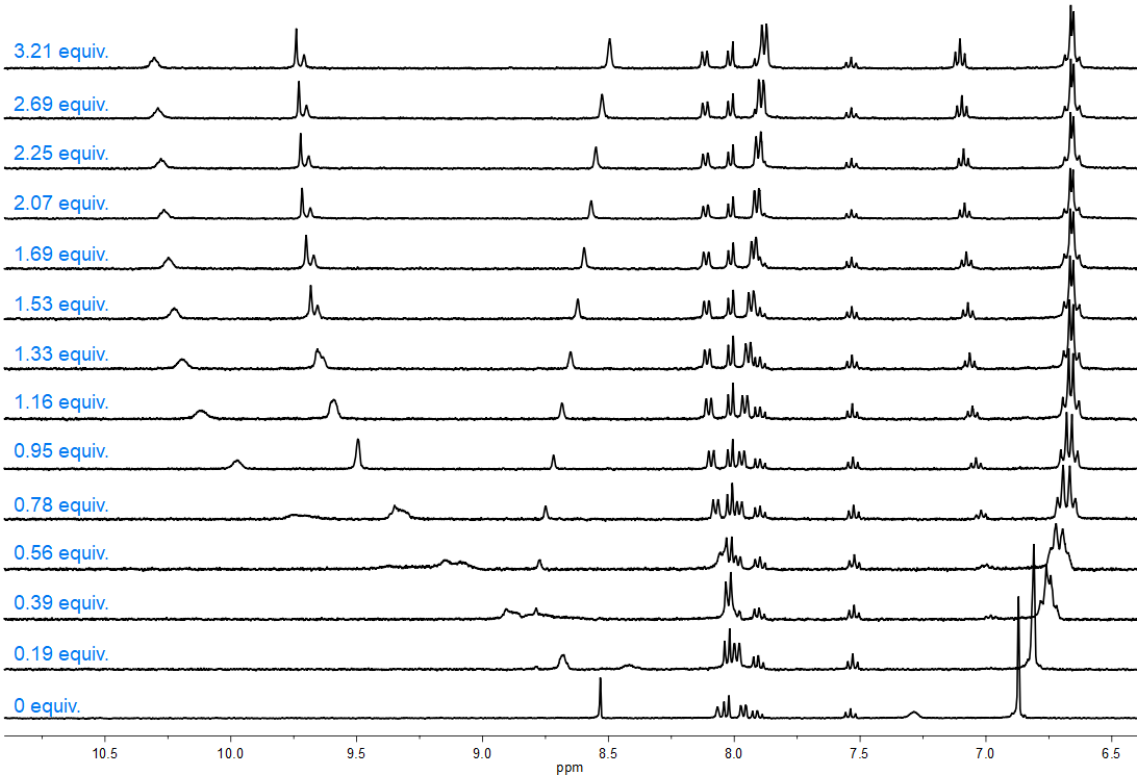

Figure S37. Partial ^{1}H NMR spectra of **8** upon addition of TBA_2·isophthalate in CD_3CN, the number of equivalents of anion (determined by integration of the ^{1}H NMR spectra) is indicated (1.0 mM **8** in CD_3CN 400 MHz, 298 K).

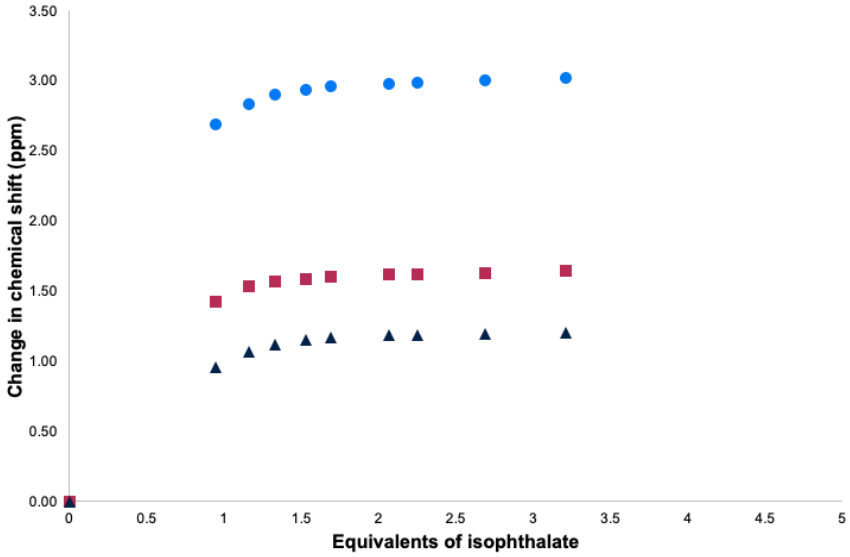

Figure S38. Change in chemical shifts of peaks corresponding to amide N–H (blue circles), interior C–H phenylene group (maroon squares) of isophthalamide motif and triazole group (navy triangles) upon addition of isophthalate (points represent data, due to the high binding strength an isotherm could not be fitted).

Binding of oxalate

The movement of the amide and phenylene protons were globally fitted to a 1:1 binding isotherm with K_a = 7665 ± 567 M^{-1}. Fitting the amide peak movement alone gave a value of 7577 ± 851 M^{-1}, fitting the phenylene peak movement alone gave a value of 8552 ± 1064 M^{-1}. Significant peak broadening was observed at low equivalents of anion meaning that these peaks could not be resolved.

Bindfit link: http://app.supramolecular.org/bindfit/view/4f42571e-392a-447e-b74f-8f75ca04805b

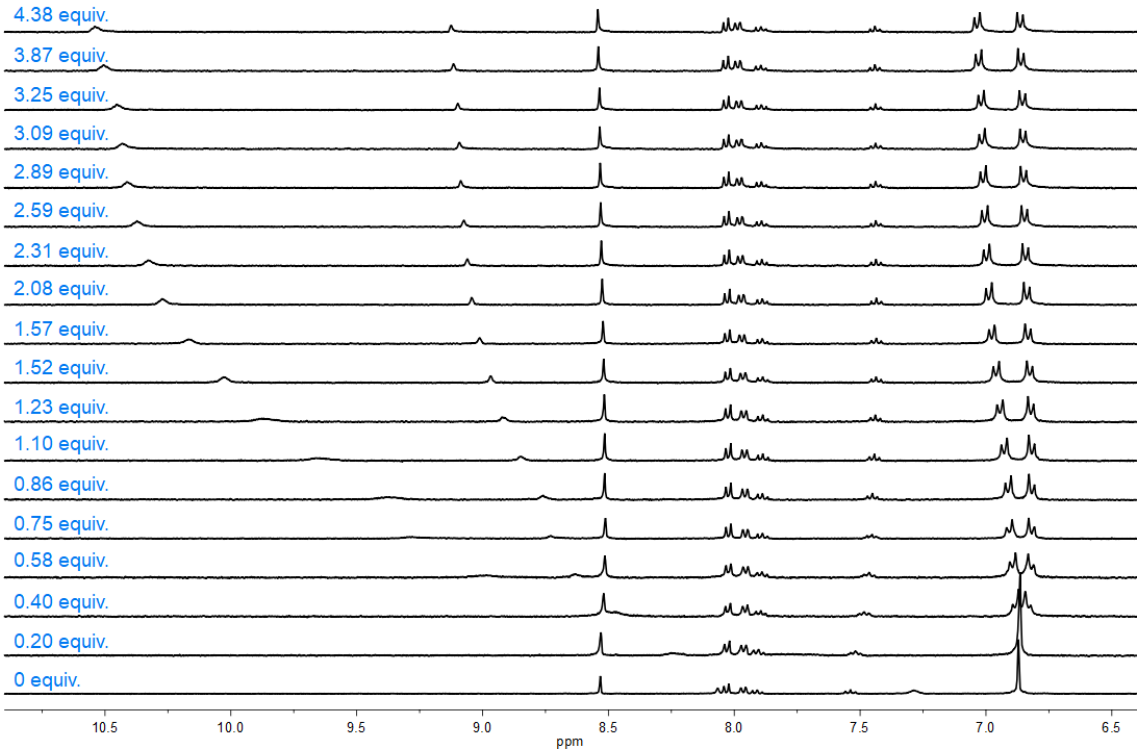

Figure S39. Partial ^{1}H NMR spectra of **8** upon addition of TBA_2·oxalate in CD_3CN, the number of equivalents of anion (determined by integration of the ^{1}H NMR spectra) is indicated (1.0 mM **8** in CD_3CN 400 MHz, 298 K).

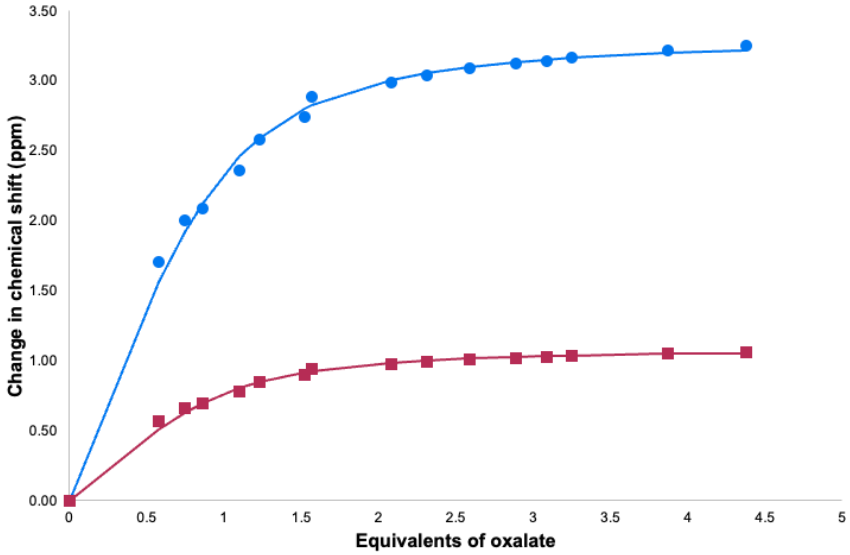

Figure S40. Change in chemical shifts of peaks corresponding to amide N–H (blue circles) and interior C–H phenylene group (maroon squares) of isophthalamide motif upon addition of oxalate (points represent data, curves represent 1:1 binding isotherms fitted using *Bindfit*[14]).

2.5 Anion complexation by [Pd·8·CH$_3$CN](BF$_4$)$_2$

We studied the binding of halide anions by [Pd·**8**·CH$_3$CN](BF$_4$)$_2$ using ^{1}H NMR spectroscopy. Studies were conducted in CD$_3$CN, with 50 mM solutions of the anions as their TBA$^+$ salts added to a 1.0 mM solution of [Pd·**8**·CH$_3$CN](BF$_4$)$_2$. These showed initial quantitative formation of a new species, believed to be [Pd·**8**·X]BF$_4$ (X = Cl$^-$, Br$^-$, I$^-$) in slow exchange with [Pd·**8**·CH$_3$CN](BF$_4$)$_2$ on the ^{1}H NMR timescale (Figures S41 – S43). Subsequent addition of halide anion showed downfield shifts in the amide N–H resonances as well as the interior C–H proton resonance of the isophthalamide motif, consistent with subsequent anion binding at this site. Adding more than one equivalent of halide anion also causes peaks corresponding to free **8** to reappear, as well as the formation of a precipitate. We believe that these observations are consistent with excess halide anions causing precipitation of PdX$_2$. This was most apparent and occurred at the lowest number of equivalents of anions when I$^-$ was used.

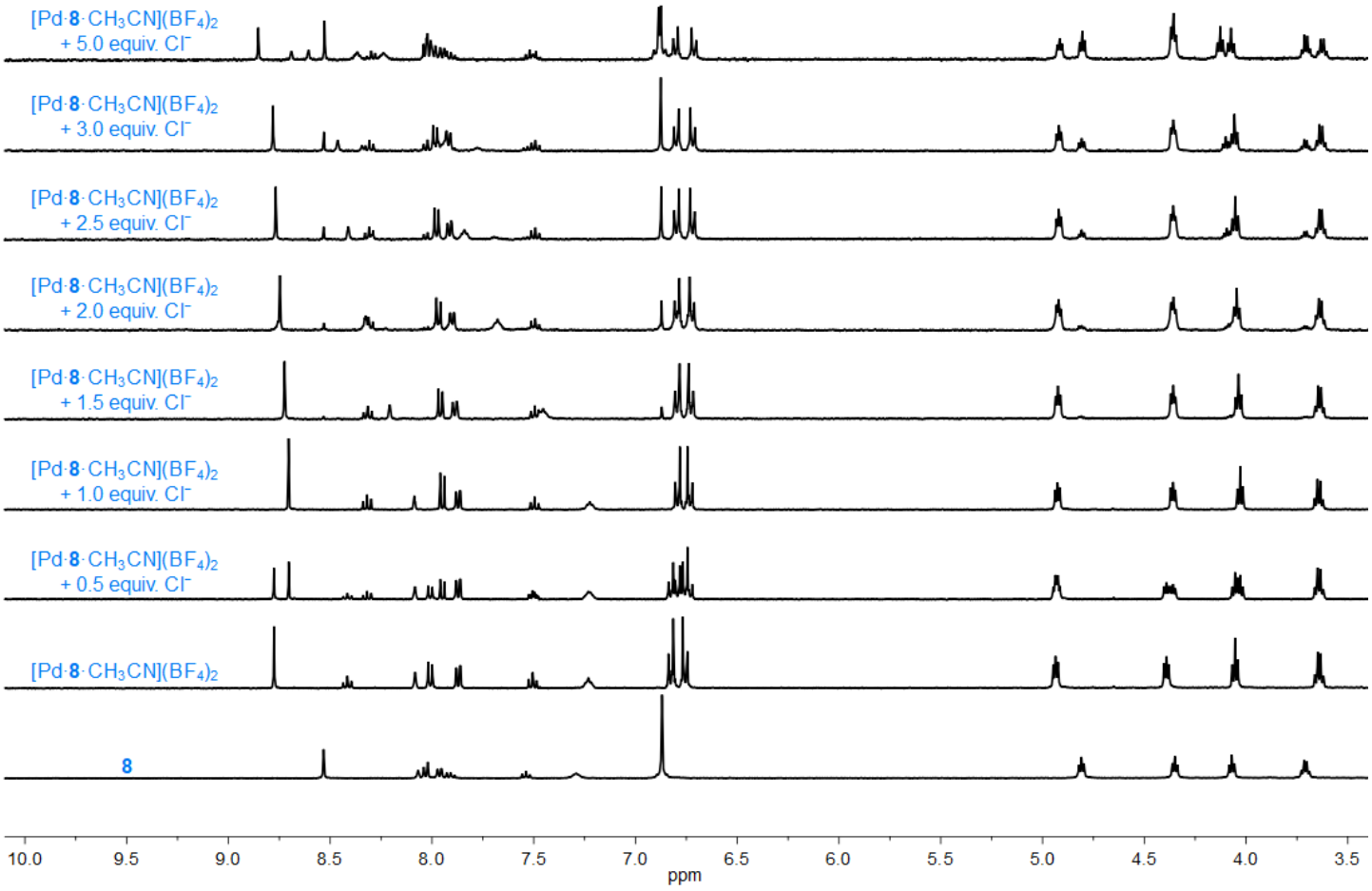

Figure S41. Partial ^{1}H NMR spectra of **8,** and [Pd·**8**·CH$_3$CN](BF$_4$)$_2$ upon the addition of TBA·Cl in CD$_3$CN (400 MHz, 298 K).

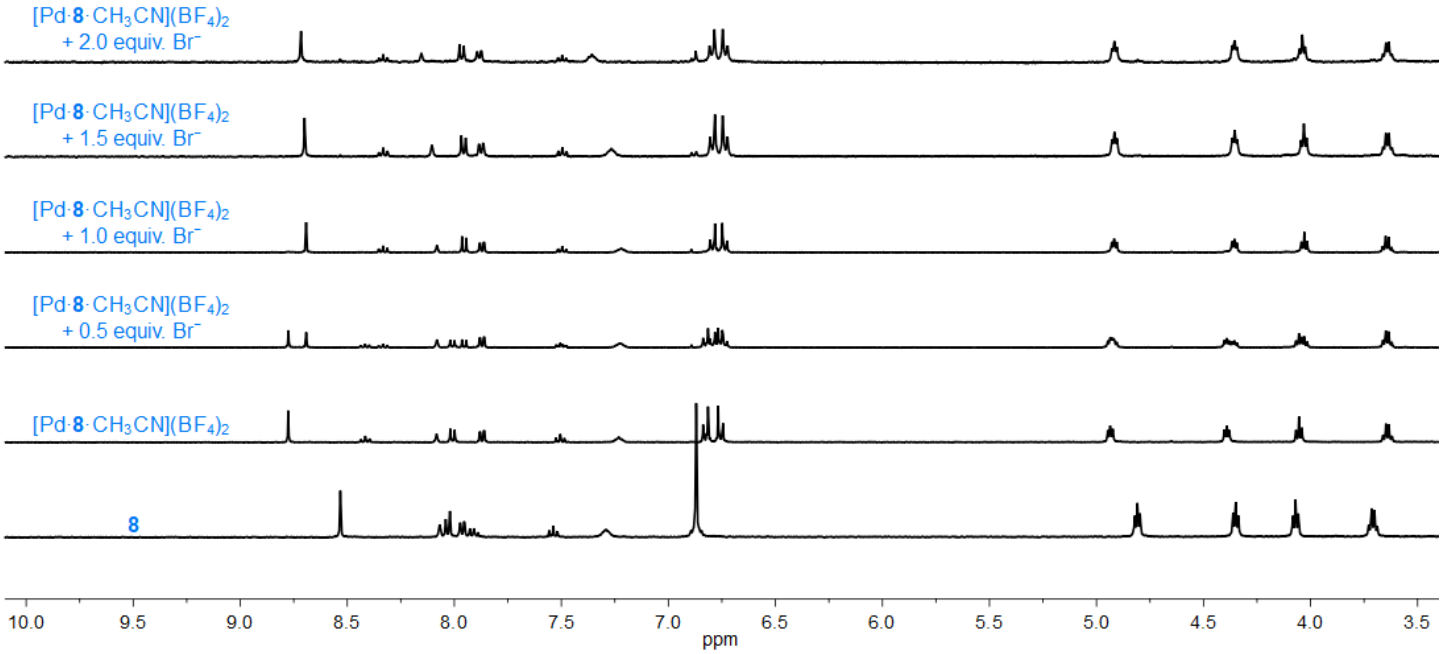

Figure S42. Partial ^{1}H NMR spectra of **8,** and [Pd·**8**·CH$_3$CN](BF$_4$)$_2$ upon the addition of TBA·Br in CD$_3$CN (400 MHz, 298 K). Significant precipitation was observed when more than 2 equivalents of TBA·Br were added.

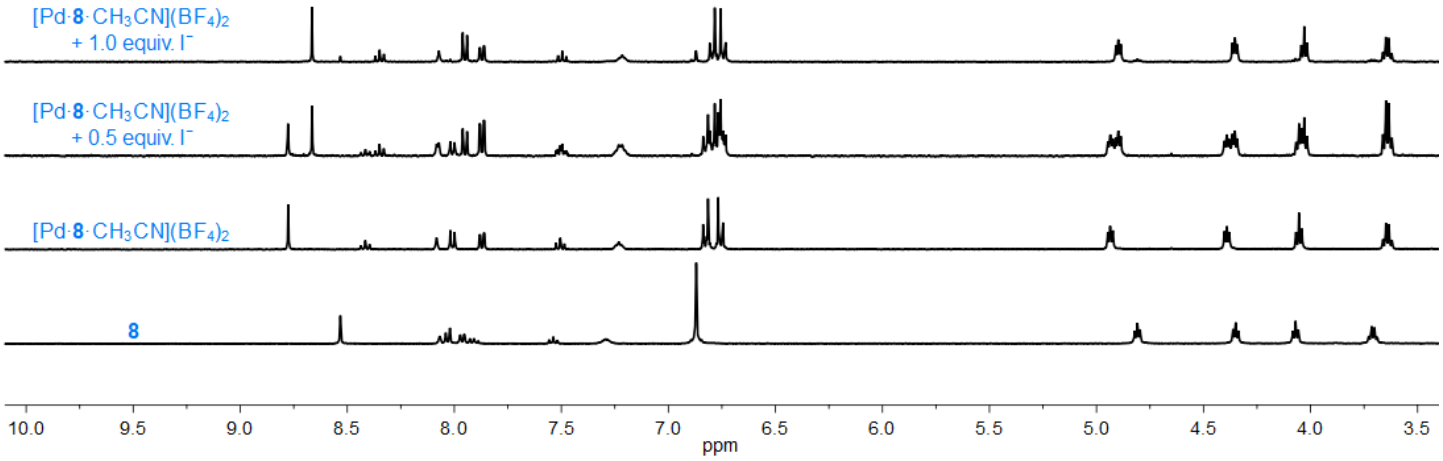

Figure S43. Partial ^{1}H NMR spectra of **8,** and [Pd·**8**·CH$_3$CN](BF$_4$)$_2$ upon the addition of TBA·I in CD$_3$CN (400 MHz, 298 K). Significant precipitation was observed when more than 1 equivalent of TBA·I was added.

3. Single crystal X-ray diffraction analysis

3.1. General remarks

Single crystal data for **[**Pd·**8**·Cl]BF_4 were collected using mirror-monochromated Mo Kα radiation on an Agilent Xcalibur diffractometer at 150 K. Data for **3**, **8**, and [Pd·**8**·Br]BF_4 from acetonitrile were collected using mirror-monochromated Cu Kα radiation on an Agilent SuperNova diffractometer at 150 K. Raw frame data (including data reduction, interframe scaling, unit cell refinement and absorption corrections) were processed using CrysAlis Pro.[15] Structures were solved using Superflip[16] and refined using full-matrix least-squares on F^2 within the Crystals suite.[17] All non-hydrogen atoms were refined with anisotropic displacement parameters. C–H hydrogen atoms were generally visible in the Fourier difference map and the positions of these atoms were initially refined with restraints on bond lengths and angles, after which the positions were used as the basis for a riding model.[18] N–H hydrogen atoms were visible in the Fourier difference map and their positions were refined with restraints on N–H bond lengths and C–N–H angles.

Single crystal data for [Pd·**8**·Br]BF_4 from chloroform/methanol and [Pd·**8**·I]BF_4 were collected using synchrotron radiation at 100 K using beamline MX1 at the Australian Synchrotron,[19] single crystal data for TBA·**8**·Br were collected using synchrotron radiation at 100 K using beamline MX2 at the Australian Synchrotron.[20] Raw frame data (including data reduction, interframe scaling and unit cell refinement) were processed using XDS.[21] The structures were solved using Superflip[16] and refined using full-matrix least-squares on F^2 within the Crystals suite.[17] All non-hydrogen atoms were refined with anisotropic displacement parameters. C–H hydrogen atoms were generally visible in the Fourier difference map and the positions of these atoms were initially refined with restraints on bond lengths and angles, after which the positions were used as the basis for a riding model.[18] N–H hydrogen atoms initially inserted at calculated positions and then their positions were refined with restraints on N–H bond lengths and C–N–H angles.

Single crystal data for [Zn·**8**·$(OH_2)_2$·MeOH]$^{2+}$ were collected using synchrotron radiation at 100 K using beamline MX2 at the Australian Synchrotron.[20] Raw frame data (including data reduction, interframe scaling and unit cell refinement) were processed using XDS.[21] The structure was solved using ShelXT[22] and refined using ShelXL[23] inside OLEX2.[24] All non-hydrogen atoms were refined with anisotropic displacement parameters. Data are of relatively low quality and so hydrogen atoms were inserted at calculated positions.

Individual structures are discussed in more detail in the following pages, and thermal ellipsoid plots are provided in Figures S44 – S51. Full crystallographic data in CIF format are provided as Supporting Information (CCDC Numbers: 2225115 – 2225121, 2225744) and selected crystallographic data are provided in Table S1.

3.2. Structure of 3

Crystals were grown by slowly cooling a solution (approx. 2 mg mL^{-1}) of **3** in hot DMF (approx. 80 °C). Crystals were thin long needles, which grew in clusters. Even after many attempts to split a single crystal from the cluster, diffraction images suggested the presence of either a split crystal or a second minor crystal. After data processing, this resulted in 17 reflections that had observed intensities that were significantly higher than calculated by the model. We suspect these were due to the split crystal, and so these reflections were removed manually by inspection of the F_o/F_c plot. Two additional reflections appeared to have been obscured by the beamstop and so were also removed. Apart from this, data refinement proceeded smoothly and no crystallographic restraints were necessary.

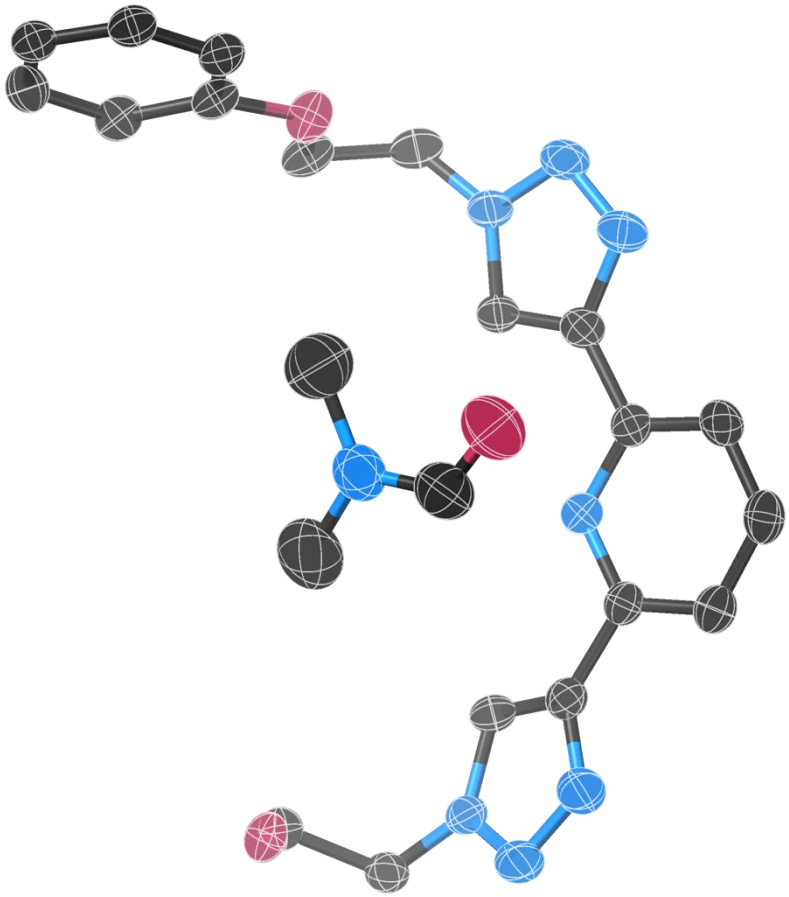

Figure S44. Thermal ellipsoid plot showing the asymmetric unit of **3**. Ellipsoids are shown at 50% probability, hydrogen atoms are omitted for clarity.

3.3. Structure of 8

Crystals were grown by vapour diffusion of diethyl ether into a solution of **8** in a mixture of DMSO, dichloromethane and methanol. C–H hydrogen atoms were visible in the Fourier difference map and were initially refined with restraints on bond lengths and angles, after which the positions were used as the basis for a riding model. Amide N–H hydrogen atoms were visible in the Fourier difference map and were refined with restraints on bond lengths and angles. Other than restraints on hydrogen atoms (N–H bond lengths and C–N–H bond angles), it was not necessary to use any crystallographic restraints during refinement.

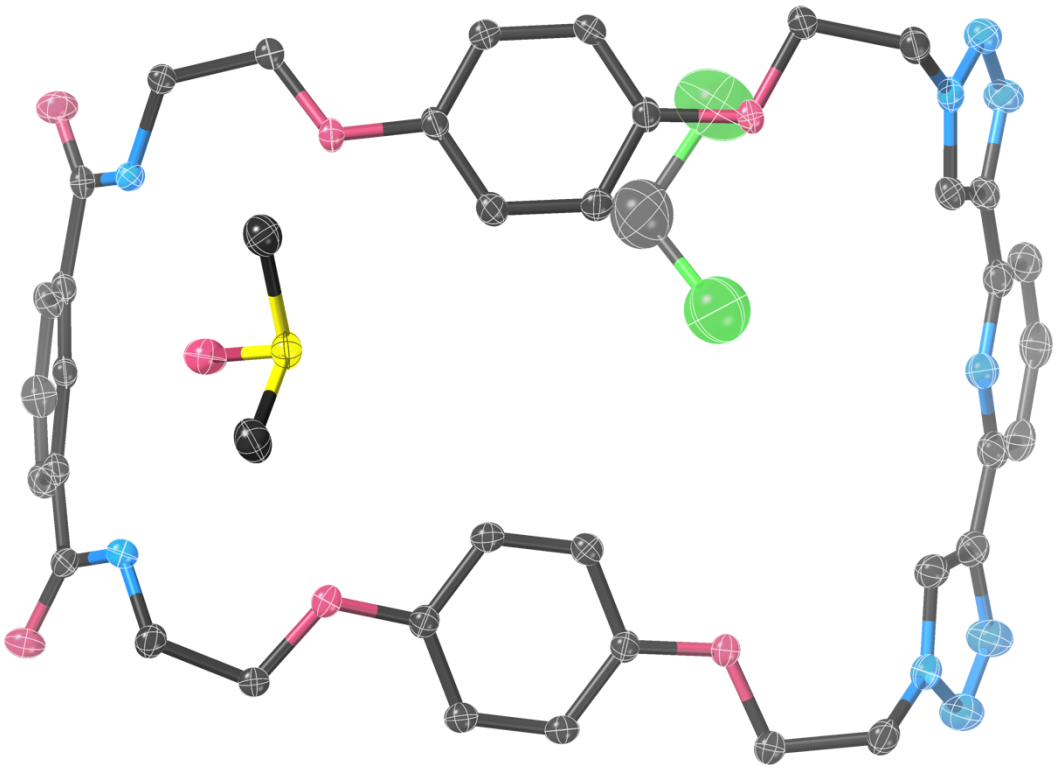

Figure S45. Thermal ellipsoid plot showing the asymmetric unit of **8**. Ellipsoids are shown at 50% probability, hydrogen atoms are omitted for clarity.

3.4. Structure of TBA·8·Br

Crystals were grown by vapour diffusion of diethyl ether into an acetonitrile solution containing **8** and a large excess of TBA·Br. C–H hydrogen atoms were visible in the Fourier difference map and were initially refined with restraints on bond lengths and angles, after which the positions were used as the basis for a riding model. Amide N–H hydrogen atoms were visible in the Fourier difference map and were initially refined with restraints on bond lengths and angles, after which the positions were used as the basis for a riding model. There is a half occupancy water molecule located close to the crystallographic centre of inversion such that one of its hydrogen atoms is located on the centre of inversion; the other hydrogen atom for this partial occupancy water molecule was inserted at an idealised hydrogen bonding position. The positions of these hydrogen atoms were then used as the basis for a riding model. It was not necessary to use any crystallographic restraints during refinement.

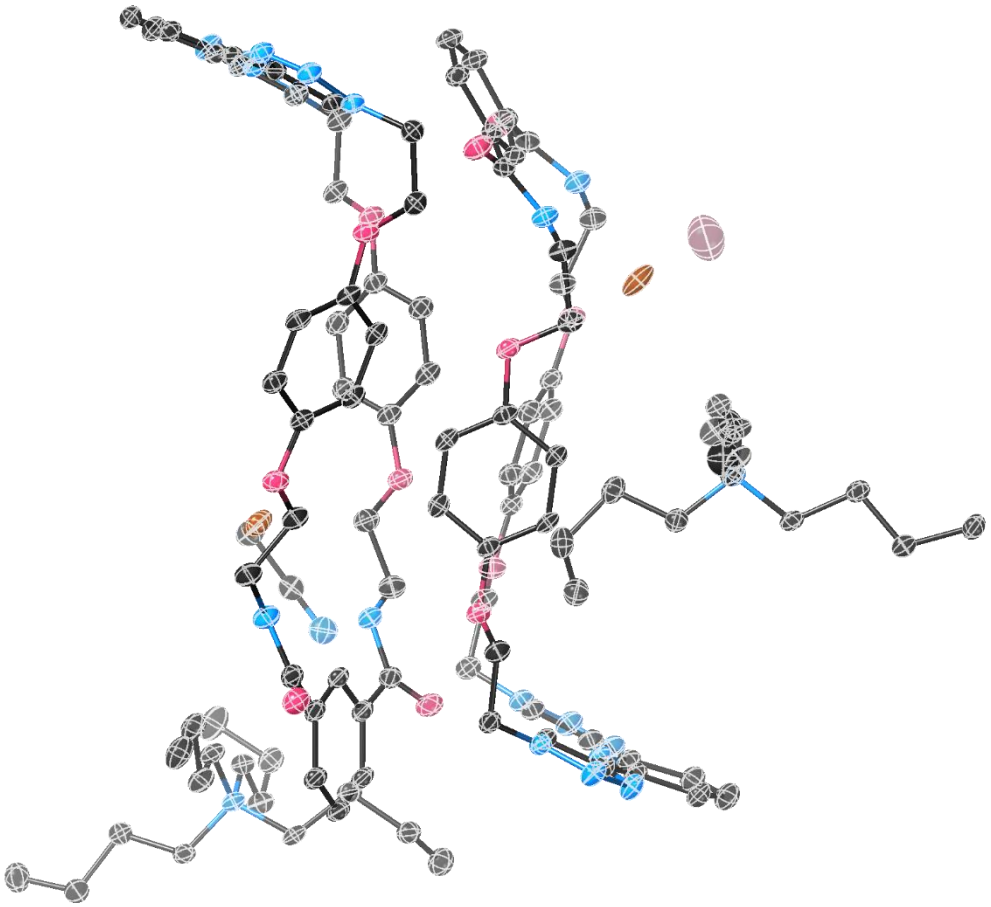

Figure S46. Thermal ellipsoid plot showing the asymmetric unit of TBA·**8**·Br. Ellipsoids are shown at 50% probability, hydrogen atoms are omitted for clarity.

3.5. Structure of [Pd·8·Cl]BF_4

Crystals were grown by vapour diffusion of diethyl ether into an acetonitrile solution containing [Pd·**8**·MeCN]$(BF_4)_2$ and one equivalent of TBA·Cl. C–H hydrogen atoms were visible in the Fourier difference map and were initially refined with restraints on bond lengths and angles, after which the positions were used as the basis for a riding model. Amide N–H hydrogen atoms were visible in the Fourier difference map and were refined with restraints on bond lengths and angles. Refinement proceeded smoothly and apart from restraints on N–H bond lengths and C–N–H bond angles, it was not necessary to use any crystallographic restraints.

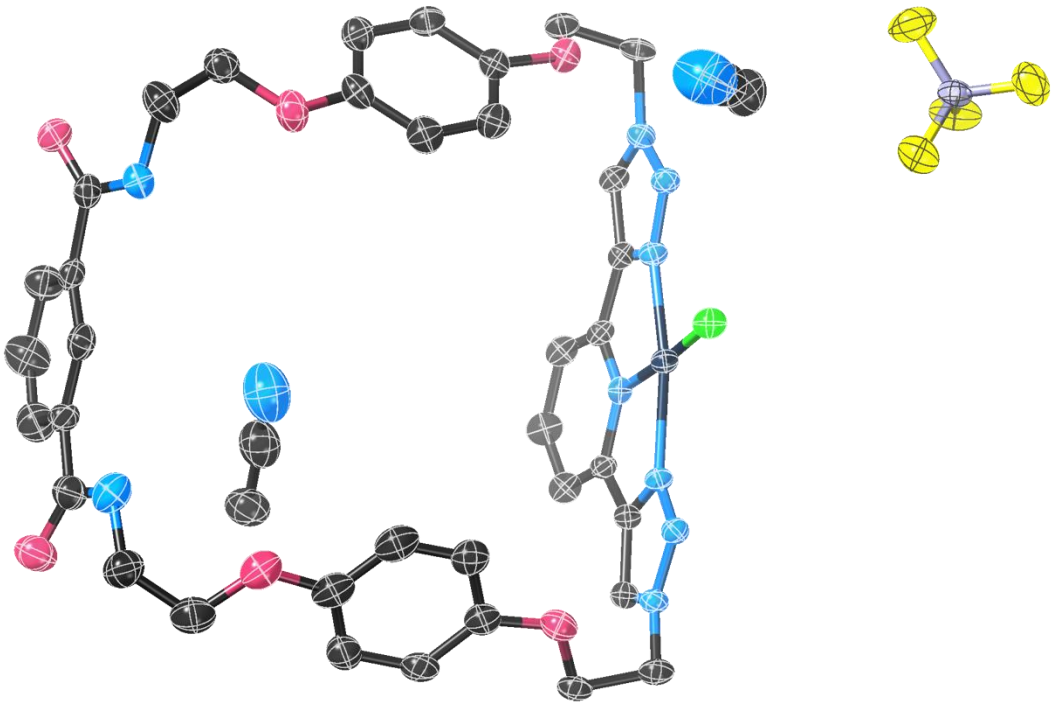

Figure S47. Thermal ellipsoid plot showing the asymmetric unit of [Pd·**8**·Cl]BF_4. Ellipsoids are shown at 50% probability, hydrogen atoms are omitted for clarity.

3.6. Structure of [Pd·8·Br]BF_4 from acetonitrile

Crystals were grown by vapour diffusion of diethyl ether into an acetonitrile solution containing **8** and $[Pd(CH_3CN)_4](BF_4)_2$. The structure contains an adventitious bromide anion; as discussed in the manuscript, it is not clear where this Br^- has come from. Most of the structure refines very smoothly. The exception is a diethyl ether solvent molecule located in the centre of the macrocycle. This was modelled as disordered over two parts (occupancies 0.5:0.5), and required the use of bond distance, bond angle, planarity and thermal and vibrational ellipsoid restraints for this disordered solvent. Despite these restraints, the thermal ellipsoids for the diethyl ether atoms are relatively large.

With the exception of the disordered diethyl ether solvent molecule, C–H hydrogen atoms were visible in the Fourier difference map and were initially refined with restraints on bond lengths and angles, after which the positions were used as the basis for a riding model. Amide N–H hydrogen atoms were visible in the Fourier difference map and were refined with restraints on bond lengths and angles. Given the difficulties in modelling the disordered diethyl ether solvent, the hydrogen atoms on this group were inserted at calculated positions and these positions used as the basis for a riding model.

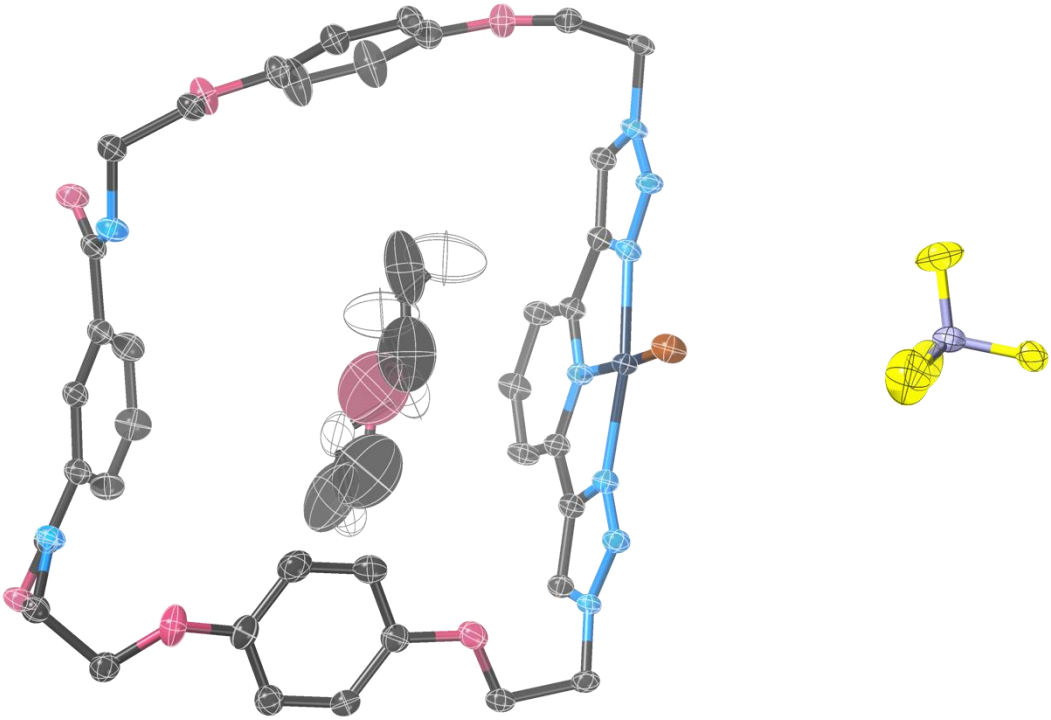

Figure S48. Thermal ellipsoid plot showing the asymmetric unit of **[**Pd·**8**·Br]BF_4 from acetonitrile. Ellipsoids are shown at 50% probability, hydrogen atoms are omitted for clarity, the two positions of the disordered diethyl ether solvent are shown in different colours.

3.7. Structure of [Pd·8·Br]BF_4 from chloroform/methanol

Crystals were grown by vapour diffusion of diethyl ether into a solution containing **8** and $[Pd(CH_3CN)_4](BF_4)_2$ in 1:1 chloroform:methanol. The structure contains an adventitious bromide anion; as discussed in the manuscript, it is not clear where this Br^- has come from. Most of the structure refines very smoothly. The exception is a diethyl ether solvent molecule located in the centre of the macrocycle. This was modelled as disordered over two parts (occupancies 0.65:0.35), and required the use of bond distance, bond angle, thermal and vibrational ellipsoid restraints for this disordered solvent. Despite these restraints, the thermal ellipsoids for the diethyl ether atoms are relatively large.

C–H hydrogen atoms were visible in the Fourier difference map and were initially refined with restraints on bond lengths and angles, after which the positions were used as the basis for a riding model. Amide N–H hydrogen atoms were initially inserted at calculated positions and were then refined with restraints on N–H bond lengths and C–N–H angles.

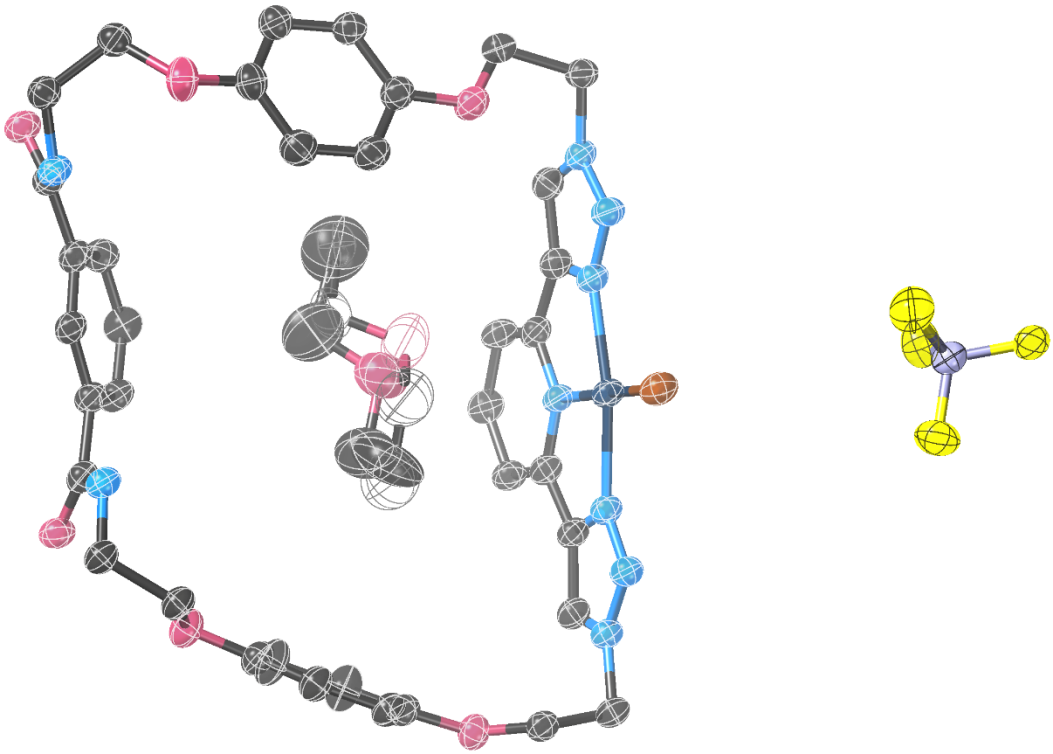

Figure S49. Thermal ellipsoid plot showing the asymmetric unit of [Pd·**8**·Br]BF_4 from chloroform/methanol. Ellipsoids are shown at 50% probability, hydrogen atoms are omitted for clarity, the two positions of the disordered diethyl ether solvent are shown in different colours.

3.8. Structure of [Pd·8·I]BF_4

Crystals were grown by vapour diffusion of diethyl ether into an acetonitrile solution containing [Pd·**8**·MeCN]$(BF_4)_2$ and one equivalent of TBA·I. Crystals were small and weakly-diffracting, and even with the use of synchrotron radiation, it was not possible to obtain diffraction data beyond 0.90 Å. Despite this, the structure solves and refines readily. Restraints were added to the B–F bond lengths and thermal and vibrational ellipsoid parameters of the BF_4^- anion.

C–H hydrogen atoms were visible in the Fourier difference map and were initially refined with restraints on bond lengths and angles, after which the positions were used as the basis for a riding model. Amide N–H hydrogen atoms were initially inserted at calculated positions and then were refined with restraints on N–H bond lengths and C–N–H angles.

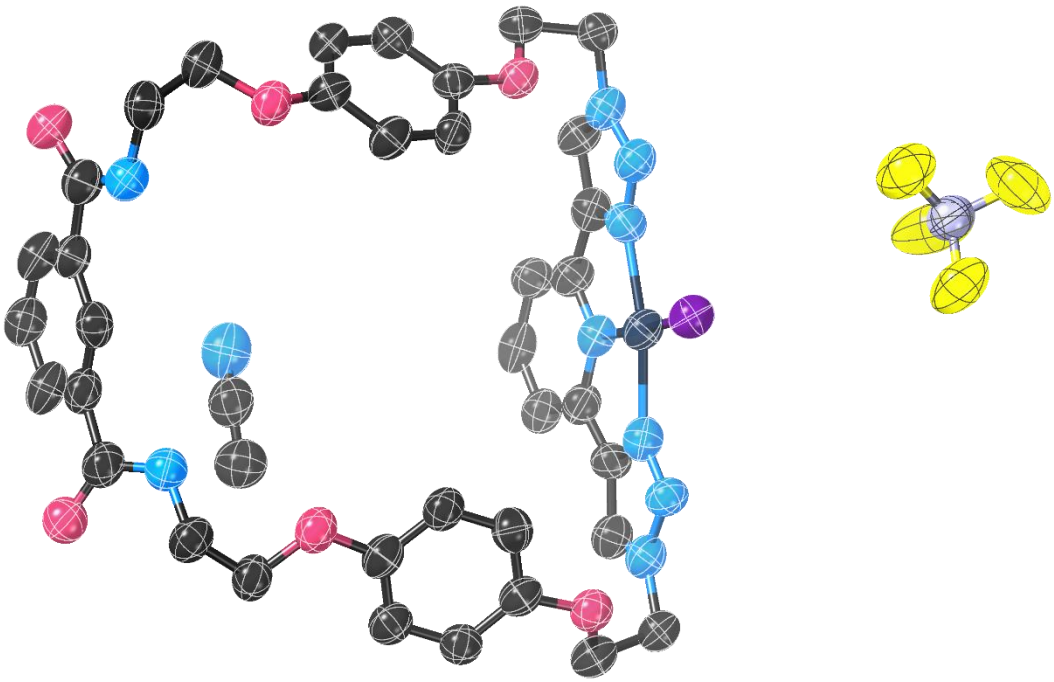

Figure S50. Thermal ellipsoid plot showing the asymmetric unit of [Pd·**8**·I]BF_4. Ellipsoids are shown at 50% probability, hydrogen atoms are omitted for clarity.

3.9. Structure of $[Zn{\cdot}8{\cdot}(OH_2)_2{\cdot}MeOH]^{2+}$

Crystals were grown by vapour diffusion of diethyl ether into a solution of **8** and a large excess of $[Zn(OH_2)_6](ClO_4)_2$ in a 1:1 mixture of chloroform and methanol. These crystals were small and very weakly diffracting and it was necessary to use synchrotron radiation to obtain data. Even using microfocus synchrotron radiation, no data could be obtained beyond a resolution of 0.85 Å. The data are of relatively low quality and it was not possible to sensibly model the positions of the perchlorate anions, or of the (numerous) solvent molecules. The diffuse electron density from these species was included in the model using the OLEX solvent mask feature.[24]

It appears that the zinc(II) ion is coordinated to two water molecules and one methanol, although given the quality of the data, it is possible that these vary (*i.e.* that sometimes the water molecules are methanol and vice-versa). It was necessary to apply DFIX restraints to phenyl rings, four CH_2–CH_2 bonds and the two phenyl-amide carbon bonds in order to achieve a sensible refinement. Due to the low data quality, hydrogen atoms were inserted at calculated positions.

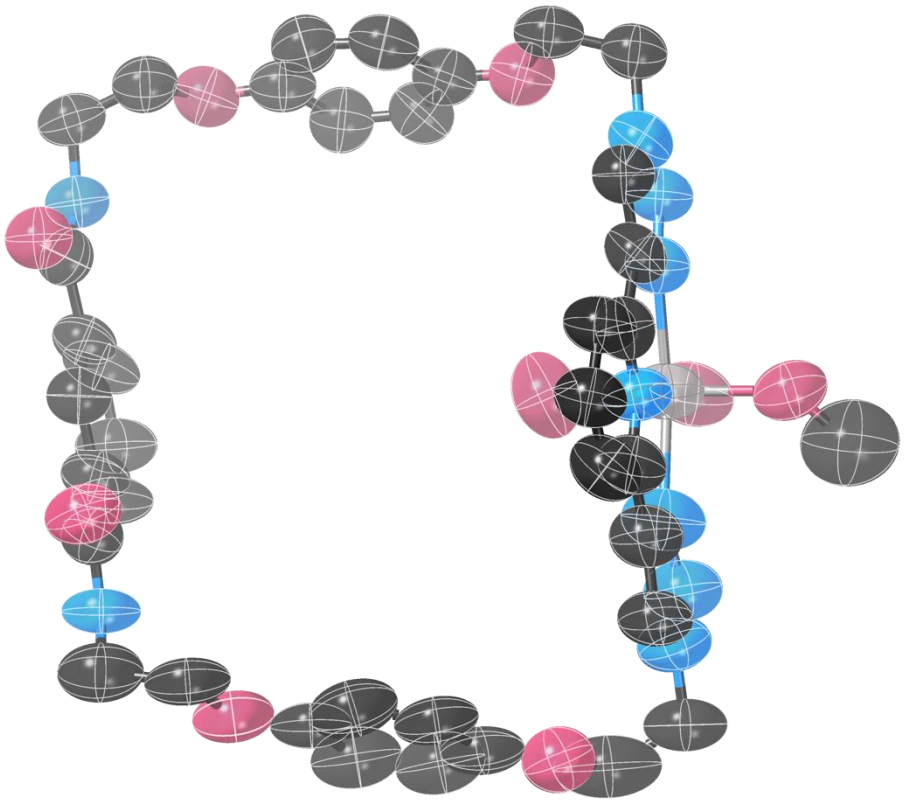

Figure S51. Thermal ellipsoid plot showing the asymmetric unit of $[Zn{\cdot}\mathbf{8}{\cdot}(OH_2)_2{\cdot}MeOH]^{2+}$. Ellipsoids are shown at 50% probability, hydrogen atoms are omitted for clarity.

3.10. Structure of $[Zn{\cdot}\mathbf{1}_2]^{2+}$

We grew crystals by diffusing diethyl ether vapour into a 1:1 chloroform:methanol solution of diazide **1** and either 0.5 or 1.0 equivalents of either $[Zn(OH_2)_6](ClO_4)_2$ or $Zn(BF_4)_2{\cdot}nH_2O$. We collected data for several of these on both an in-house diffractometer and on beamline MX2 of the Australian Synchrotron.[20] In all cases we obtained crystals having the same unit cell (a = 20.4, b = 26.1, c = 29.3 Å, α = 90, β = 108.0, γ = 90 °, $P2_1/c$), which appear to have two ML_2 complexes in the asymmetric unit. In all of these structures, the central zinc **btp** cores of the complexes are relatively well-resolved, but the azido-alkyl-hydroquinone arms of the structure as well as the anions and any solvent molecules cannot be resolved at all. Despite numerous attempts to model these data using copious restraints and PLATON-SQUEEZE[25] to include electron density arising from poorly-resolved parts of the structure in the model, we were unable to achieve a stable structure refinement. A view of the initial SHELXT[22] solve of the structure is shown in Figure S52. A "tidied" version of this where atoms types have been corrected and atoms not corresponding to the $[Zn{\cdot}\mathbf{1}_2]^{2+}$ parts of the molecule removed is presented in Figure S53. While we cannot obtain any useful information about the chemical structure of the molecule from this crystal structure, we believe it provides further evidence of a ML_2 geometry, as determined using ^{1}H NMR titration data.

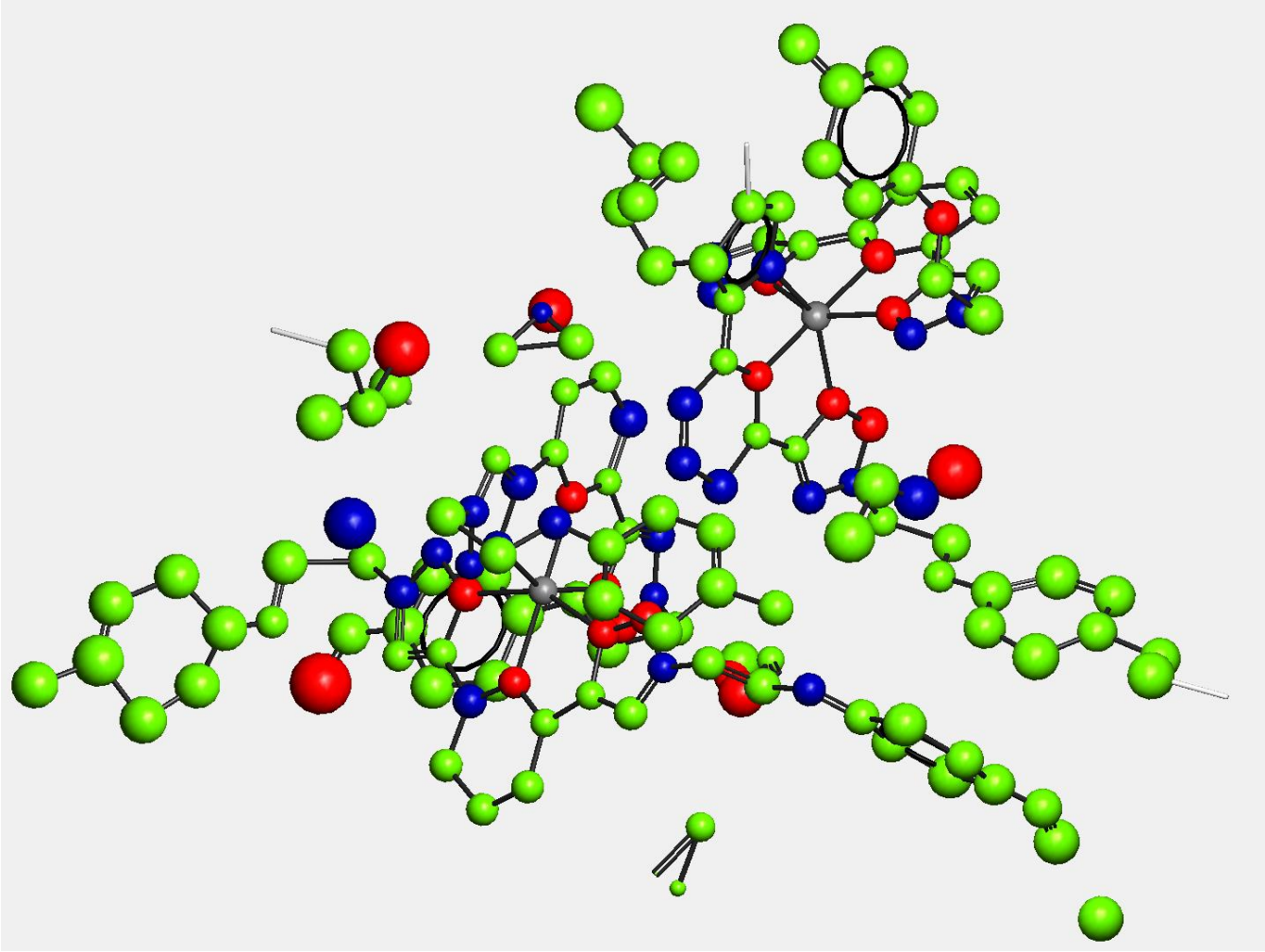

Figure S52. View of the initial SHELXT[22] solve of the structure of $[Zn{\cdot}\mathbf{1}_2]^{2+}$. This could not be refined despite numerous efforts. Note: SHELXT has misassigned some atom types.

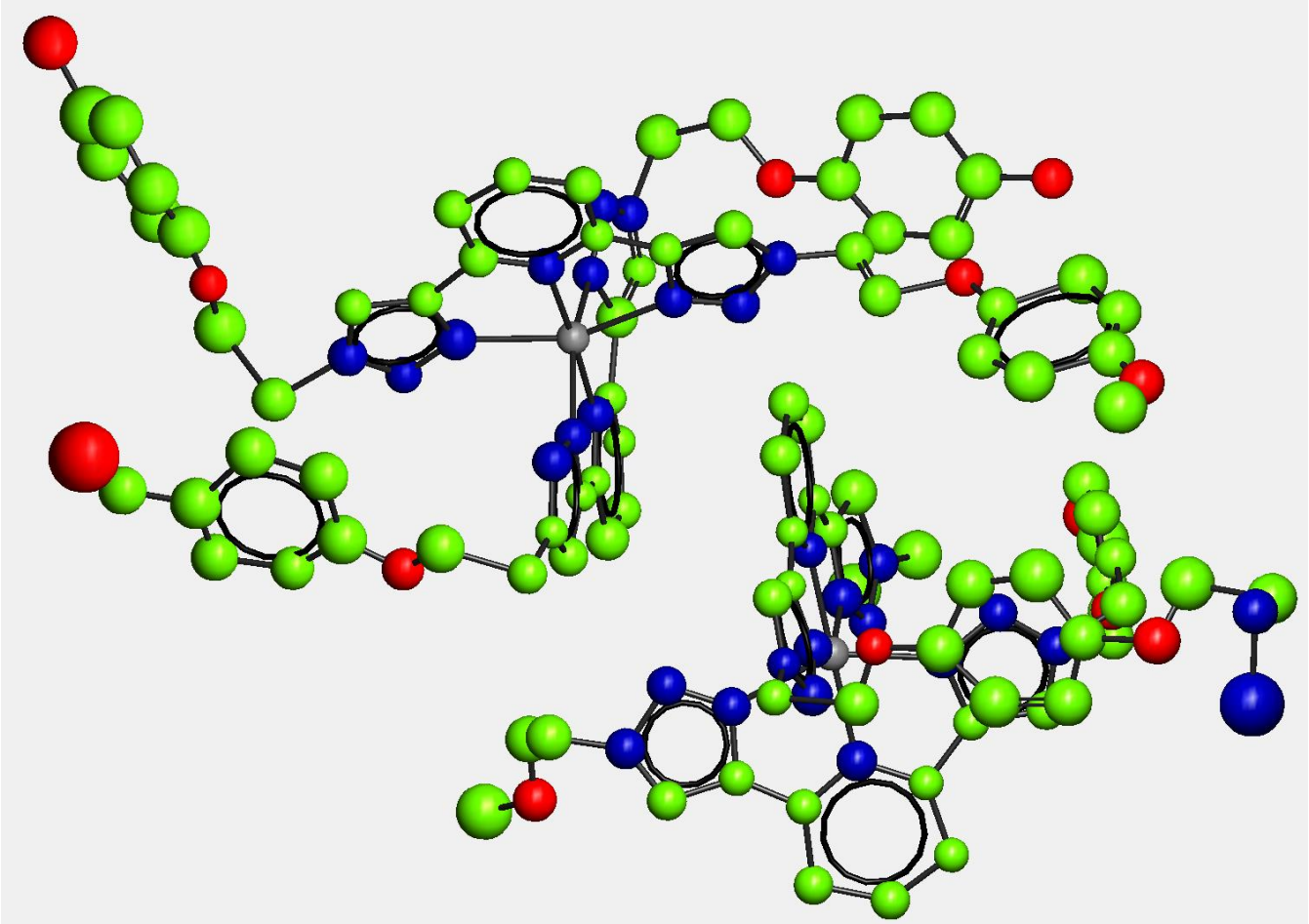

Figure S53. View of the initial SHELXT[22] solve of the structure of $[Zn{\cdot}\mathbf{1}_2]^{2+}$ with mis-assigned atom types corrected, and atoms not corresponding to the $[Zn{\cdot}\mathbf{1}_2]^{2+}$ part of the structure removed.

3.11. Table of crystallographic data

Table S1. Selected crystallographic data.

Compound	**3**	**8**	**TBA·8·Br**
Radiation type	Cu (λ = 1.54184 Å)	Cu (λ = 1.54184 Å)	Synchrotron (λ = 0.71075 Å)
Temperature (K)	150	150	100
Formula	$C_{38}H_{34}N_{14}O_4 \cdot (C_3H_7NO)_2$	$C_{37}H_{35}N_9O_6 \cdot C_2H_6OS \cdot CH_2Cl_2$	$(C_{37}H_{35}N_9O_6)_2 \cdot (C_{16}H_{36}N)_2 \cdot (Br)_2 \cdot C_2H_3N \cdot (H_2O)_{0.5}$
Formula weight	896.97	864.79	2098.29
a (Å)	24.3689(9)	20.1781(4)	16.286(3)
b (Å)	6.0698(2)	22.0626(4)	16.323(3)
c (Å)	32.7063(13)	19.6871(3)	21.177(4)
α (°)	90	90	106.89(3)
β (°)	107.273(4)	109.6762(19)	90.64(3)
γ (°)	90	90	92.77(3)
Unit cell volume (Å^3)	4619.6(3)	8252.58(14)	5378(2)
Crystal system	monoclinic	monoclinic	triclinic
Space group	*C2/c*	*C2/c*	*P–1*
Z	4	8	2
Reflections (all)	16692	33265	37252
Reflections (unique)	4649	8309	20284
R_{int}	0.042	0.034	0.048
R_1 [$I > 2\sigma(I)$]	0.076	0.067	0.062
wR_2 (all data)	0.195	0.197	0.177
CCDC number	2225120	2225115	2225744

Compound	**[Pd·8·Cl]BF_4**	**[Pd·8·Br]BF_4 from acetonitrile**	**[Pd·8·Br]BF_4 from $CHCl_3$/CH_3OH**	**[Pd·8·I]BF_4**	**[Zn·8·$(OH_2)_2$·MeOH]$^{2+}$** [a]
Radiation type	Mo (λ = 0.71073 Å)	Cu (λ = 1.54184 Å)	Synchrotron (λ = 0.71075 Å)	Synchrotron (λ = 0.71075 Å)	Synchrotron (λ = 0.71075 Å)
Temperature (K)	150	150	100	100	100
Formula	$C_{37}H_{35}ClN_9O_6Pd \cdot BF_4 \cdot (C_2H_3N)_2$	$C_{37}H_{35}BrN_9O_6Pd \cdot BF_4 \cdot C_4H_{10}O$	$C_{37}H_{35}BrN_9O_6Pd \cdot BF_4 \cdot C_4H_{10}O$	$C_{37}H_{35}IN_9O_6Pd \cdot BF_4 \cdot C_2H_3$	$C_{38}H_{43}N_9O_9Zn$[a]
Formula weight	1012.50	1048.97		1062.90	835.18
a (Å)	9.3736(4)	13.2676(3)	13.238(3)	9.660(19)	13.835(3)
b (Å)	14.5616(7)	13.9658(4)	13.973(3)	13.938(3)	26.238(5)
c (Å)	17.2045(5)	14.0241(4)	14.000(3)	17.090(3)	17.570(4)
α (°)	75.166(3)	66.859(3)	66.81(3)	109.45(3)	90
β (°)	77.178(3)	81.243(2)	81.10(3)	100.95(3)	111.89(3)
γ (°)	75.894(4)	71.620(2)	71.56(3)	100.13(3)	90
Unit cell volume (Å^3)	2169.50(16)	2266.39(12)	2256.8(10)	2057.9(10)	5929(2)
Crystal system	triclinic	triclinic	triclinic	triclinic	monoclinic
Space group	*P–1*	*P–1*	*P–1*	*P–1*	*P2$_1$/n*
Z	2	2	2	2	4
Reflections (all)	27393	28193	28059	17348	66965
Reflections (unique)	7728	9052	7831	4968	10091
R_{int}	0.063	0.026	0.030	0.033	0.064
R_1 [$I > 2\sigma(I)$]	0.045	0.035	0.052	0.080	0.137
wR_2 (all data)	0.099	0.092	0.153	0.256	0.351
CCDC number	2225121	2225119	2225116	2225117	2225118

[a] OLEX2 solvent mask feature used to remove diffuse electron density.[24]

3.12. Survey of Pd···Pd interactions in the Cambridge Structural Database

The Cambridge Structural Database[26] (Version 5.42 + Sep 2021 updates) was surveyed to compare the Pd···Pd close contacts observed in the structures of [Pd·**8**·Cl]BF_4 and [Pd·**8**·Br]BF_4 with other crystallographically characterised complexes containing such contacts.

An initial search revealed 1780 structures containing Pd···Pd contacts in the range 2.15 – 4.30 Å (50–100% of the sum of the van der Waals radii[27] of two Pd atoms). Subsequently, we searched for the PdN_3X fragment shown in Figure S54, *i.e.* a four-coordinate Pd bonded to three nitrogen and one halogen/halide donor to look for complexes that are broadly similar to [Pd·**8**·X]BF_4. There are 363 structures that match this search fragment in the CSD. Of these 363 structures, 79 (22%) feature a Pd···Pd contact to another PdN_3X fragment with a distance in the range 2.15 – 4.30 Å (range of values observed: 3.28 – 4.29 Å). The properties of these short contacts are summarised in Table S2 and represented graphically in Figure S55.

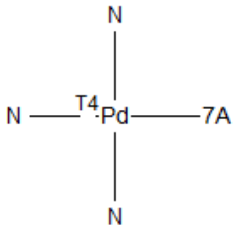

Figure S54. Search fragment used to search Cambridge Structural Database.

Table S2. Parameters of Pd···Pd contacts in PdN_3X complexes from CSD search

Parameter	Value[a]
Number of complexes containing Pd···Pd contacts	79
Number of Pd···Pd contacts	91
Shortest Pd··Pd contact	3.279 Å (76%)
Longest Pd···Pd contact	4.285 Å (>99%)
Mean Pd···Pd contact	3.716 Å (86%)
Median Pd···Pd contact	3.704 Å (86%)

[a] Values in parentheses are expressed as a percentage of the sum of the van der Waals radii.[27]

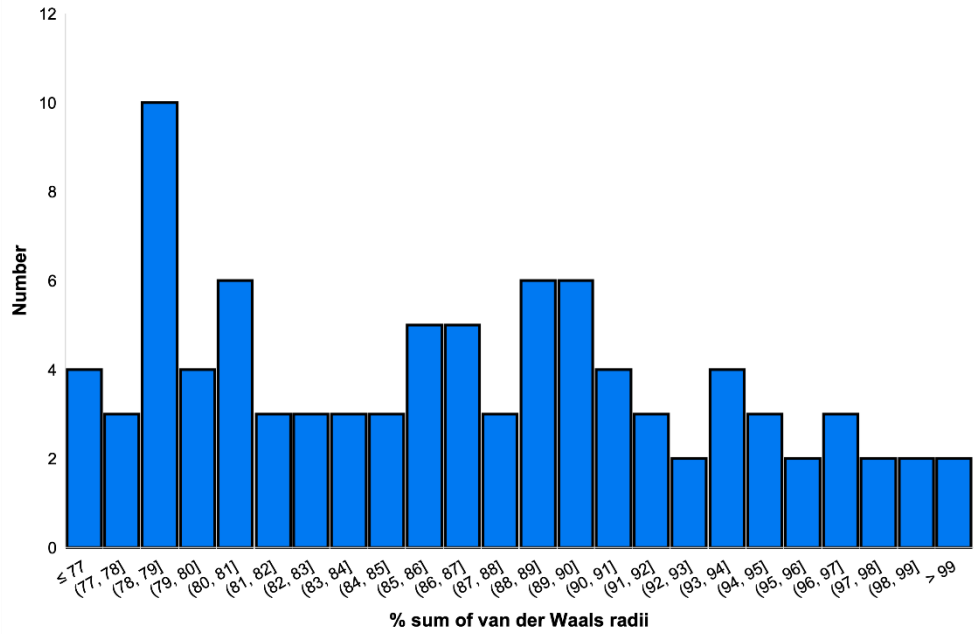

Figure S55. Histogram showing lengths of Pd···Pd contacts of PdN_3X complexes as a percentage of the sum of the van der Waals radii.[27]

The lengths of the Pd···Pd contacts in the three structures in this work ([Pd·**8**·Cl]BF_4, [Pd·**8**·Br]BF_4 from acetonitrile, [Pd·**8**·Br]BF_4 from chloroform/methanol) are 3.338, 3.294 and 3.287 Å, *i.e.* 78, 77 and 76% of the sum of the van der Waals radii, respectively. This puts them at the shorter end of such contacts, and only slightly longer than the shortest such contact in the Cambridge Structural Database.

4. Computational modelling

4.1. Simulation protocol

Computational calculations were undertaken to investigate whether a catenane formed using a metal templated reaction of two equivalents of **1** and a dialkyne such as 2,6-diethynylpyridine (see main text) was geometrically plausible. Note that these calculations offer no insight into whether such a reaction is likely, just whether there are any major steric or conformational barriers to the product forming.

Putative catenanes prepared from two molecules of either tetra-triazole macrocycle **3** or ditriazole diamide macrocycle **8** and a zinc(II) template, *i.e.* $[Zn{\cdot}\mathbf{3_2}]^{2+}$ or $[Zn{\cdot}\mathbf{8}_2]^{2+}$ were initially prepared and energy minimised using the default molecular mechanics forcefield within Spartan20.[28]

All subsequent calculations (including molecular dynamics simulations) were conducted in implicit acetonitrile at a semi-empirical level of theory using the GFN2-xTB methodology[29] within xTB6.4.1[30] using the Australian National Computational Infrastructure. An initial geometry optimisation of the crude models from Spartan20 was then conducted. After this initial optimisation, molecular dynamics simulations were conducted to sample conformational space. These simulations were conducted for 500 ps. Simulations were conducted in the NVT ensemble with the system temperature maintained at 298 K and bonds were constrained using the SHAKE algorithm.[31] The energies over the course of the simulations are shown in Figures S56 and S58 (data from the first 5 ps of the simulations were discarded due to the unreliability of data from the very start of dynamics simulations). After these molecular dynamics simulations, the lowest energy structure for each catenane was taken and again geometry optimised. These optimised structures are shown in Figure S57 and S59. Atomic coordinates for these structures are provided as .xyz files (as Supporting Information). Inspection of the calculated IR spectra showed that no imaginary frequencies were present for either optimised structure.

4.2. Computational modelling of $[Zn{\cdot}\mathbf{3}_2]^{2+}$

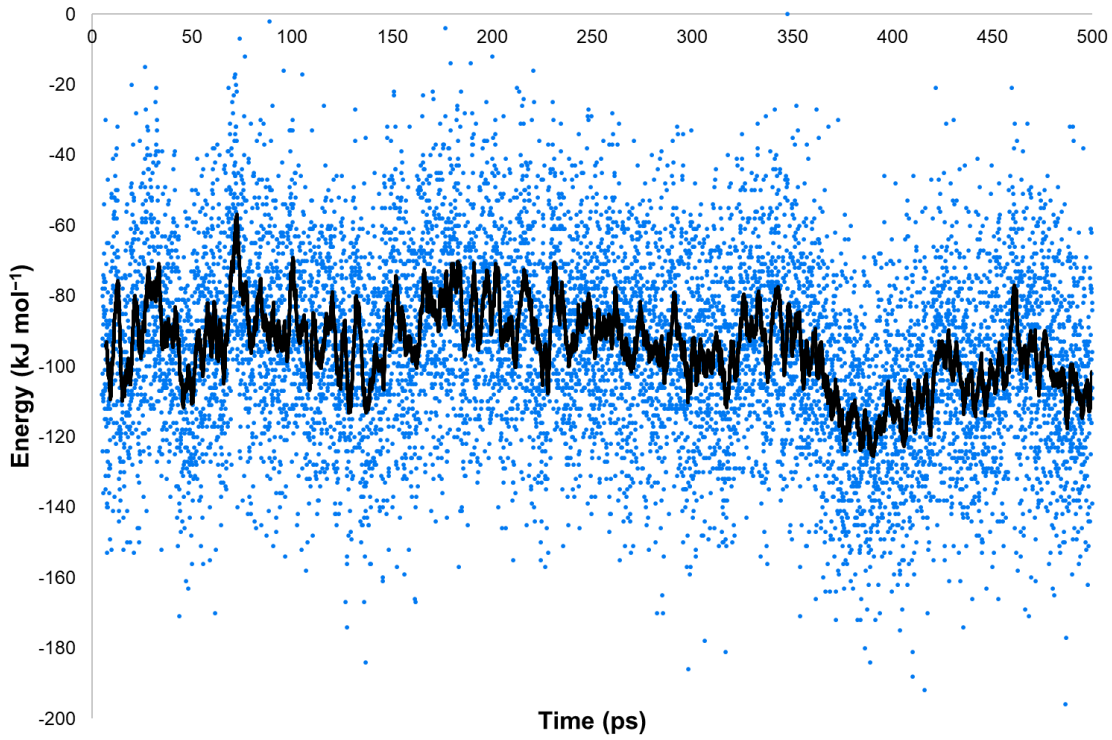

Figure S56. Energies of structures obtained during GFN2-xTB molecular dynamics simulations of $[Zn{\cdot}\mathbf{3}_2]^{2+}$. Blue circles represent datapoints, black line is a 2 ps rolling average. The first 5 ps have been removed.

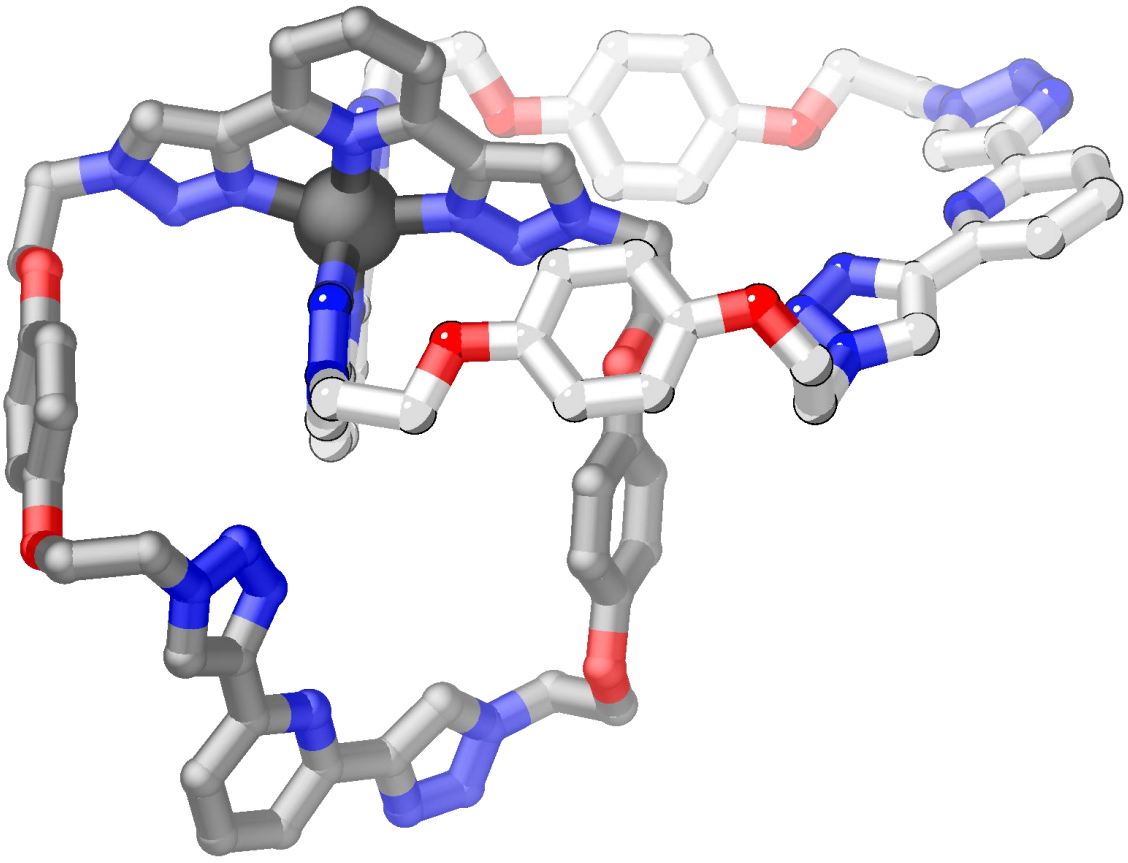

Figure S57. GFN2-xTB optimized structure of $[Zn{\cdot}\mathbf{3}_2]^{2+}$ in implicit acetonitrile.

4.3. Computational modelling of $[Zn\cdot\mathbf{8}_2]^{2+}$

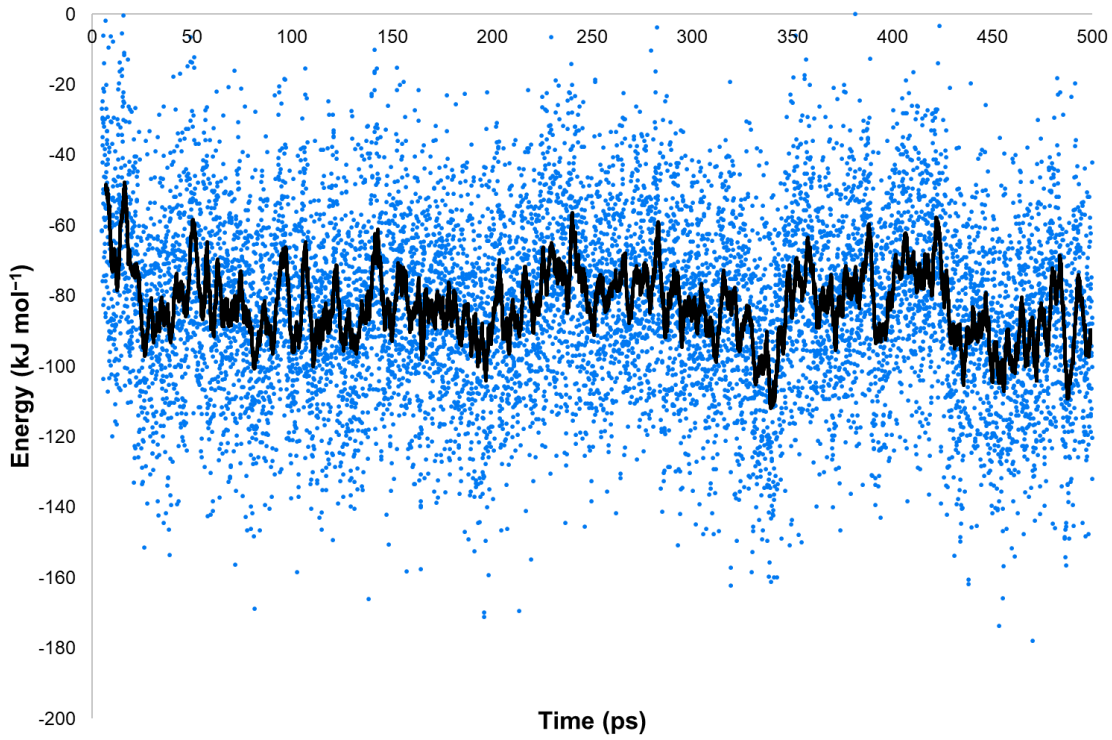

Figure S58. Energies of structures obtained during GFN2-xTB molecular dynamics simulations of $[Zn\cdot\mathbf{8}_2]^{2+}$. Blue circles represent datapoints, black line is a 2 ps rolling average. The first 5 ps have been removed.

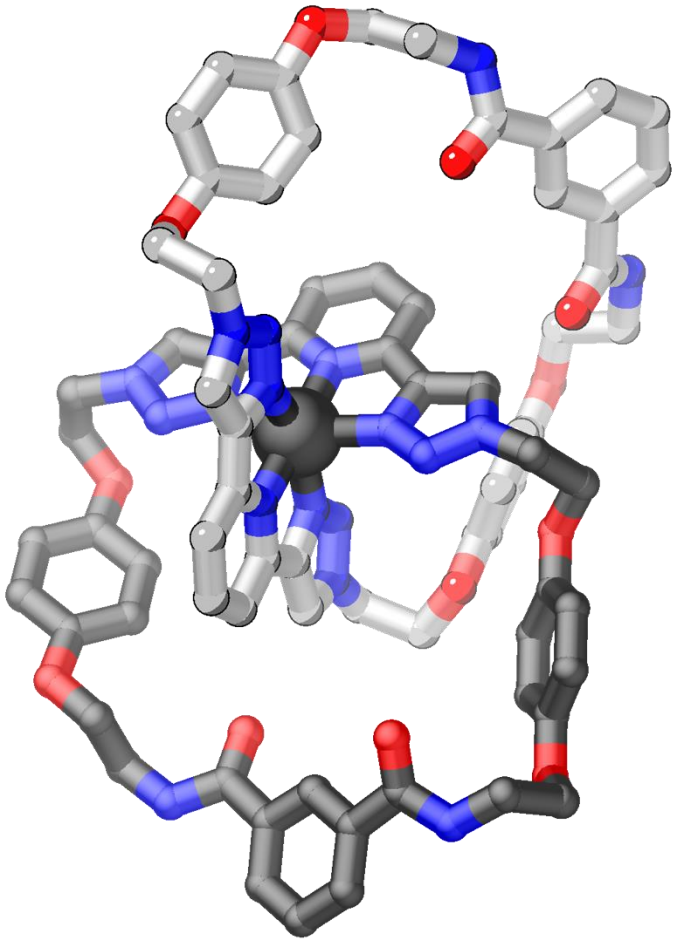

Figure S59. GFN2-xTB optimized structure of $[Zn\cdot\mathbf{8}_2]^{2+}$ in implicit acetonitrile.

5. References

1 T. R. Chan, R. Hilgraf, K. B. Sharpless, V. V. Fokin, Polytriazoles as Copper(I)-Stabilizing Ligands in Catalysis, *Org. Lett.* **2004**, *6*, 2853–2855.
2 A. Orita, K. Miyamoto, M. Nakashima, F. Ye, J. Otera, Double Elimination Protocol for Convenient Synthesis of Dihalodiphenylacetylenes: Versatile Building Blocks for Tailor-Made Phenylene-Ethynylenes, *Adv. Synth. Catal.* **2004**, *346*, 767–776.
3 B. T. Holmes, C. W. Padgett, M. Krawiec, W. T. Pennington, Alkynolpyridines and Their Complexes with Triphenylphosphine Oxide, *Cryst. Growth Des.* **2002**, *2*, 619–624.
4 M. Más-Montoya, D. Curiel, C. Ramírez de Arellano, A. Tárraga, P. Molina, Preorganized Fluorescent Receptor for the Preferential Binding of the Glutarate Anion, *Eur. J. Org. Chem.* **2016**, 3878–3883.
5 M. Thomas, T. Anglim Lagones, M. Judd, M. Morshedi, M. L. O'Mara, N. G. White, Hydrogen Bond-Driven Self-Assembly between Amidinium Cations and Carboxylate Anions: A Combined Molecular Dynamics, NMR Spectroscopy, and Single Crystal X-Ray Diffraction Study, *Chem. Asian J.* **2017**, *12*, 1587–1597.
6 A. J. Lowe, F. M. Pfeffer, Size Matters-Strong Binding of the Terephthalate Dianion by Thiourea Functionalised Fused [n]Polynorbornane Hosts, *Chem. Commun.* **2008**, 1871–1873.
7 H. E. Gottlieb, V. Kotlyar, A. Nudelman, NMR Chemical Shifts of Common Laboratory Solvents as Trace Impurities, *J. Org. Chem.* **1997**, *62*, 7512–7515.
8 D. E. Phipps, P. D. Beer, A [2]Catenane Containing an Upper-Rim Functionalized Calix[4]Arene for Anion Recognition, *Tetrahedron Lett.* **2009**, *50*, 3454–3457.
9 E. J. O'Neil, K. M. DiVittorio, B. D. Smith, Phosphatidylcholine-Derived Bolaamphiphiles via Click Chemistry, *Org. Lett.* **2007**, *9*, 199–202.
10 R. E. Conrow, W. D. Dean, Diazidomethane Explosion, *Org. Process Res. Dev.* **2008**, *12*, 1285–1286.
11 B. T. Holmes, P. Deb, W. T. Pennington, T. W. Hanks, Synthesis and Polymerization Behavior of Tridentate Diacetylene Hosts, *J. Polym. Res.* **2006**, *13*, 133–144.
12 S. L. Broman, C. L. Andersen, M. Jevric, C. G. Tortzen, O. Hammerich, M. B. Nielsen, Metal Cation Binding to Acetylenic Tetrathiafulvalene–Pyridine Conjugates: Affinity Tuned by Preorganization and Cavity Size, *Tetrahedron*, **2016**, *72*, 5831–5842.
13 J. E. M. Lewis, R. J. Bordoli, M. Denis, C. J. Fletcher, M. Galli, E. A. Neal, E. M. Rochette, S. M. Goldup, High Yielding Synthesis of 2,2′-Bipyridine Macrocycles, Versatile Intermediates in the Synthesis of Rotaxanes, *Chem. Sci.* **2016**, *7*, 3154–3161.
14 *Bindfit*, accessed at supramolecular.org.
15 CrysAlis Pro, Oxford Diffraction, **2011**.
16 L. Palatinus, G. Chapuis, SUPERFLIP. A Computer Program for the Solution of Crystal Structures by Charge Flipping in Arbitrary Dimensions, *J. Appl. Crystallogr.* **2007**, *40*, 786–790.
17 P. W. Betteridge, J. R. Carruthers, R. I. Cooper, K. Prout, D. J. Watkin, CRYSTALS Version 12: Software for Guided Crystal Structure Analysis, *J. Appl. Crystallogr.* **2003**, *36*, 1487.
18 R. I. Cooper, A. L. Thompson, D. J. Watkin, CRYSTALS Enhancements: Dealing with Hydrogen Atoms in Refinement, *J. Appl. Crystallogr.* **2010**, *43*, 1100–1107.
19 N. P. Cowieson, D. Aragao, M. Clift, D. J. Ericsson, C. H. Gee, N. Mudie, S. Panjikar, J. R. Price, A. Riboldi-Tunnicliffe, R. Williamson, T. Caradoc-Davies, MX1: A Bending-Magnet Crystallography Beamline Serving Both Chemical and Macromolecular Crystallography Communities at the Australian Synchrotron, *J. Synchrotron Radiat.* **2015**, *22*, 187–190.
20 D. Aragao, J. Aishima, H. Cherukuvada, R. Clarken, M. Clift, N. P. Cowieson, D. J. Ericsson, C. L. Gee, S. Macedo, N. Mudie, S. Panjikar, J. R. Price, A. Riboldi-Tunnicliffe, R. Rostan, R. Williamson, T. T. Caradoc-Davies, MX2: A High-Flux Undulator Microfocus Beamline Serving Both the Chemical and Macromolecular Crystallography Communities at the Australian Synchrotron, *J. Synchrotron Radiat.* **2018**, *25*, 885–891.
21 W. Kabsch, XDS, *Acta Crystallogr.* **2010**, *D66*, 125–132.
22 G. M. Sheldrick, SHELXT - Integrated Space-Group and Crystal-Structure Determination, *Acta Crystallogr.* **2015**, *A71*, 3–8.
23 G. M. Sheldrick, *Acta Crystallogr.* Crystal Structure Refinement with SHELXL, **2015**, *C71*, 3–8.
24 O. V. Dolomanov, L. J. Bourhis, R. J. Gildea, J. A. K. Howard, H. Puschmann, OLEX2: A Complete Structure Solution, Refinement and Analysis Program, *J. Appl. Crystallogr.* **2009**, *42*, 339–341.
25 A. L. Spek, PLATON SQUEEZE: A Tool for the Calculation of the Disordered Solvent Contribution to the Calculated Structure Factors, *Acta Crystallogr.* **2015**, *C71*, 9–18.
26 R. Taylor, P. A. Wood, A Million Crystal Structures: The Whole Is Greater than the Sum of Its Parts, *Chem. Rev.* **2019**, *119*, 9427–9477.
27 S. Alvarez, A Cartography of the van Der Waals Territories, *Dalton Trans.* **2013**, *42*, 8617–8636.
28 Spartan20, Wavefunction Inc.
29 C. Bannwarth, S. Ehlert, S. Grimme, GFN2-XTB—An Accurate and Broadly Parametrized Self-Consistent Tight-Binding Quantum Chemical Method with Multipole Electrostatics and Density-Dependent Dispersion Contributions, *J. Chem. Theory Comput.* **2019**, *15*, 1652–1671.
30 C. Bannwarth, E. Caldeweyher, S. Ehlert, A. Hansen, P. Pracht, J. Seibert, S. Spicher, S. Grimme, Extended Tight-Binding Quantum Chemistry Methods, *WIREs Comput. Mol. Sci.* **2021**, *11*, e1493.
31 J.-P. Ryckaert, G. Ciccotti, H. J. C. Berendsen, Numerical Integration of the Cartesian Equations of Motion of a System with Constraints: Molecular Dynamics of n-Alkanes, *J. Comput. Phys.* **1977**, *23*, 327–341.